UNIVERSITÀ DELLA CALABRIA

Dipartamento di Matematica e Informatica

Dottorato di Ricerca in Matematica e Informatica

Con il contributo della

Secretaría Nacional de Educación Superior, Ciencia, Tecnología e Innovación (SENESCYT - ECUADOR)

XXVII CICLO

TITOLO TESI

CELLULAR AUTOMATA FOR MODELING AND SIMULATING COMPLEX PHENOMENA: LAHARS

Case Studies of Primary and Secondary Lahars in Ecuador

Settore Scientifico Disciplinare

INF/01 - INFORMATICA

Coordinatore: Prof. Nicola Leone

Firma _____

Supervisori: Prof. Salvatore Di Gregorio

Firma _____

Dr. Valeria Lupiano

Firma _____

Dottorando: Dott. Guillermo E. Machado Sotomayor

Firma _____

Dedicated to my loving parents, my sons Alexander and Jhordan, and my family for always having faith in me.

Declaration

I hereby declare that except where specific reference is made to the work of others, the contents of this dissertation are original and have not been submitted in whole or in part for consideration for any other degree or qualification, or to any other university. This thesis is my own work and contains nothing which is the outcome of work done in collaboration with others, except as specified in the text and Acknowledgments. This thesis contains fewer than 65,000 words including a bibliography, appendices, footnotes, tables and equations and has fewer than 50 figures.

Guillermo Machado Sotomayor
November 2015

Acknowledgements

Foremost, I would like to express my gratitude to all those individuals and institutions who have supported me during my doctoral studies and have helped me to make this research a reality.

Firstly, I want to express my grateful and appreciation to my thesis advisors: Prof. Salvatore Di Gregorio and Dr. Valeria Lupiano, for their invaluable guidance throughout the years. I could not have imagined having better advisors and mentors for my PhD study. Salvatore Di Gregorio, for giving me the opportunity to work in this thrilling approach of modeling and simulation of complex natural phenomena with Cellular Automata, for his contributions and support that were not limited to the transmission of knowledge and ideas for the development of the thesis, in themselves very valuable, but reached the human side of those who have been fortunate, as me, in to meet and work with him. Valeria Lupiano, who was present at all times, given me guidance and unconditional support, without her guidance and valuable ideas, this study would not have been successfully completed. I am deeply grateful for all their constructive comments and critical spirits that allowed me to move forward with this research.

Many thanks to:

My sponsors, Secretaría Nacional de Educación Superior, Ciencia, Tecnología e Innovación (SENESCYT) and Universidad Nacional de Chimborazo from Ecuador, by the financing granted to my studies and research.

The teaching and administrative staff of the Department of Mathematics and Computer Science of the University of Calabria.

The technical staff of the Geophysical Institute of the National Polytechnic of Ecuador for its predisposition and support.

I am grateful to many scientists for obtaining precious data, useful information, advices and comments. I remember just Gustavo Cordoba Guerrero, Professor at the University of Nariño, Colombia, Patricia Mothes and IGEPN staff, Michel Sheridan, Professor Emeritus at the University of Buffalo, USA. Salvatore Straface, Professor at the University of Calabria, Italy.

I have been very fortunate to have unconditional colleagues and friends at the UNICAL: Barbara, Marek, Weronika, Carmine, Giovanni, Mario, Luigi, William, Maria Vittoria, Francesco, Donato, Rocco, Paolo, Alessia and Angelo, who have given me their friendship and a hand when I needed them.

A heartfelt thanks to my family and friends for the moral support and affection that I have always received from them, especially to Lorena, Cristian and Leticia for their enormous unconditional support and timely advice.

Finally, I would like to express my sincere and special gratitude to the Machado Sotomayor family for their unconditional love and full support, thank you for your prayers and words of encouragement in difficult times that I had to overcome.

Thanks, thanks my God and to my beautiful angel Alexander forever be with me.

Abstract

Lahars represent one of the most destructive natural disasters regarding the loss of human lives and property damage in their path. Lahars are very complex surface flows of two types: primary lahars originated directly from eruptive volcanic activity, and secondary lahars originated in post-eruptive events or quiescent periods.

Lahars are a complex combination of many interrelated processes besides the process of surface flow: rainwater percolation in the soil (secondary lahars), volcanic stratum erosion, water inclusion and extrusion in lahar, ice melting and mixing with volcanic emissions (primary lahars). Evaluating the hazard posed by lahars constitutes a significant challenge within the framework of modeling and simulation of complex systems for reducing hazard in many, sometimes very populous, inhabited areas next some dangerous volcanoes.

A variety of approaches has been taken to modeling the behaviors of lahars and the hazards posed to downstream communities: empirical models based on smart correlations of phenomenon observables, simple rheological and hydrological models and Partial Differential Equations (approximating numerical methods of fluid dynamics).

Cellular Automata (CA) represent an alternative approach for modeling and simulating complex systems evolving on the base of local interactions of their elementary components. Lahars may be classified as such a type of phenomenon. Moreover, a CA modeling methodology has been developed for simulating surface flows.

CA are a parallel computational paradigm for modeling complex systems by defining 'simple' laws at a local level that generate a global 'complex' evolution. The research, reported in this thesis, adopts a Multicomponent (or Macroscopic) Cellular Automata (MCA) approach that was applied to other complex surface flows. The model LLUNPIY has been developed in this frame, and successful simulations of real events were performed.

The goal of this thesis has been to develop a CA model, LLUNPIY (**L**ahar modeling by **L**ocal rules based on an **UN**derlying **PI**ck of **Y**oked processes, from the Kichwa word llunp'iy meaning flood), which is based on the CA semi-empirical approach to macroscopic phenomena of Di Gregorio and Serra, in order to simulate the complex dynamics of lahars, taking into account experience of models like SCIDDICA, SCIARA, PYR, VALANCA and SCAVATU.

This work is focused on the CA modeling of the complex phenomenon of primary and secondary lahars, whose dynamics and processes are considered in this thesis to be divided into three main phases:

Generation phase: In the case of primary lahars, these are generated from pyroclastic flows and melting of the volcano's icecap, due to the interaction of eruptive products with a summit glacier. In the case of secondary lahars, heavy rainfalls mobilize abundant unconsolidated sediments on steep slopes by percolation of an adequate water quantity, which determines the collapse of cohesion forces of the soil components.

Flood phase: Lahar flows develop along the volcano steep slopes with high gravitational potential energy and turbulence with bulking by soil erosion and water inclusion along watercourses.

Exhaustion phase: Lahar flow reduces its kinetic energy and velocity in flat areas; a rapid decrease of turbulence causes deposit formation by water extrusion. In this latter, in some cases, the lahar can partially 'be diluted' and 'disappear', if it runs into a watercourse with a water flow, sufficiently large to englobe the lahar matter.

Before and during the development of the model, a comprehensive study was carried out on models not only for modeling complex macroscopic phenomena with Cellular Automata, but also two main models have been studied, which have previously modeled the lahars. LAHARZ is an empirical model, which computes the inundation area on the base of lahar volume and channel sections. TITAN2D model (for simulating granular, mud, debris flows and lahars) is based on physical Partial Differential Equations (PDE), related to the Coulomb mixture theory. Both LAHARZ and TITAN2D did not account for all the processes of the previous cited three phases. An example is the erosion process. The erosion process does not exist in LAHARZ, because of the simplicity of the model. In the case of TITAN2D, it was necessary to omit the erosion process because the calculation times are not sustainable because of the complexity of the complete differential equations system. The MCA incremental method of modeling, applied in this research, permitted to LLUNPIY model to manage the erosion process and other ones with satisfactory results.

This research considered real events of primary and secondary lahars to develop and validate the model. CA modeling and simulation of lahars needs a time-space correspondence, which may be explicitly established between the model and the real world to compare phenomenon development with simulation progress. To find sufficient data with an appropriate precision according to MCA methodology was not easy. Data about 1877 Cotopaxi primary lahar were found, analyzed, compared and interpreted. Analog study was performed with less effort for the more recent 2005 and 2008 Tungurahua secondary lahars. The candidate collected important data for developing the model directly on the field in the first person.

The LLUNPIY model was validated through simulations of the three selected events: the 2005 and 2008 Tungurahua secondary lahars and afterward the 1877 Cotopaxi primary lahar.

Results of the LLUNPIY simulations demonstrate that modeling choices, allowed by CA properties, permit to account for more processes (e.g., erosion process) that are not considered in other models. Therefore, LLUNPIY extends the potentiality of analysis and scenarios development in applications that needs computer simulations of real or conjectured lahar events.

Sommario

I lahar rappresentano uno dei disastri più distruttivi in termini di perdita umane e di danno a strutture e infrastrutture. I lahar sono flussi di superficie molto complessi, distinguiamo due tipi: I lahar primari che si originano in concomitanza di eruzioni vulcaniche, e i lahar secondari che si originano durante eventi post-eruttivi o nei periodi di quiescenza del vulcano.

I lahar sono una complessa combinazione di molti processi variamente combinati: oltre ai flussi di superficie si riscontrano fenomeni di filtrazione di acqua piovana nel suolo (lahar secondari), erosione dello strato piroclastico, inclusione ed estrusione di acqua, scioglimento di ghiacciai con aliquote di acqua che si mescola a emissioni vulcaniche (lahar primari).

Valutare il pericolo generato dai lahar al fine di ridurre il pericolo in molte, a volte popolose, aree vulcaniche, costituisce una sfida significativa nel contesto della modellizzazione e simulazione di sistemi complessi.

La comunità scientifica mette a disposizione un varietà di approcci per definire il comportamento dei lahar e per valutare i pericoli ad essi connessi. Esistono, infatti, modelli empirici basati sulle correlazioni intelligenti dei fenomeni osservabili, modelli semplici reologici e idrologici, e modelli basati sulla risoluzione di Equazioni Differenziali Parziali (metodi approssimativi numerici della dinamica dei fluidi).

Gli Automi Cellulari (AC) rappresentano un approccio alternativo per modellare e simulare sistemi complessi che si evolvono sulla base delle interazioni locali dei loro componenti elementari. I lahar rientrano in questa casistica e come tali possono essere trattati tramite modelli ad AC.

Gli AC sono un paradigma computazionale parallelo che consentono di modellare sistemi complessi previa definizione di “semplici” leggi locali che generano un’evoluzione globale e “complessa” del sistema.

La ricerca, sostenuta in questa tesi, adotta un approccio a Multicomponenti (o Macroscopico) Automi Cellulare (ACM) già applicati ad altri flussi complessi di superficie. Il modello LLUNPIY è stato sviluppato in questo contesto, e sono state ottenute con successo simulazioni di eventi reali.

L’obiettivo di questa tesi è stato quello di sviluppare il modello ad AC, LLUNPIY (dalla parola Kichwa llunp’iy che significa inondazione). Tale modello è basato sull’approccio ad automi cellulari di tipo semi-empirico descritto da Di Gregorio e Serra,

allo scopo di simulare le complesse dinamiche dei lahar, tenendo in conto l'esperienza dei modelli come SCIDDICA, SCIARA, PYR, VALANCA e SCAVATU.

Questo lavoro si basa sul modello AC del fenomeno complesso dei lahar primari e secondari, le cui dinamiche e processi sono considerate in questa tesi divisi in tre fasi principali:

Fase della generazione: nel caso dei lahar primari, l'innesco è generato dai flussi piroclastici incandescenti che sciolgono la callotta di ghiaccio del vulcano. Nel caso di lahar secondari, piogge eccezionali sono in grado di mobilitare i sedimenti poco consolidati presenti sui ripidi pendii attraverso l'infiltrazione di quantità sufficienti d'acqua. Ciò determina il collasso delle forze di coesione delle particelle di suolo con conseguente innesco di fenomeni di flusso.

Fase dell'inondazione: I flussi dei lahar si sviluppano lungo i ripidi pendii del vulcano, utilizzando il reticolo fluviale esistente, con un'alta turbolenza, alta energia gravitazionale potenziale e alta capacità erosiva.

Fase di esaurimento: il flusso del lahar riduce la sua energia cinetica e la sua velocità quando raggiunge aree pianeggianti; la rapida diminuzione di turbolenza causa la formazione di deposito attraverso l'estrusione dell'acqua. In alcuni casi, il lahar può essere parzialmente "diluito" o "scomparire", quando si immette in un fiume sufficientemente grande da inglobare i flussi del lahar.

Prima e durante lo sviluppo del modello, è stato eseguito uno studio completo sui modelli esistenti, non solo quelli basati sugli Automi Cellulari, ma anche i modelli, che hanno in precedenza simulato i lahar con altre metodologie. Per esempio: LAHARZ e TITAN2D. LAHARZ è un modello empirico, che calcola l'area di inondazione sulla base del volume del lahar e delle sezioni del canale di flusso. Il modello TITAN2D (nato per simulare flussi e colate di tipo granulare) è basato sulle equazioni differenziali parziali, legate alla teoria della miscela di Coulomb. Sia LAHARZ sia TITAN2D non prendono in considerazione i processi delle tre fasi descritte precedentemente. Un esempio è il processo di erosione. Esso non esiste in LAHARZ, a causa della semplicità del modello. Nel caso di TITAN2D, si omette il processo di erosione perché i tempi di calcolo non sono sostenibili a causa della complessità dei sistemi di equazioni differenziali. Il metodo incrementale ad ACM, applicato in questa ricerca, permette al modello LLUNPIY di considerare il processo di erosione e varie altri processi, tipici del fenomeno, con resultati soddisfacenti.

Questa ricerca è stata applicata a eventi reali sia di lahar primari che di lahar secondari allo scopo di sviluppare e testare il modello. La modellizzazione e la simulazione con Automi Cellulari dei lahar necessita di una corrispondenza spazio-temporale, che può

essere esplicitamente stabilita fra il modello e il mondo reale per mettere a confronto simultaneamente lo sviluppo del fenomeno con quanto realmente accaduto. Trovare dati sufficienti con un'adeguata precisione per poter applicare la metodologia descritta non è stato facile. Sono stati recuperati, analizzati, e confrontati i dati del lahar primario che si è generato nel 1877 lungo i fianchi del vulcano Cotopaxi. Una ricerca analoga è stata eseguita, con meno sforzo, per i più recenti lahar secondari del vulcano Tungurahua. Il candidato ha raccolto importanti dati, necessari al modello, direttamente sul campo e in prima persona. Il modello LLUNPIY è stato testato attraverso le simulazioni di tre diversi eventi: i lahar secondari del vulcano Tungurahua avvenuti nel 2005 e nel 2008 e in seguito il lahar primario del vulcano Cotopaxi del 1877.

I resultati delle simulazioni del modello LLUNPIY dimostrano che le scelte di modellazione, consentite dalle proprietà degli AC, permettono di tenere in conto di più processi (tra cui il processo di erosione), che non sono considerati in altri modelli. Se ne conclude che LLUNPIY estende la potenzialità di analisi, con possibilità di messa a punto di scenari evolutivi, dei lahar siano essi reali o ipotizzati.

Resumen

Los lahares representan uno de los desastres naturales más destructivos en términos de pérdida de vidas humanas y daños materiales a su paso. Los lahares son flujos superficiales muy complejos, se distinguen dos tipos: lahares primarios que se originan directamente de la actividad eruptiva volcánica y lahares secundarios que ocurren en eventos post-eruptivos o en periodos de inactividad.

Estos eventos se caracterizan por tener una combinación compleja de muchos factores interrelacionados, además del proceso de flujo de superficie: percolación del agua-lluvia en el suelo (lahares secundarios), erosión del estrato volcánico, inclusión y extrusión de agua en el lahar, fusión del hielo y la mezcla con las emisiones volcánicas (lahares primarios). Evaluar el peligro que representa el lahar, constituye un reto importante en el contexto de la modelización y simulación de sistemas complejos para reducir el riesgo en muchas y a menudo muy pobladas, áreas residenciales cercanas a algunos volcanes peligrosos.

Varios enfoques se han adoptado para modelar los comportamientos de los lahares y los peligros que representan para las comunidades aguas abajo, tales como: modelos empíricos basados en correlaciones inteligentes de fenómenos observables, modelos reológicos e hidrológicos simples y ecuaciones diferenciales parciales (que se aproximan a los métodos numéricos de dinámica de fluidos).

Los Autómatas Celulares (AC) representan un enfoque alternativo para el modelado y simulación de sistemas complejos que evolucionan sobre la base de las interacciones locales de sus componentes elementales. Los lahares pueden ser clasificados como tal tipo de fenómeno. Por otra parte, una metodología de modelado de AC ha sido desarrollada para simular flujos de superficie.

Los AC representan un paradigma de cálculo paralelo para el modelado de sistemas complejos mediante la definición de leyes "simples" a nivel local que generan una evolución global "compleja". La investigación, reportada en esta tesis, adopta un enfoque de Autómatas Celulares Multicomponente (o Macroscópicos) (ACM) que ha sido aplicado a otros flujos complejos de superficie. El modelo LLUNPIY se ha desarrollado en este contexto y ha permitido la realización de simulaciones exitosas de eventos reales.

La tesis tuvo como objetivo principal desarrollar un modelo de AC denominado LLUNPIY (término que proviene de la palabra Kichwa llunpi’y que significa inundación), fundamentado en el enfoque semi-empírico de AC propuesto por Di Gregorio y Serra para fenómenos macroscópicos, con la finalidad de simular la dinámica compleja de los lahares,

tomando en cuenta la experiencias previas con modelos como SCIDDICA, SCIARA, PYR, VALANCA y SCAVATU.

Este trabajo se enfocó sobre el modelo de AC para fenómenos complejos, tanto de lahares primarios como secundarios, cuyas dinámicas y procesos se consideran en esta tesis y se dividen en tres principales fases:

Fase de generación: En el caso de lahares primarios, éstos se generan a partir de flujos piroclásticos y la fusión del casquete glaciar del volcán, debido a la interacción de los productos eruptivos con la cima del glaciar. En el caso de lahares secundarios, las fuertes lluvias movilizan abundantes sedimentos no consolidados en pendientes pronunciadas por la percolación de una cantidad de agua, lo que determina el colapso de las fuerzas de cohesión de los componentes del suelo.

Fase de inundación: Los flujos de lahar se desarrollan a lo largo de las empinadas laderas del volcán con una alta energía potencial gravitacional y una turbulencia con un incremento de volumen debido a la erosión del suelo y la inclusión de agua a lo largo de los causes de los ríos.

Fase de agotamiento: El flujo del lahar reduce su energía cinética y velocidad en las áreas planas; la rápida disminución de la turbulencia causa la formación de depósitos a través de la estrucción de agua. En ésta última, en algunos casos, el lahar puede parcialmente “ser diluido” y “desaparecer”, si converge a un flujo de agua lo suficientemente grande como para ser embebido el material del lahar.

Antes y durante el desarrollo del modelo, se llevó a cabo un estudio exhaustivo sobre modelos, no sólo para modelar fenómenos macroscópicos complejos con Autómatas Celulares, sino además, se estudiaron dos modelos principales, los cuales previamente han modelado lahares, estos son: LAHARZ, es un modelo empírico que calcula el área de la inundación sobre la base del volumen del lahar y las secciones transversales del canal y el modelo TITAN2D (para simular flujos granulares, lodo y escombros), basado en las ecuaciones diferenciales parciales físicas, relacionado con la teoría de la mezcla de Coulomb. Tanto el LAHARZ como el TITAN2D, no tuvieron en cuenta todos los procesos de las tres fases citadas anteriormente. Un ejemplo es el proceso de erosión que no existe en LAHARZ, debido a la simplicidad del modelo. En el caso de TITAN2D, era necesario omitir el proceso de erosión debido a los tiempos de cálculo que no son sostenibles por la complejidad del sistema completo de ecuaciones diferenciales. El método incremental del modelado de ACM, aplicado en esta investigación, ha permitido al modelo LLUNPIY considerar el proceso de erosión y otros, con resultados satisfactorios.

Esta investigación ha considerado eventos reales de lahares primarios y secundarios con la finalidad de desarrollar y validar el modelo. La modelización y simulación de lahares

con Autómatas Celulares requiere una correspondencia espacio-temporal, que puede establecerse de forma explícita entre el modelo y el mundo real con el propósito de comparar el comportamiento del fenómeno con el progreso simultáneo. El encontrar suficientes datos con la precisión adecuada utilizando la metodología de ACM, no ha sido fácil. Los datos sobre el lahar primario del Cotopaxi 1877 han sido encontrados, analizados, comparados e interpretados. Un estudio similar y reciente se llevó a cabo con menos esfuerzo, para los lahares secundarios del volcán Tungurahua en el 2005 y 2008. El candidato recolectó directamente importantes datos de campo para desarrollar el modelo. El modelo LLUNPIY fue validado a través de las simulaciones de tres diferentes eventos seleccionados: los lahares secundarios ocurridos en el volcán Tungurahua tanto en el 2005 como en el 2008, y posteriormente el lahar primario del volcán Cotopaxi en 1877.

Los resultados de las simulaciones del modelo LLUNPIY demuestran que las opciones de modelado, permitidas por las propiedades de los Autómatas Celulares, posibilitan tomar en cuenta más procesos (por ejemplo, el de erosión), aspectos fundamentales que no son considerados en otros modelos. Por lo tanto, LLUNPIY amplía la potencialidad del análisis y desarrollo de posibles escenarios en aplicaciones que requieren simulaciones por ordenador de eventos de lahares reales o conjeturados.

Table of Contents

List of Figures

List of Tables

Chapter 1

Introduction

"Complexity is almost a theological concept; many people talk about it, but nobody knows what 'it' really is"

Daniel L. Stein

1.1 Background

Modeling and simulation are becoming increasingly important enablers for the study, analysis and description of complex systems in all the sectors of science and engineering. Very many systems that are composed of interconnected and mutually interacting parts exhibit highly complex behaviors [146]. Many systems of the physical, socioeconomic, urban and biological worlds can be defined as complex systems. Some examples of complex systems are the motion of fluids, the economic transformation of a region, the growth of an urban center, the life of an organism, etc.

Different types of natural macroscopic phenomena are fully included in the class of such systems. Some types of 'surface flows' are of particular interest, such as lava flows, pyroclastic flows, debris flows and lahars, both for environmental impact and because they are a grave danger to people and property in many parts of the world. Concerning volcanic hazard, approximately more than 1,000 volcanoes have populations within proximity. About 10 % of the global population live on the flanks of active volcanoes and could suffer the acute effects of even a moderate-sized eruption [108] [30] [135].

Many international studies have attempted to characterize surface flows in detail, often for the purpose of preparing defense measures and mitigating risk. In some cases, studies were aimed at evaluating 'temporal' hazards [45] [145]. For instance, they identify the likely

moment, when a landslide or eruption of magma from a crater will be triggered, while other analyses attempt to estimate 'susceptible' territorial sectors, or the 'spatial' hazard. In this case, the purpose of the study is generally to create valid simulation models that reproduce as faithfully as possible the dynamics and effects of phenomena of interest, such as the debris flow, lahars, lava flow, etc.

With regard to surface flow models, two basic research models have been developed and consolidated. The first is based on the analysis of Differential Partial Equations (PDE). It describes the phenomenon and its evolution through analytical numerical methods (used mostly to study general properties, but could be impractical to apply to real events because of complexity) or approximated numerical methods [79] [74] [86]. As an alternative to these methods, which are based on the analysis of physical equations, a methodological approach was developed based on the computational paradigm of Cellular Automata [42]. Henceforth the notation CA is used both for Cellular Automaton and Cellular Automata, when the context is evident, in other instances, the full name will used.

CA are able to represent non-linear dynamic systems at discrete intervals in time and space. First, they were introduced in 1947 by mathematician John von Neumann in a study that investigated the mechanisms which regulate the self-reproduction of living organisms [159]. CA are parallel calculation models whose evolution is governed by purely local laws. Codd and Langton ([22], [80]) proved that CA has self-reproduction capabilities, but CA probably became most well known due to the famous "Game of life" as developed by Conway [23]. After that, Wolfram ([166], [167], [168]) contributed significantly to the further evolution of CA. The global dynamics of the complex systems simulated with CA 'emerges' from the 'local interactions' of their 'elementary components', even when they are based on a set of simple local rules, CA could generate very complex global patterns that are often not unlike complex processes observed in natural phenomena.

The classical concept of Cellular Automata consists of a d-dimensional space partitioned in cells of uniform size. Each cell starts from an initial state and all cell states are updated synchronously at discrete steps according to a simple local rule [12]. The new state of each cell depends on the previous state of the cell itself, and of the state of its nearest neighbors [77].

Cellular Automata can be used to study both the theoretical and applicative aspects of many phenomena. Theoretical studies regard computability theory (parallel computing), artificial life, complex systems, etc. Applicative studies relate to Modeling and Simulation (M&S) of many various complex phenomena, whose behavior is mainly based on local interactions of their constituent parts (the word 'localism' could be used for specifying such a property): e.g., different aspects of fluid-dynamics, forest fires, traffic, soil bioremediation,

population dynamics, coffee percolation, etc. For processes related to the theory of dynamical systems such as turbulence, chaos theory, fractal dynamics and other complex dynamic systems [156] [14], the studies about CA provide an efficient modeling instrument.

1.2 Research Scope and Objectives

In the last years, the research into simulations of CA in fluid dynamics, as an important field for CA applications, is being pursued in many directions. One of the research directions concerns the modeling and simulation of flow-type landslides, such a research has been carried out by several authors with satisfactory results since 1986 [10]. More recently an extension of the CA paradigm for macroscopic systems and a related modeling methodology were established in order to simulate the fluid-dynamical phenomena [42]. Good simulation results were obtained for some types of 'macroscopic' surface flows; for instance lava flows were simulated on the base of the model SCIARA [31]; pyroclastic flows were simulated according to the model PYR [32]; debris, mud, granular flows were simulated in relation to various versions of the model SCIDDICA [4]; snow avalanches were simulated according to the model VALANCA [6]. Other significant MCA models were developed for flow-type landslides [21] [126].

After the eruptions of Mt. St. Helens (Washington, USA) in 1980 [169] and Nevado del Ruiz (Colombia) in 1985 [113], the international scientific community began to focus its attention on lahars or volcanic debris flows, which constitute one of the most important and devastating phenomena associated with volcanic activity. Computational science may be considered a powerful tool to study, analyze and model such type of phenomenon, thanks to the rapid evolution of computing power, improvements in the methods and creation of new methodologies.

The present research activity is directed at the interdisciplinary problem of Modeling and Simulation of lahars by methods related to the Computational Paradigm of Cellular Automata.

Lahar, as before mentioned, is one of the most destructive natural catastrophic events in terms of number of victims and property damage in the communities located near the flanks of volcanoes. Volcanic eruptions can generate direct (primary lahars) or indirect (secondary lahars) catastrophic surface flows that are a mixture of volcanic debris and water occurring on and around the volcanoes [154]. Like some complex fluid-dynamical phenomena, they are difficult to model through standard approaches, such as partial differential equations. Hence the simulation of lahars could be an important tool for risk management in threatened regions.

The deep motivation for this research is born from the desire to contribute to the mitigation of volcanic risk in my country, Ecuador. This motivation takes shape by exploring possible applications of Cellular Automata modeling and simulation of lahars (real and hypothetical) in terms of very complex dynamical systems, hazard scenarios and eventually impacting of possible protective pro works.

A proper validation of the model is important according to the today requirements of the scientific community. In this context, the objectives of the research are related to the study and implementation of innovative techniques and algorithms in the field of Computational Science for modeling geological processes and fluid dynamics by the computational paradigm based on Cellular Automata, with interactive three-dimensional representation and visualization of scientific data related to simulations. To achieve the overall objective, it is necessary to develop the following partial objectives:

- Analysis of the lahar dynamics in the different disciplinary contexts of the phenomenon (physics and geology), various theoretical approaches, study methodologies and possible integration in modeling ambit.
- Design and development of a framework for real-time rendering of scientific simulations of both primary and rainfall-induced (secondary) lahars by the Computational Paradigm of Cellular Automata.
- Assessment of the results of the proposed model under a methodological approach for large scale modeling of this complex phenomenon.

The research, discussed in this work, forms part of the methodological context described by Di Gregorio and Serra [42], with the objective of deriving valid simulation models for surface flows that take place on a large scale. Particular reference was made to ‘primary’ and ‘secondary’ types of lahars, with the study of Cotopaxi’s last important eruption activity in 1877, such event produced lahars comparable in size to those that buried Armero, Colombia in 1985 by the eruption of the Nevado del Ruiz volcano, or the importance of several rain-generated lahars that have been registered at Tungurahua volcano since 1999.

The model, developed by the candidate (identified below as LLUNPIY model) and presented in this work, is derived from the CA models developed by the interdisciplinary research group of M&S at the University of Calabria, Italy.

1.3 Thesis Outline

The research is structured as follows. The first chapter introduces the research background and motivation, the description of the research problems and the related methodologies.

The second chapter presents a brief historical introduction, along with the principal characteristics of deterministic and homogeneous Cellular Automata, finally providing a classical formal definition. The chapter also depicts a brief description of the most important theoretical results of CA, and some applications that are considered important. This is followed by some definitions and topics related to the classes of complexity, which cannot be neglected in a general overview of CA. Lattice Gas and Lattice Boltzmann models are classes of Cellular Automata developed for modeling and simulating fluid dynamics. These are addressed in the last part of the chapter.

The third chapter discusses the application of Cellular Automata in modeling complex macroscopic phenomena. The chapter also illustrates the semi-empirical method of Di Gregorio and Serra.

The fourth chapter reviews characteristics and fundamentals of lahar generation, as well as approaches that have been adopted for modeling lahar behavior, which are variously informed by theoretical analysis and assessed for their strengths and weaknesses.

The fifth chapter, which illustrates the research carried out by the candidate, is entirely dedicated to describing the new model developed for lahar simulations and the sixth chapter presents several applications to the different lahars that occurred in the Tungurahua volcano, 2005-2008, and the Cotopaxi volcano of 1877. Finally, the research concludes with a general discussion of the work carried out. In addition, unsolved problems and recommendations for future exploration are outlined.

Chapter 2

The Computational Paradigm of Cellular Automata

"In the history of science it is fairly common that new technologies are ultimately what make new areas of basic science develop. And thus, for example, telescope tecnology was what led to moderm astronomy, and microscope technology to modern biology. And now, in much the same way, it is computer technology that has led to the new kind of science..."

Stephen Wolfram

2.1 Introduction

Cellular Automata are spatially and temporally discrete, abstract computational systems that can exhibit chaotic behavior and self-organization and lend themselves to description in rigorous mathematical terms, these have proven useful both as general models of complexity of non-linear dynamics and in a diversity of scientific fields. The computational model for the growth of a snowflake is an example of the CA. It is represented by a uniform array of numerous identical cells, where each cell may assume only a few states and interact with only a few adjacent cells. The elements of the system (the cells and the rule to calculate the subsequent state of a cell) can be very simple, yet nonetheless give rise to a notably complex evolution [67].

In its essential description, CA can be seen as a space, partitioned in cells, each one embedding an identical input/output computing unit. Each cell is characterized by its state. S is the finite set of the states. Input for each cell is local and is given by the states of m neighboring cells, where the neighborhood conditions are given by a pattern invariant in time and space. At time 0, cells are in arbitrary states (initial conditions of the system) and the CA evolves changing simultaneously the state at discrete times, according to local evolution rules, which are functions of the states of the cell itself and its neighbors.

This chapter introduces the notion of the CA, the basis for many models of complex systems in many disciplines, which depict the fundamental aspects of the classical cellular automata modeling paradigm. One of the fundamental ideas underlying the concept of CA is the successful reconstruction of the complex behavior of a system, the fundamental mechanism start from 'simple' rules which describe the interaction of the micro-components into the system itself [168]. Therefore, it could be said that the basic idea of CA is to describe a complex system, not 'from above' using complex equations, as result of the interaction of cells that follow simple rules, thus allowing complexity to emerge from such interactions.

CA were introduced by John von Neumann more than sixty years ago [159], on suggestion from Stanislaw Ulam, for the purpose of studying the formal (and computational) properties of self-reproducing organisms, with the most general notion of self-reproduction in mind, to be combined with the notion of universal calculability. Interest in CA by the scientific community had been intermittent, but today they have been firmly established as a parallel calculation model and a tool to model and to simulate complex systems. This chapter will begin by addressing the origins of CA and will conclude with a formalization of CA.

2.2 A Brief History of Cellular Automata

The history of CA as a computational paradigm started during the Second World War by mathematicians John von Neumann and Stanislaw Ulam while they were contemporaries at Los Alamos National Laboratory. John von Neumann in the late 1940s conceived a self-replication system that would proceed from an iterative, limited state computational machine [158]. In other words, von Neumann was trying to conceive a system capable of producing exact copies of itself. However, following a suggestion of his colleague Stanislaw Ulam, von Neumann focused on a discrete two-dimensional system, instead of just black-or-white cells, von Neumann's automaton used 29 different states and a rather complicated dynamic that was capable of self-reproduction. John von Neumann died prematurely in 1957, and did not have time to complete his "Theory of Self-Reproducing Automata", edited and published posthumously in 1966 by A.W. Burks [159].

John von Neumann's principal goal was to devise a simple system capable of reproducing like a living organism; that is, to find formulas for models that simulate the complexity of the biological phenomena. As he was interested in the logical principles that govern the capacity of a self-reproducing system rather than the physical and chemical details of such processes, von Neumann concentrated on the modes of interaction between elementary entities, Finite Automata (which he called Elementary Automata, *ea* for future reference), precisely due to the extreme simplicity of their individual behavior [159].

John von Neumann's guiding idea (to give an intuitive idea of the definition of CA) was to consider a plane tessellated with square cells of the same size, each one incorporating an *ea* of the same type, whose input is given by the states of adjacent cells. At step 0 of the CA, the state of the *ea* is initialized; in subsequent steps, the cells synchronously change their state by applying the transition function of the *ea*. A complex global behavior would have to emerge in the evolution of the cellular space.

Parallelism and 'localism' are thus the distinctive properties of CA, whose evolution is prompted by the interaction of each *ea* with the *ea* of adjacent cells.

von Neumann's CA was also the first discrete parallel computational model in history formally shown to be a universal computer, i.e., capable of emulating a universal Turing machine and computing all recursive functions [22] [150].

In 1970, the mathematician John Conway introduced his famous "Game of Life" [58], a two-dimensional square lattice with simple update rules but complex dynamics, arguably the most popular automaton ever seen and one of the simplest computational models ever proved to be a universal computer [160]. The next wave of CA research was the application of CA to physics, Tommaso Toffoli [152] used cellular automata to directly model physical laws, and in the process laid the foundations for the study of reversible CA.

In the 80s Stephen Wolfram produced a systematic study of one-dimensional, 2–state automata showing that deterministic rules in such a limited system could yield not only complex dynamics, but also truly chaotic dynamics as well as nearly perfect random dynamics [167]. Cellular Automata can be designed to resemble and model many different physical systems [76] [168] [18] [40]. CA have been especially successful in the modeling of fluids.

Cellular Automata used for modeling fluids are known as lattice gas automata [166]. One of the first successful lattice gas automata was the HPP lattice gas [66]. Its name HPP model is derived from the initials of three authors (Hardy, Pomeau and Pazzis). An interesting example is the FHP fluid model proposed by Frisch, Hasslacher and Pomeau in 1986, which can be viewed as a fully discrete molecular dynamics and yet behaves as predicted by Navier-Stokes equation when the observation time and length scales are much larger than the lattice and automaton time step [55].

Currently this computational paradigm is applied in many scientific fields, thanks to a group of researchers. Prof. Salvatore Di Gregorio, who was ACRI Conference's founder together with Eng. Domenico Spezzano, named ACRI 1994 (in Italian means: Automi Cellulari per la Ricerca e l'Industria, i.e., Cellular Automata for Research and Industry) began it in Rende-Italy. ACRI is focused on challenging problems and new researches not only in theoretical but also in applicative aspects of Cellular Automata, including cellular automata tools and computational issues. These forums are for both scientists and innovation managers in academia and industry, permitting them to express and discuss their viewpoints on current and future trends from a variety of scientific fields. Applications and solutions of problems from the fields of physics, engineering, environment science, social science and life sciences are presented in these biennial meetings.

2.3 Cellular Automata Description: Basic Definitions

In order to understand how some scientific groups, enrolled in this new computational paradigm, have proceeded and are proceeding to incorporate CA into their investigations, it is necessary to describe the CA approach, deduced by generalizing from the initial work of von Neumann such as a large class of discrete models with homogeneous interactions; there are several fundamental properties common among all the models. They have the following characteristics:

- They are formed from a d-dimensional space divided into regular cells (triangles, squares, hexagons, cubes, etc.) or, equivalently, by a regular d-dimensional grid.
- Each cell has a state. The number of possible states must be finite
- Evolution occurs in discrete steps
- Each cell changes its state simultaneously with all the others, in accordance with the same transition rule.
- The transition rule depends on the state of the cell itself and the state of its neighboring cells.
- The neighborhood relationship is local, uniform, and invariant over time

2.3.1 Dimension and Geometry of Cellular Automata

The definition of CA require the discretization of space into cells. For one-dimensional Cellular Automata, the only possibility is a sequence of cells aligned one beside the other,

or a one-dimensional grid. In this regard, some surprising discoveries have been made with a simple row of cells. There are other alternatives for Cellular Automata of greater size: triangular, square, or hexagonal grids can be adopted for two-dimensional CA, while cubic cells are usually used for three-dimensional Cellular Automata.

For a model that simulates the growth of a snowflake, for example, a two-dimensional hexagonal matrix would be adequate: in most contexts, a rectangular grid, made up of identical squares, would be selected. Fig. 2.1 illustrates some examples of cellular spaces of one, two, and three dimensions.

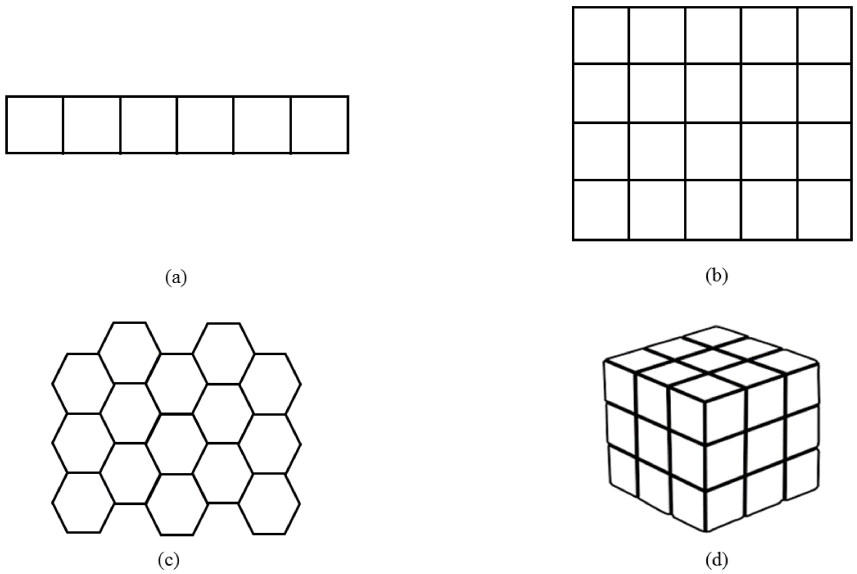

Fig. 2.1 Examples of cellular spaces that are (a) one-dimensional, (b) two-dimensional with square cells, (c) two-dimensional with hexagonal cells, and (d) three-dimensional with cubic cells.

With regard to two-dimensional CA, although square tessellation can easily be represented through a matrix, and does not present problems in graphic representation (for example, each element of the matrix can be viewed using one pixel of the screen matrix), in some applications they may present problems which arise from anisotropy. When this occurs, it is preferable to adopt a hexagonal tessellation, which assures the lowest anisotropy for two-dimensional CA and minimizes the problem of spurious symmetries [166]. It improves simulations and, in some cases, is indispensable for correctly modeling some phenomena [161]. Unfortunately, there is no three-dimensional equivalent of the hexagonal cellular space.

2.3.2 Number of Cell States

The number of cell states must be finite, and is determined in relation to the particular context of study or application. In the first theoretical studies after von Neumann, who saw CA as abstract computational models [22][150], the number of cell states was usually rather small. With only two states, for example, it is possible to represent, in the initial configuration the information that the CA must process, the specification of the state (0 or 1) of all the cells in the cellular space at the time $t = 0$. Even when the cellular automaton is used to describe systems of particles and model their interactions, the number of states is rather contained [147] [161]. Conversely, studying systems that may be found in a continuum of possible states can require a rather large number of cell states, provided that the model is significant [42].

2.3.3 Neighborhood Relationship

The cell's neighborhood relationship, which will be related to the name of the central cell, depends on the geometry of the cells. According to the definition given, it must have the following properties:

- It must be local, that is, it must involve only a limited number of cells in proximity to the central cell.
- It must be uniform, e.g., the same for every cell in the cellular space
- It must be invariant over time

One-dimensional CA are usually related to their neighbor in terms of range r, which defines a neighborhood composed of $n = 2r + 1$ cells [165]. For example, a range of $r = 1$ identifies a neighborhood of $n = 2r + 1 = 3$ cells: the central cell, the adjacent cell to the left and the adjacent cell to the right. Fig. 2.2 illustrates two examples of neighborhoods with a range of $r = 1$ and $r = 2$ for a one-dimensional CA.

In the case of 2-dimensional CA with square tessellation, there are several neighborhoods schemes, for example: von Neumann, Moore and Margous neighborhoods. Fig. 2.3 shows the most frequently used neighborhoods, which is named after von Neumann, who used it in his studies of self-reproducing machines.

A diamond-shaped neighborhood can be used to define a set of cells surrounding a central cell (x_0, y_0) that may affect the evolution of a 2-dimension cellular automaton on a square grid. The von Neumann neighborhood of range r is defined by

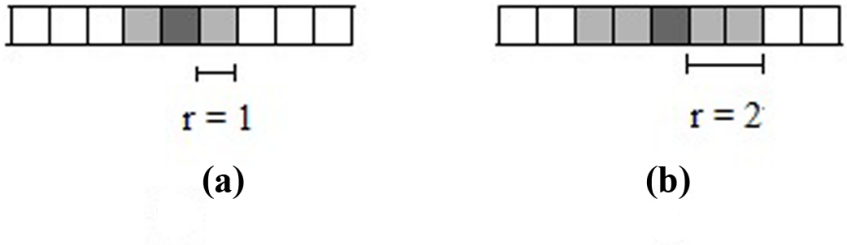

Fig. 2.2 Example of neighborhood with a range of (a)$r = 1$ and (b)$r = 2$ for a 1-dimensional cellular automata. The dark gray cells are the central cell, the light gray cells are the neighbors

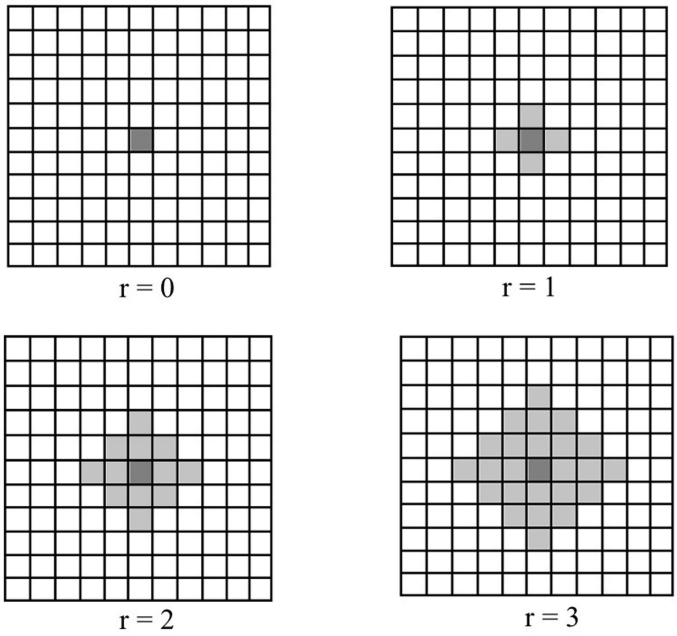

Fig. 2.3 von Neumann's neighborhoods for a two-dimensional cellular automaton with square tessellation. The dark gray cells are the central cells, the light gray cells are the neighbors.

$$N^{v}_{(x_0,y_0)} = \{(x,y)/\,|x-x_0|+|y-y_0| \leq r\} \tag{2.1}$$

John von Neumann neighborhoods for ranges $r = 0,1,2$, and 3 are illustrated above. The number of cells in this neighborhood of range r is the centered square number $n = 2r(r+1)+1$, the first few of which are 1, 5, 13, 41, etc. [62] [138].

When the range of neighborhood $r = 1$, especially for the square meshes in d-dimension, a cell has the number of neighbors with 2^d.

In the case of a square-shaped neighborhood, the Moore neighborhood of range r is defined by

$$N^{M}_{(x_0,y_0)} = \{(x,y)/\,|x-x_0| \leq r, |y-y_0| \leq r\} \tag{2.2}$$

Moore neighborhoods for ranges $r = 0,1,2$, and 3 are illustrated in the Fig. 2.4. The number of cells in the Moore neighborhood of range r is the odd squares $n = (2r+1)^2$, the first few of which are 1, 9, 25, 49, 81, etc. Therefore, for d-dimensional square meshes with $r = 1$, the number of neighbors for the cell could be calculated as $(3^d - 1)$ [62][138].

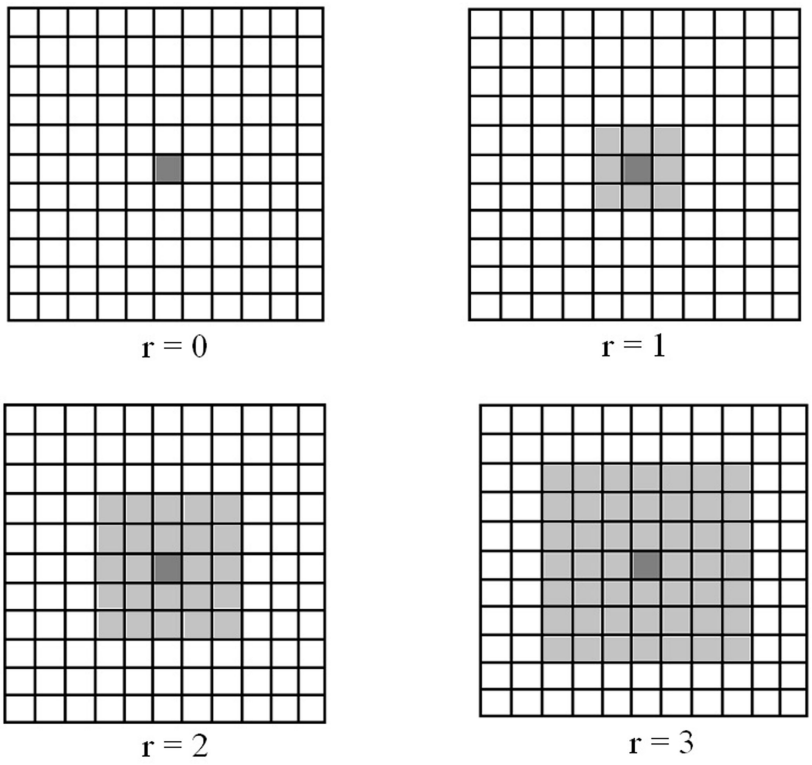

Fig. 2.4 Moore's neighborhoods for a two-dimensional cellular automaton with square tessellation. The dark gray cells are the central cells, the light gray cells are the neighbors.

Fig. 2.5 shows a typical neighborhood for two-dimensional hexagonal CA composed of cells in the North-West, North-East, East, South-East, South-West and West.

Naturally, it is possible to define neighbor relationships other than these illustrated. In simulating the diffusion of gas into an environment, for example, it is possible to use Margolus's neighborhood relationship [98].

2.3.4 Discrete Time and Space

Another fundamental property of CA is the discretization in space and time. CA have a status that is fundamentally different from other physical models. The most common stratagem to

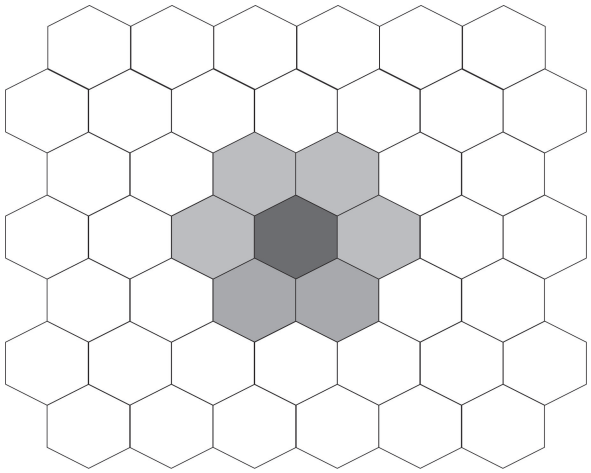

Fig. 2.5 Hexagonal neighborhood for two-dimensional CA with hexagonal tessellation. The dark gray cells are the central cell, the light gray cells are the neighbors.

construct a mathematical model of the natural world had long been the differential equation, which can describe the change of a certain magnitude as a function of position and time. For example, Maxwell's equations provide the variation of the value of an electromagnetic field from point to point and from instant to instant. All the magnitudes in these equations vary continuously and are based on the use of real numbers. To vary continuously means that given any real number, it is always possible to find another that differs from the first by an arbitrarily small quantity. This means that, in general, real numbers can possess a virtually infinite number of decimal places. To know them exactly requires an infinite quantity of information, which means that for all practical purposes, real numbers are subject to errors of approximation.

This concept becomes crucial when we talk about chaos, where chaos essentially means the unpredictability of a system [81], i.e., the inability to precisely predict behavior over time. Indeed, since in chaotic systems a small uncertainty regarding the initial data can 'explode' the system over time, it becomes desirable to introduce mathematical tools that use finite numbers (i.e., less than a certain maximum value).

The CA lend themselves well to this purpose; they are part of a family of new mathematical models adapted to the study of complex systems. This family of new methods tends to address complex and discontinuous systems in the same way that Newton's infinitesimal calculus addressed the physics of smooth and continuous processes. A Cellular Automaton is a totally discrete system [147]. The space is therefore not a continuum but a matrix of cells; even time is fragmented into discrete steps, and while the intensity of a field can change on a continuous domain, the cells of a CA can have only a finite number of states. Of course, real space, time, and many physical variables are believed to be continuous rather than discrete.

CA makes explicit this 'discretization' on a computer. Moreover, their evolution over time can be precisely calculated without the need of approximations [67]. Therefore, to say that space is discrete means that the components of the CA, or the *ea* located in each small cell, at all times occupies a small square (if the matrix is square) of a grid pattern. Moreover, discretization time requires that the components (*ea*) move from one state to another at constant intervals (see Fig. 2.6). Thus, temporal coordination is provided by a nonnegative integer t, and it will not concern with what happens in the intermediate time between t and $t+1$; this will be constituted by instants of the type $t = 0, 1, 2...$

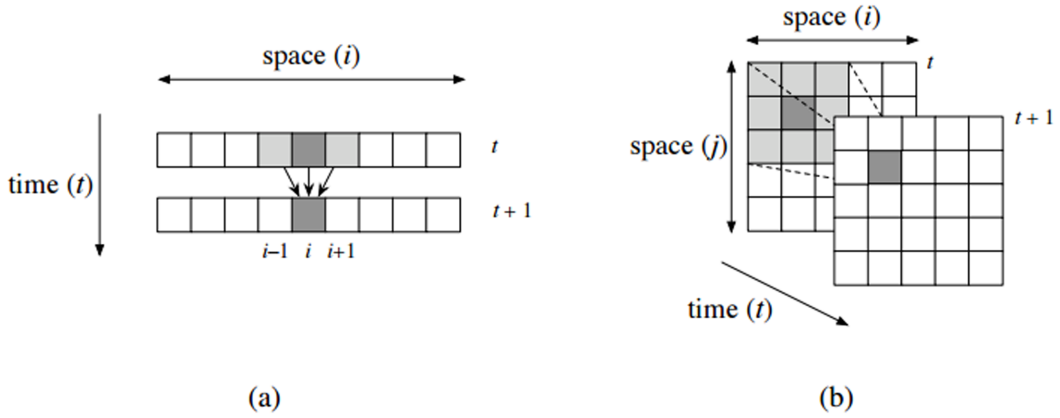

Fig. 2.6 Illustration of (a) 1-dimensional CA and (b) 2-dimensional CA. The light gray cells are the neighboring cells of the dark gray cell.

2.3.5 Cell State Transition Function

The fifth and final property of CA is the transition rule (or transition function). The principal source of variety in the CA universe is the enormous number of possible rules to establish the future state of a cell based on the current configuration of its neighborhood. If k is the number of states per cell and n is the number of cells included in the neighborhood, there will be $p = k^n$ possible configurations and k^p possible rules. For example, for a CA with two states per cell (binary CA) in a von Neumann neighborhood (where n is 4), there are more than 65,000 possible rules, while in a Moore neighborhood (where n is 8) there are 10^{77}. Only an insignificant fraction of such rules have been examined.

Wolfram, for example, started with the study of binary rules with a range of 1, where the neighborhood of each cell is given by the cell itself and the cells to its left and its right ($n = 3$); the states are 0 and 1 ($k = 2$). From the above, the states therefore have $2^3 = 8$ possible configurations (0,0,0),(0,0,1)...(1,1,1) and $2^8 = 256$ possible rules exist. Each rule

must assign a 0 or a 1 to each configuration, and may be viewed as an 8-bit string. For example, the rule given in the following table assigns the state 0 to the configuration (0,0,0), the state 1 to (0,0,1), and so on (Table 2.1).

Table 2.1 Rule 90.

current pattern	000	001	010	011	100	101	110	111
the new state for center cell	0	1	0	1	1	0	1	0

This rule can be identified with the number 01011010, corresponding to the decimal number 90, and is therefore called rule 90. Let's suppose that it is wanted the box be black if its state is 1, otherwise to leave it white. At a certain moment, the automaton will appear as a string of black or white boxes. In Fig. 2.7, stacking the strings atop each other gives a visual representation of the evolution.

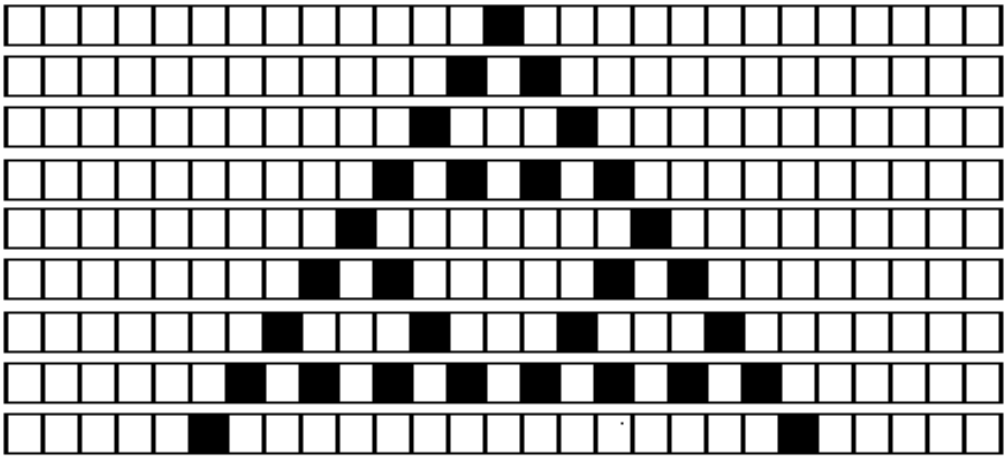

Fig. 2.7 Evolution of Wolfram's rule 90.

The classification of these rules (which Wolfram divides into 4 classes) is a topic that is still open for research and will be better addressed in the section 2.5.2. Considering what has been said, it can deduce that the new state of a cell depends only on the number of adjacent cells in a given state and by the rule adopted, not by their position. Therefore, the rule adopted is the local transition function.

At every step of the CA, the transition function is applied simultaneously to all the cells in the cellular space, determining the new state of each one according to the state of the cells in the neighborhood. In this way, the CA's computation assumes characteristics of parallelism and decentralization. When the number of states is small, it is customary to define the transition function through a table (called a lookup table, e.g., Table 2.1), which

specifies the new state of the central cell for each possible neighborhood configuration [168]. Conversely, when the number of CA states is too large, the transition function is usually defined through the explication of an algorithm [42].

2.4 Formal Definition of the Cellular Automata

At this point a formal definition of CA must be provided, which was created, through immediate generalization of von Neumann's CA, by those who sought to investigate the properties of the new paradigm immediately after the posthumous publication of his work. It is possible to find many definitions of CA in the literature, each of which has its own applications and strengths. The formal definition given in this paragraph is the uniform definition of CA, with a transition function of finite automaton, which can be easily replaced by one that is probabilistic or a mix of deterministic and probabilistic. Moreover, it is not limiting, since most of the other definitions can be traced back to it. As stated before, each cell of the CA incorporates an identical Finite Automaton. In the specific case of deterministic uniform CA, it is dealing with a finite automaton that is also uniform and deterministic. It is appropriate, therefore, to first provide the definition for this.

2.4.1 The Finite Automaton

The *finite state automaton*, or more concisely, *finite automaton* (*fa*), is probably the simplest calculation model in Computing Science. Intuitively, a *fa* is a system that can be found in a finite number of different states and, as a consequence of some input, can effect a transition from one state to another. As with CA, it is possible to find numerous definitions of the *fa* in the literature. The *fa* presented below is the definition of the *fa* as a recognizer (acceptor) of languages [60]. The model of the *fa* used in CA, presented in the next paragraph, is a further simplified model called the elementary automaton.

Definition 2.1 (Formal Definition of Deterministic Finite Automaton) *A deterministic finite automaton (fa) [60], as recognizer of languages, is formally defined as a quintuple*

$$fa = \langle I, S, \sigma, q_0, O \rangle \tag{2.3}$$

where:

- I is the finite set of input symbols (input)
- S is the finite set of states of the *fa*

- $\sigma : I \times S \longrightarrow S$ is the transition function that modifies the states through input
- $q_0 \in S$ is the initial state of the *fa*
- $O \subseteq S$ is the set of final states of the *fa*

Definition 2.2 (Language) *Let I^* be the set of all the possible strings that may be constructed on the input symbol set I. The language L accepted by the fa is defined as follows:*

$$L = \{x \in I^* : \sigma(q_0;\, x) \in O\} \tag{2.4}$$

where $\sigma(q_0;\, x)$ indicates the state in which the *fa* is found at the end of the computation. Therefore, a string $x \in I^*$ is accepted by the *fa* if it, after having read the entire string, finds it to be in a final state.

Fig. 2.8 illustrates a *fa* that recognizes binary strings of any length in which at least three consecutive 0 symbols appear. In this case $I = \{0,1\}$, $S = \{q_i, q_1, q_2, q_f\}$, $q_0 = q_i$ and $O = \{q_f\}$. At step $t = 0$, the *fa* is in initial state q_i and the first symbol of the string is read. The transition function is applied as many times as there are symbols in the input string and determines the new state of the *fa* based on the current state and the input. Having exhausted the input, the string is recognized if and only if the *fa* is found to be in the final state q_f. The string $x_1 = 100110$ is not recognized by the *fa*. In fact, the sequence of transitions of states $\sigma(q_i;\, x_1)$ does not terminate in the final state q_f:

$$q_i \xrightarrow{\sigma(1,q_i)} q_i \xrightarrow{\sigma(0,q_i)} q_1 \xrightarrow{\sigma(0,q_1)} q_2 \xrightarrow{\sigma(1,q_2)} q_i \xrightarrow{\sigma(1,q_i)} q_i \xrightarrow{\sigma(0,q_i)} q_1$$

But the string $x_2 = 100011$ is recognized by the *fa*, since the sequence of transitions of state $\sigma(q_i;\, x_2)$ terminates in the final state q_f:

$$q_i \xrightarrow{\sigma(1,q_i)} q_i \xrightarrow{\sigma(0,q_i)} q_1 \xrightarrow{\sigma(0,q_1)} q_2 \xrightarrow{\sigma(0,q_2)} q_f \xrightarrow{\sigma(1,q_f)} q_f \xrightarrow{\sigma(0,q_f)} q_f$$

The CA cells incorporate a type of *fa*, called elementary (*ea*), which is a further simplification of the simple model just described. It is not relevant whether the *ea* terminates its calculation in a final state or in some other state, because its initial state is not specified. What matters is the change of state in itself and the distinction between the set of states S and that the set of final states $O \subseteq S$ is not present. The finite set of input symbols is implicitly defined by the number of states of the *ea* and the number of cells in the neighborhood.

Definition 2.3 (Formal Definition of Elementary Automaton) *The elementary automaton (ea) is formally defined as a triple:*

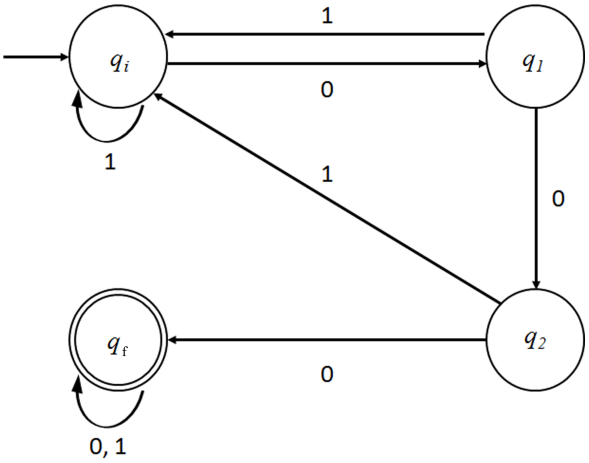

Fig. 2.8 The finite automaton that recognizes the binary strings in which at least three consecutive 0 symbols appear. The nodes indicate the states of the *fa*, the transition arcs. At the start of the computation, the *fa* is in initial state q_i; if the input symbol 0 is read, a transition is made toward the state q_1; conversely, if the symbol 1 is read, the *fa* remains in initial state q_i. The *fa* recognizes the input string if it is found in the final state q_f at the end of the computation.

$$ea = \langle S, I, \sigma \rangle \tag{2.5}$$

where:

- S is the finite set of states of the *ea*
- $I \equiv S^n$ is the finite set of input symbols, with n being the number of cells in the neighborhood.
- $\sigma : I \longrightarrow S$ is the transition function that modifies the states through input

2.4.2 Deterministic Homogeneous Cellular Automata

Definition 2.4 (Classical Formal Definition) *Cellular Automaton [72] is formally defined as a quadruple*

$$A = \langle Z^d, X, S, \sigma \rangle \tag{2.6}$$

where:

- $Z^d = \{i \equiv \langle i_1, i_2, .., i_k, ..i_d \rangle / i_k \in Z\}$ is the set of cells identified by integer coordinate points in a d-dimensional Euclidean space, Z is the set of the integers.

- $X = \langle \xi_0, \xi_1, .., \xi_{m-1} \rangle$ is the relationship (or index) of neighborhood[1], a ordered finite set of d-dimensional vectors that defines the set $V(X,i)$ of neighbors of the cell i (also called the central cell) $i = \langle i_1, i_2, ..., i_d \rangle$ as follows: if $m = \#X$, then $V(X,\ i) = \langle i + \xi_0, i + \xi_1, ..., i + \xi_{m-1} \rangle$.

- S is the finite set of the states of the elementary automaton

- $\sigma : S^m \longrightarrow S$ is the deterministic transition function of the elementary automaton; this can also be probabilistic, non-deterministic, or mixed: deterministic/probabilistic.

Example 2.1 *To consider a 2-dimensional CA with von Neumann neighborhood (Fig. 2.3 with $r = 1$) and the cell i of coordinates for example $(5,5)$. The neighborhood relation that defines the von Neumann neighborhood is:*

$$X = \langle \xi_0, \xi_1, \xi_2, \xi_3, \xi_4 \rangle = \{(0,0); (0,-1); (1,0); (0,1); (-1,0)\}$$

Therefore, the set of coordinates of the neighboring cells to the cell $(5,5)$ are defined from the set:

$$\begin{aligned} V(X,\ i) &= \{i + \xi_0, i + \xi_1, i + \xi_2, i + \xi_3, i + \xi_4\} \\ &= \{(5,5) + (0,0); (5,5) + (0,-1); (5,5) + (1,0); (5,5) + (0,1); (5,5) + (-1,0)\} \\ &= \{(5,5); (5,4); (6,5); (5,6); (4,5)\} \end{aligned}$$

Let $C = \{c / c : Z^d \longrightarrow S\}$ be the set of possible assignments of state to A and be called the set of configurations of the CA; $c(i)$ is the state of the cell i, then the evolution of the CA that is moving in a step from one configuration to another, is specified by the global transition function τ: let $c(V(X,i))$ be the ordered set of states of the neighborhood of i, then

$$\tau : C \longrightarrow C \longmapsto [\tau(c)(i) = \sigma(c(V(X,i)))]$$

Definition 2.5 *Is defined quiescent state a state $q_0 \in S$ such that*

$$\sigma(q_0, q_0, ..., q_0) = q_0$$

[1]For the following, ξ_0 is posited as the null vector, and therefore every cell is part of its own neighborhood. This cell is refereed as the 'central cell'. However, a CA in which the cell is not part of its own neighborhood is certainly conceivable.

The formal definition 2.4 can easily be extended to different types of space (e.g. Riemannian spaces, etc.), different topologies (e.g., the torus in two-dimensional CA), or different tessellations (e.g. hexagonal or triangular in two-dimensional CA). In actual cases, only finite regions of the cellular space are considered.

2.4.3 'Parallelism' and 'Localism'

It is important to highlight here the two notable characteristics that arise from the definition of the CA: '*parallelism*' and '*localism*'. Here, the word 'localism'(Oxford Dictionary: " Preference for one's own area or region, especially when this results in a limitation of outlook ") assumes the accentuated meaning of 'dependent on local conditions'. These two properties assume a particular meaning in context: it is specified the property of a complex system that evolves exclusively on the base of the 'local' interactions of its components. Hence, parallel and local behaviors of CA, in fact are amalgamated to coincide.

Parallelism and localism can be seen in the very structure of CA, ideally composed by infinite locally interacting calculation units, well known as finite automata (probably the simplest designed calculation models) within the CA, where the cell's state is identified by its output.

The French epistemologist Jean Petitot in 1977 discussed from a philosophical view point the opposite notions of "centrato/acentrato", under the entry of Italian Enciclopedia Einaudi [109]. The word "centrato" is centered, while the word "acentrato" is an objective neologism that means, not centralized.

Professor Di Gregorio used the English word "acentric" that is a word in the Biology Scientific language as an extension of meaning and used the word "acentrism" (its neologism in English) in order to specify the property to be "acentric".

The word 'local' instead of "acentric" and the word 'localism' for "acentrism" are used in this thesis with a meaning related with the property of a complex system that evolves depending only of the local conditions and interactions of its constituent parts.

CA, as have been defined, become part of the problem of localism. The focal problem of 'localism'is to identify in what extent a system (whose components act only according to local information) is capable of pursuing global ends. In this sense, a CA is a special case of a non-centered system, which can be thought of as an enormous and stylized universe in which the space is represented by a uniform grid containing a certain number of cells.

In a certain way, the idea of the non-centered system competes, epistemologically, with a hierarchical/centered system. From a definitional point of view, CA are an extremely pure example of a non-centered system, and certainly the name 'cellular' was chosen for its assonance with the word 'cell', intending to establish an analogy with those biological

processes where a group of cells cooperate to reach a certain goal in the absence of a hierarchical order.

2.5 Theoretical Studies of Cellular Automata

This section describes some studies on Cellular Automata concerning its theoretical aspects. As most of them relate to the one-dimensional CA, it is useful for better understanding of the topics covered, to make a few definitions and conventions that have become customary.

2.5.1 One-Dimensional Cellular Automata

The simplest class of one-dimensional Cellular Automata with a neighborhood radius of $r = 1$ are elementary CA, at least from the point of view of their construction [165] [168]. There are one-dimensional CA of N cells with a binary states space ($k = 2$), labeled 0 and 1, and periodic boundary conditions (the one-dimensional cellular space is seen as a ring in which the first and last cells are adjacent). Fig. 2.9 illustrates an example of CA with periodic boundary conditions.

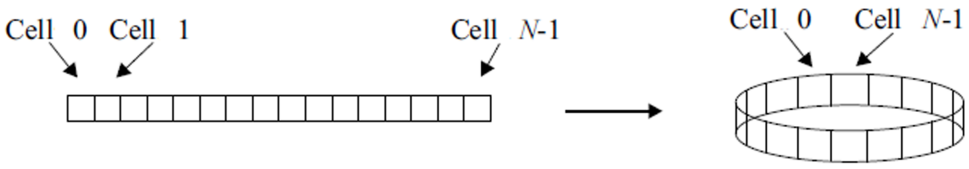

Fig. 2.9 Example of one-dimensional cellular automata with periodic boundary conditions. The first and last cells of the cellular space are neighbors in the ring representation.

The choice to adopt a cellular space made this way arises, in general, from the impossibility of managing infinite cellular spaces. A ring solution, though finite, defines an unlimited space in which the CA can evolve. The transition rule of the cell is expressed in the form of a table (look-up table). These rules were partially discussed in subsection 2.3.5. For example, if ψ indicates for a generic neighborhood configuration (recalling that the number of configurations in the neighborhood is given by $k^{2r+1} = k^n$, therefore in cases where $r = 1$ in an elementary CA, there are $2^3 = 8$ configurations), the following transition rule determines the new state, $s = \sigma(\psi)$, of the central cell (Table 2.2).

Note that in the table 2.2, the eight possible neighborhood configurations are listed in increasing order according to the binary values that they represent. Indeed, the binary number 000 corresponds to the decimal number 0, the binary number 001 corresponds to the decimal

Table 2.2 ψ a generic neighborhood configuration.

current pattern (ψ)	000	001	010	011	100	101	110	111
the new state for center cell (σ)	0	0	1	1	0	1	1	0

number 1, and so on. Finally, the binary number 111 corresponds to the decimal number 7. Adopting this convention, any transition rule for elementary CA can be defined by simply listing the new states of the central cell. Therefore, the previous rule can be defined as follows:

Table 2.3 Listing the new states of the central cell.

$\sigma_{00110110} \equiv$	000	001	010	011	100	101	110	111
	0	0	1	1	0	1	1	0

In this case as well, the transition rule σ defines a binary number. Therefore, it is referred usually to the translation rule of elementary CA through the decimal number corresponding to the binary number defined by the rule. For instance:

$$\sigma_{00000000} \equiv \sigma_0$$
$$\ldots$$
$$\sigma_{00110110} \equiv \sigma_{54}$$
$$\ldots$$
$$\sigma_{11111111} \equiv \sigma_{255}$$

Fig. 2.10 illustrates two examples of elementary CA. The initial configuration (first line of the two graphics) is generated randomly so that each cell can assume state 0 (white) or 1 (black) with equal probability. The temporal evolution is displayed from high to low as a sequence of lines.

When $r > 1$, the number of neighborhood configurations grows rapidly. For example, for $k = 2$ and $r = 2$, then $k^{2r+1} = k^n = 2^5 = 32$; as a consequence, the total number of transition rules becomes $2^{32} = 4294967296$, making an exhaustive analysis impossible. The same case applies if CA are considered with $k = 3$ and $r = 1$: in this case, the number of possible transition rules is 3^{27}.

In these cases, it is customary to restrict the field of investigation to particular subclasses, such as legal totalistic CA [165]. A CA is considered legal if it preserves the quiescent state

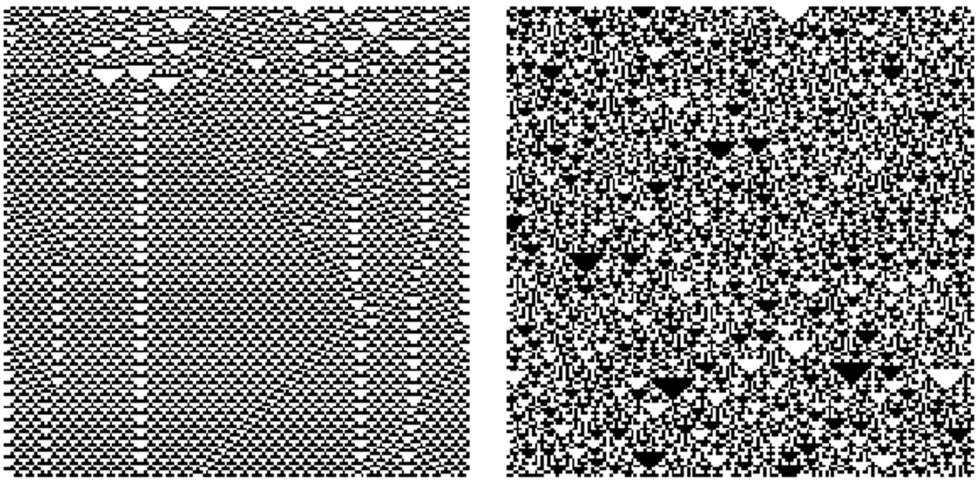

Fig. 2.10 The first 100 calculation steps of elementary CA (a) σ_{54} and (b) σ_{150}.

(usually the null state), that is, if the state of the central cell of a neighborhood in which all the cells are in the quiescent state at step t remains in the quiescent state at step $t+1$. Totalistic CA are those characterized by the fact that the new state of the cell depends exclusively on the sum of the values of the states of the cells of the neighborhood of the preceding step. In this way, for example, the legal totalistic rules for CA with k states and $r = 1$ pass from k^{k^3} to $k^{[k^2(1+k)-1]/2}$. Therefore, considering $k = 2$, it is necessary to move from 256 to 32 legal rules, while for $k = 3$, to move from 3^{27} to 3^{17} legal totalistic rules. However, the number of legal totalistic rules also grows very rapidly with k and r and therefore, the study of the properties of CA has been concentrated mostly on CA with few states and neighborhoods of few cells.

As with elementary CA, totalistic CA can also be specified through a number c called the '*rule code*'. The code c is defined so that the coefficient of 2^i in its binary representation is the expected value for the state of the central cell when the sum of the states of the cells of the neighborhood is equal to i.

2.5.2 Wolfram's Classification

Wolfram, in *A New Kind of Science* and others works dating from the mid-1980s [165][168], proposed a classification scheme which divided cellular automata rules into four categories based on their dynamic behavior. Such a classification is related to 1-dimensional CA with

infinite length, but it is possible to confine the cellular automaton in a finite region of cellular space for practical use. In order of complexity the classes are:

- Class *I*. CA evolving to a homogeneous state: CA evolve to a uniform configuration from any initial state with the same *ea* state (or to a fixed cycle) after a finite number of steps independently from the initial configuration, which do not change with time. This state can be thought of in dynamical systems terms as a "point attractor".

- Class *II*. CA evolving periodically: A series of cells tends to a fixed structure (stable patterns) or periodic structures (periodical patterns) after running for a certain period of time. CA evolve so that the state value of cells is determined in the time by initial state values of cells in a limited and connected region. This is sufficient to forecast the final states for a certain region of cells. The evolution of CA of complexity class *II* with periodic configurations can be thought of as analogous to 'limit cycles'in dynamical systems.

- Class *III*. CA evolving to a chaotic type: CA evolve so that the state value of a cell is determined in the time by initial state values of cells in a gradually more extended connected region. In this case, after a sufficient runtime, the typical CA evolution will exhibit to a non-periodic or chaotic behavior, comparable to fractal dimension features. Evolution can have typical behavior of turbulent phenomena with strange attractors, as is the case for chaotic dynamical systems.

- Class *IV*. Includes all previous cases, known as a class of *complex rules*: CA are the most interesting because of the emergence of high complexity structures in time and space. Periodic or stable structures persist for a large number of steps. This type of CA exhibit complex propagating structures that can appear during the evolution. The value of a cell state cannot be determined by a computation procedure, that is simpler than the computation by the application of the transition function. The CA behavior of class *IV* is dominated by transition phenomena from highly chaotic behavior to dynamics that is typical of strange attractors. (e.g., the game of "life" is a CA of complexity class *IV*).

Examples of CA belonging to the four classes of complexity by Wolfram are illustrated in Fig. 2.11.

Among the classes of complexity, the fourth class has been particularly interesting from the perspective of research on CA, because this class can be considered to have the virtue of 'emergent computation', which can be used as a generalized computer (Universal Computer) to simulate arbitrarily calculation processes.

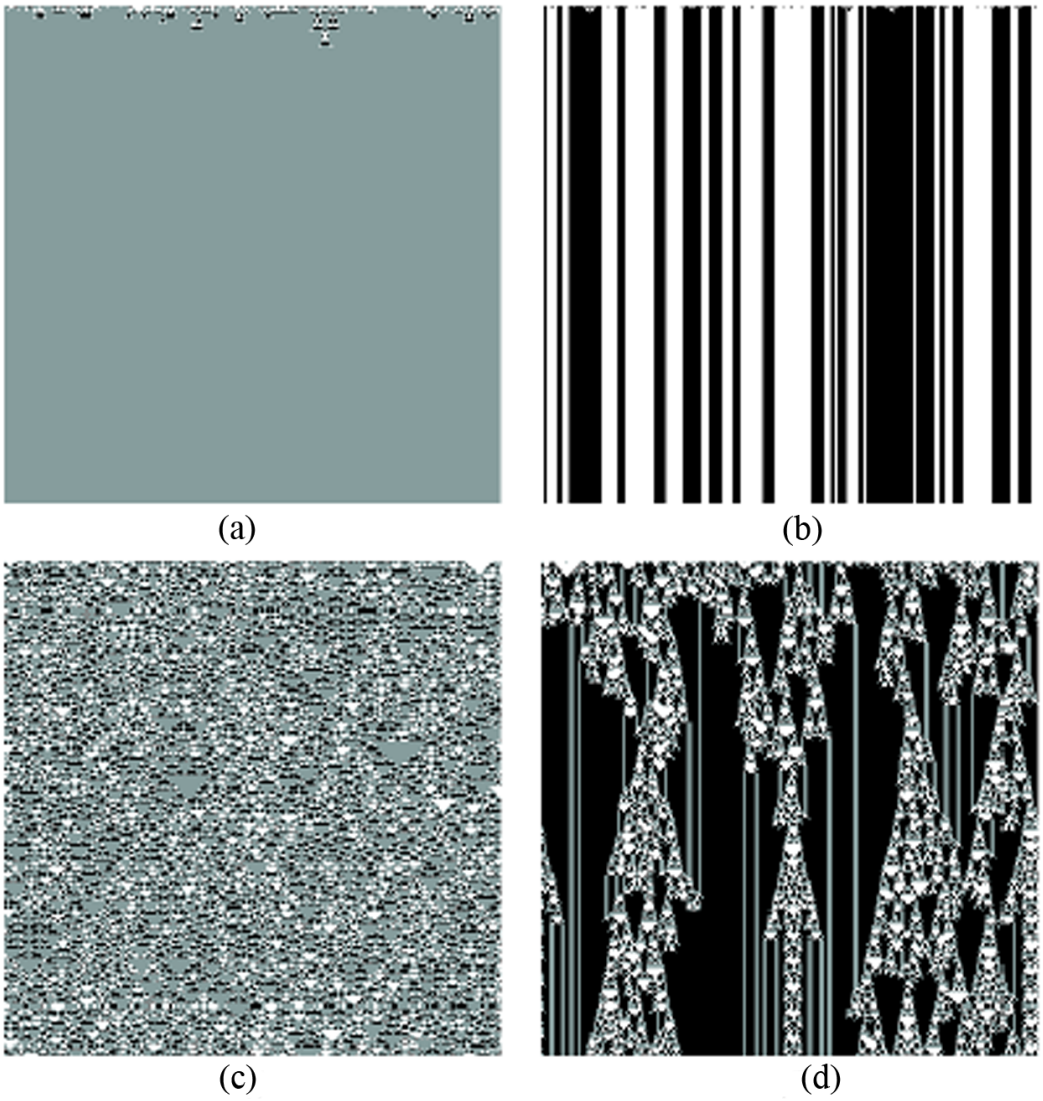

Fig. 2.11 The CA classification according to Wolfram, the initial configuration is composed of a ring of 250 cells and is generated randomly: each cell may assume the state 0 (white color), 1 (grey color) o 2 (black color) with equal probability. The time evolution is visualized from top to down as row sequences.

The distinctions between the classes of CA can be clarified by taking into consideration a simple experiment. Suppose it is assigned to a Cellular Automaton a randomly chosen initial configuration and make it evolve through many steps over time, and then record the final state. Then it is necessary returning to the starting configuration, changing the value of a single cell and making the system evolve for the same number of steps. What effect will the small change have on the final state? For a class *I* automaton, there is no consequence. In fact, a class *I* system reaches the same final state regardless of the initial state. A class *II*

automaton may show some effect, but limited to a small area near the site where the change occurred. In a class *III* system, on the other hand, the alteration of a single cell can provoke a change that propagates all along the lattice. The rules of class *IV* are the rarest and most interesting. Some rather simple transition functions fall under this class. Sensitivity to small variations in the initial conditions is even greater than in the third class. It is believed that, to predict the future state of a cellular automaton of the fourth class, there is no general procedure more effective than the one that consists of leaving the task of calculating the state to the evolution of the automaton itself. A hypothesis connected to the previous consideration suggests, therefore, that CA class *IV* can be considered as universal calculators.

Cellular Automata capable of carrying out universal computation can imitate the behavior of any calculator. Supposing that any physical process can be represented by a computational process (as it seems plausible to hypothesize), cellular automata can also imitate the behavior of any physical system.

2.5.3 The Edge of Chaos

Wolfram's hypothesis, which says that simple one-dimensional CA are capable of universal computation, was successfully taken up by Chris Langton, founder of the Artificial Life Institute at the Santa Fe Institute (California, USA).

It is not easy to explore these possibilities of life. In the case of *Life*, there is a 2-state rule with a neighborhood of 9 cells (including the central cell, which influences the next state). In fact, there are often 2^{512} rules of this type. In a 1990 work entitled "Computation at the edge of chaos: phase transition and emergent computation" [81], Langton showed that a proper parameterization of the rule space allows identification with a fair approximation of both the relations between the classes of complexity and the zones of this space in which the CA of the various classes are placed. He had an inspiration to orient himself within this myriad of rules: the *lambda parameter*. Given a CA controlled by a rule R with a number N of possible neighborhood configurations (for instance, the linear automata of Wolfram with radius 1 have 2^3 possible configurations, the CA with Moore neighborhood, as *Life* have 2^9 possible configurations, etc.), λ is defined as the probability that, based on R, one of the N configurations leads to an active cell, that is the probability of a *non-quiescent transition*. The parameter λ, therefore, parameterizes the rule space [81]: this measures the percentage of non-quiescent transitions in the function of the CA transition. The parameter λ is formally defined as follows:

$$\lambda = \frac{k^n - n_q}{k^n} = 1 - \frac{n_q}{k^n} \tag{2.7}$$

where k is the number of cell states, n is the number of cells in the neighborhood, and n_q is the number of transitions that terminate in the quiescent state. If $n_q = k^n$, all the transitions of the look-up table are toward the quiescent state and $\lambda = 0$; if $n_q = 0$, instead, there are no transitions toward the quiescent state and $\lambda = 1$; finally, when all the states are represented in the look-up table to the same extent, $\lambda = 1 - \frac{1}{k}$.

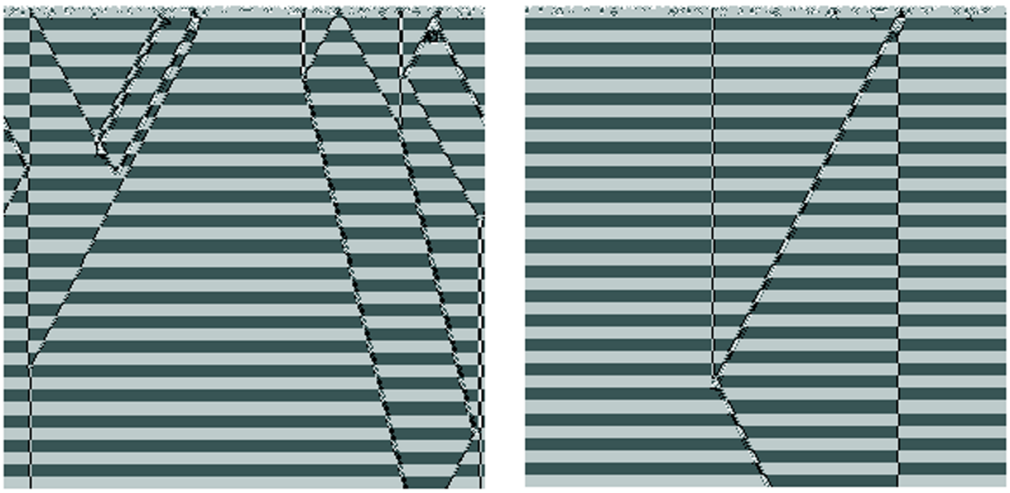

Fig. 2.12 Example of CA at the "edges of chaos". Figures (a) and (b) show the evolution of the same CA with $k = 4$ states and $r = 1$ starting from two different initial configurations. The gray scale represents the four possible states m of the cell, from white for state 0 to black for state 3.

Langton analyzed the behavior of numerous legal totalistic CA with $k = 4$ states and $r = 1$ at a variance of λ in the interval $[0; 0.75]$. The results showed that for small values of λ, the behavior of the CA analyzed is essentially ordered, typical of the complexity classes *I* and *II*, while for large values of λ, the behavior observed is essentially chaotic, typical of class *III*. Between these two zones (order and chaos), however, Langton observed a third, very small one, close to the value $\lambda = 0.45$. In this zone, defined by Langton himself as the "*edge of chaos*", the dynamics of the CA are capable of generating both static structures and structures capable of propagating in space and time, typical of Wolfram's class *IV*. Fig. 2.12 illustrates an example of a CA at the edge of chaos.

Unlike the first two zones, only at the edge of chaos can the information codified in the initial configuration of the CA propagate itself over long distances, a necessary condition for speaking of computation. Furthermore, as can be seen in Fig. 2.12, within the edge of chaos, the dynamics of the CA depend substantially on the initial configuration. In this way, according with Wolfram's hypothesis, the CA is capable of "discriminating" between

different information (program and data) codified in the initial string, thus making effective processing potentially possible.

Langton coined the term *edge of chaos* to indicate the zone at the borders between the "orderly" states (stable or periodic) and the chaotic states, where complexity is found, shown particularly in the capacity for universal computation. In this computer cosmos, in the narrow and rugged zone of the borders of the edges of chaos, are there other lives outside of Life? No one has found them. Moreover, since Life is capable of universal computation, each "algorithmic" life is, in principle, reproducible in itself.

2.5.4 Universal Computation

Among the classes of complexity, class *IV* is particularly interesting for the presence of structures (gliders) capable of propagating in space and time, so much so as to have pushed Wolfram to advance the hypothesis, as was stated previously, that CA of this class may be capable of universal computation. A calculator can be seen as a system capable of transforming an initial bit sequence into a final sequence codifying the result of the computation. The initial sequence can be considered the codifying of the information that must be processed by the program that must be executed, while the final sequence, or part of it, can be considered a result of the computation.

Therefore, the CA studied by Wolfram can be seen as calculators: the initial configurations codify data and programs and the final configurations (obtained through a sufficient number of calculation steps) codify the result of the computation. If the CA, analyzed by Wolfram, were capable of universal computation, then with a preset transition rule, it should be possible to represent every possible program in the initial configuration.

In fact, the computational universality of CA has been known from their beginnings. von Neumann's construction of a machine capable of self-reproducing is actually based on the demonstration of the existence of a universal calculator/constructor in a CA with 29 states [159]. Later, Codd [22], Thatcher [150], Berlekamp et al, [15], Fredkin and Toffoli [52], to name only a few, demonstrated the computational universality for the simplest CA. The hypothesis of computational universality for the even simpler CA studied by Wolfram arose from the observation that gliders can operate as '*processors*' of the information codified in the initial configuration. By means of gliders, the state of a cell in a particular position of the cellular space can actually influence, over time, the states of the cells in arbitrarily distant positions (Fig. 2.11d). Furthermore, gliders can interact among themselves in an extremely complex manner, and through them, it is theoretically possible to reproduce, as demonstrated in John Horton Conway's Game of Life [15] [59], the fundamental logic gate of a universal digital computer.

Therefore, it is known that some CA are capable of universal computation, but the question remains open on whether that particular CA is capable of universal computation with the smallest number of states and possible neighbors. The possibility of universal computation implies that every computation can be executed through CA. Furthermore, the information-processing mechanisms observed in many natural processes appear closer to CA than to the Turing Machine. For this reason, these processes can be simulated more efficiently through CA than through other calculation models [168]. When finally is considered that with current technological knowledge, a simple universal one-dimensional CA with many millions of cells can be easily realized on a single wafer of silicon with very low 'time step' time, on the order of billionths of a second, it is understood that the question related to the design of dedicated hardware could open new prospects in terms of performance for the simulation of those phenomena (physical, biological, economic, etc.), which readily lend themselves to being described in terms of Cellular Automata [165]. Wolfram supposes that one-dimensional CA can be the simplest well-defined systems capable of complex self-organization behavior. In nature, many continuous dynamic systems have this capacity: they evolve from a random start state into a highly ordered structure, being one example the snowflake.

2.5.5 Computational Mechanics

Wolfram's study of CA classification is placed within the context of a purely macroscopic analysis, since it is based exclusively on the observation of space-time configurations generated by CA, completely disassociated from the causes by which the configurations emerge. In diametric opposition, Langton's attempt to characterize the rule space through the parameter λ, that is placed within a purely microscopic approach, since it is based exclusively on the analysis of local interactions defined by the transition rule. Both approaches can be subject to criticism. For example, Wolfram's classification scheme is subjective and, as a consequence, different observers could fail to agree on the classes to which the CA belong. Langton's work, on the other hand, is in some sense the antithesis of the well-known principle that, in non-linear systems, the equation that defines the system (the transition rule in the case of CA) does not directly determine the behavior of the system over the long term [33]. Indeed, the less-than-absolute precision of λ is well-known: not all the rules at the edge of chaos are actually complex, and, conversely, complex rules can also be located outside of this zone.

In consideration of this, Wuensche [171] [170] proposed the parameter Z, which better describes the behavior of CA starting from analysis of the transition rule.

Computational mechanics, proposed by Crutchfield [34] and applied to CA by Crutchfield and by Hanson [35] [64] [65], is an approach placed intermediately between the micro- and

macroscopic in the study of emergent computation in discrete dynamic systems. Applied to CA, the objective of computational mechanics is to discover an appropriate basic configuration from which to describe the fundamental emergent structural components and their interactions. A basic configuration consists of a set of formal languages

$$\Lambda = \left\{\Lambda^i, i = 0, 1, \dots\right\} \tag{2.8}$$

For example, the basic configuration of elementary CA σ_{18}, illustrated in Fig. 2.13, is $\Lambda = \left\{\Lambda^0 = (0^*)^+\right\}$, where, in the specific context of computational mechanics, the symbol * is a *wildcard* symbol that can assume both the value 0 and the value 1, while the apex $^+$ indicates a sequence equal to what is contained within the parentheses. In other terms, in many regions in the space-time configuration of CA σ_{18}, the states of the cells are instances of the language Λ^0, for example $0101\dots01$, or $0000\dots00$.

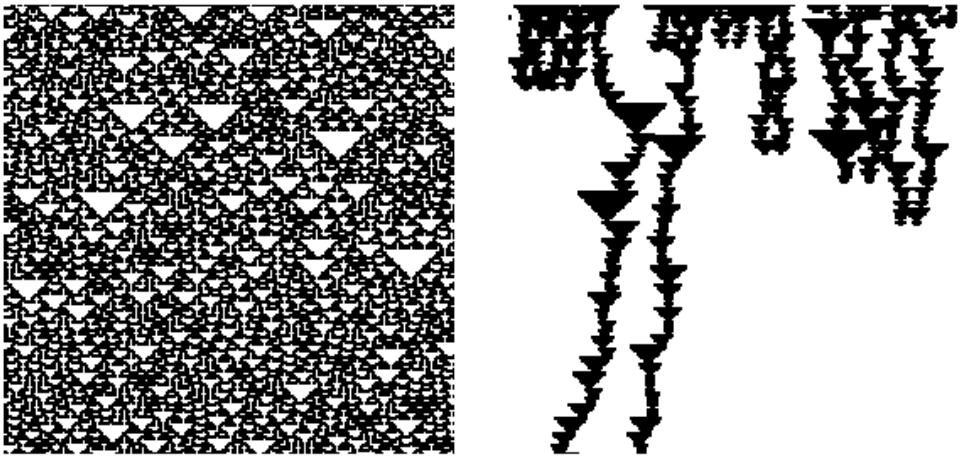

Fig. 2.13 Space-time diagram (a) of elementary CA σ_{18} and (b) of the same CA in which the instances of language Λ^0 were 'filtered' and the emergent particles highlighted in black.

Crutchfield and Hanson define regular domain *j* as a region of the space-time configuration of CA, invariant with respect to both space and time such that it is a regular language. Identifying a regular domain means, at least in part, understanding the dynamics of CA.

In fact, the regular domains define causes of 'regularity' in the corresponding zones of the space-time diagrams. The domains can be filtered, emphasizing the zones of demarcation. These zones are in fact gliders, which, in the typical terminology of computational mechanics, are called particles. The particles that emerge through filtering the single regular domain Λ^0 of the CA σ_{18} are instances of the language $P = \{1(00)^n 1, n = 0, 1, 2, \dots\}$.

Fig. 2.13 illustrates the space-time configuration of CA σ_{18}, in which the cells of Λ^0 are white, while the cells of P are black. To analyze the behavior of CA, domains and particles are shown in a catalog. For AC σ_{18}, the catalog is particularly simple (see Table 2.4).

Table 2.4 Catalog AC elementary σ_{18}.

Regular domains	$\Lambda = \{\Lambda^0 = (0^*)^+\}$ $(^* = 0\ or\ ^* = 1)$
Particles	$\alpha \sim P = \{1(00)^n 1, n = 0, 1, 2, \dots\}$
Interactions	$\alpha + \alpha \longrightarrow 0(\Lambda^0)$

The result is that CA σ_{18} can be analyzed structurally, rather than simply defining it as chaotic according to Wolfram's classification. The emergent particles carry with them various types of information related to the regions of the initial configuration of the CA from which they arise. Their interactions act as information processors.

2.6 Some Applications of Cellular Automata

The application areas of CA are many and diverse ranging from various fields of computer science, physics, chemistry, mathematics, biology, ecology, sociology, geography, environmental science, information theory, and other disciplines.

In certain areas the application of CA gave results comparable, or even greater than, to those obtained using more traditional approaches, for instance:

In Computer Science, Cellular Automata can be seen as a parallel computer and are used to study parallel computing [165]. Besides, CA are also used in computer graphics research. With regard to mathematics, Cellular Automata are used to study number theory, for instance Fischer designed primes filter (Prime Number Sieves) [49].

In physics, a particularly significant example is the application to the modeling of the behavior of turbulent fluids through models known by the name of Lattice Gas and of Lattice Boltzmann models. CA simulation is also applied to magnetic field theory, electric field, and others, as well as to thermal diffusion, thermal conductivity and mechanical analog waves.

In addition, due to the stability of CA dynamics [57], the most widely spread CA application refers to modeling dynamical physical systems. CA have been used to model the laws of physics as an alternative to differential equations [153], Moreover, CA have been successfully engaged to model geography and urban growth [78], in information science (information storage, image processing and pattern recognition [41] [124]), sociology (formation and outbreak processes of economic crisis, social behavior of individuals, popular

phenomena), environmental science (CA are used to simulate oil spill behavior [63], waste water pollution, gas dispersion, and other diffusion processes [137]).

In the last years, the research into simulations of CA in fluid-dynamics, as an important field for CA applications, is accelerating in many directions. One of the beaten research directions concerns modeling and simulation of flow-type landslides that have been carried out by several authors with satisfactory results since 1986 [10]. An extension of the CA paradigm for macroscopic systems and a related modeling methodology were established in order to simulate also fluid-dynamical phenomena [42]. Good simulation results were obtained for some types of 'macroscopic' surface flows, for instance, lava flows and pyroclastic flows for volcanic eruptions, debris, mud, granular flows for landslides and snow avalanches respectively with various versions of the models SCIDDICA, SCIARA, PYR and VALANCA (e.g., Avolio et al.[4], Crisci et al. [32] [31], Avolio et al. [6]). Other significant MCA models were developed for flow-type landslides [21], [126].

In chemistry, Cellular Automata can be used to study chemical reactions and interactions by simulating atoms, molecules, and other microscopic particles in a chemical reaction. Also other CA applications to simulated the polymerization [8] [106].

In biology, CA are applied on growth of tumor cells, exploring the mechanism of the human brain [157], intracellular activity, cell-cell interactions, population organism, DNA sequences, HIV infection process [136], and self-reproductive biological phenomena such as the latest popular clone technology [46].

Equally important in ecology, CA were used for population dynamic process simulation, such as rabbit-grass, shark-fish interactions etc., which demonstrated satisfactorily the dynamic effects; Cellular Automata were also successfully applied to ants, geese, migratory fish and other animals simulating group behavior. Additionally, CA based biomes dispersion model has become to be a hot item currently.

Many CA applications in fluid dynamics exist, most of these based on microscopic approaches, for example: lattice gas automata modeled were introduced to described the motion and collision of particles interacting according to appropriate laws on a lattice space [54].

Below is a brief description of some application examples in the field of Lattice Gas.

2.7 Fluid Dynamics

Fluid dynamics is the branch of physics concerned with the behavior of gases and liquids [56]. The basic equations of this discipline have a very simple fundamental logic; they correspond to the mathematical transcription of the laws of conservation of mass, energy and momentum,

and are today universally known as Navier-Stokes equations [55], for the names of the researchers who proposed them during the last century. They are, in the two-dimensional case:

$$\frac{\partial \rho u}{\partial t} = -\frac{\partial \rho uu}{\partial x} - \frac{\partial \rho uv}{\partial y} - \frac{\partial p}{\partial x} + \mu \left(\frac{\partial^2 u}{\partial^2 x} + \frac{\partial^2 u}{\partial^2 y} \right)$$

$$\frac{\partial \rho v}{\partial t} = -\frac{\partial \rho uv}{\partial x} - \frac{\partial \rho vv}{\partial y} - \frac{\partial p}{\partial x} + \mu \left(\frac{\partial^2 v}{\partial^2 x} + \frac{\partial^2 v}{\partial^2 y} \right) \tag{2.9}$$

u and v being the velocity of the fluid in directions x and y of a particular orthogonal Cartesian system, ρ the density of fluid, p the pressure exercised on the fluid, and t the time. The first element represents the variation, with respect to the time, of the momentum per unit of volume. This variation is due to three effects: the flow due to the flow field of the fluid (the first two terms for the second element), called the convection term, the forces of pressure (third term), and dissipation (fourth and fifth terms). It should be noted that the non-linearity of these equations is entirely contained in the convection term: it is really the term that, despite its simple physical origin, gives rise to those mathematical difficulties that make the Navier-Stokes equations so difficult to solve. Therefore, the convection term is the principal cause of the difficulty in solving for non-idealized cases [147], pushing some researchers to try an alternative approach to the study of fluid dynamics based on CA, which is called *lattice gas*.

2.7.1 Lattice Gas and Lattice Boltzmann Models

Many physical phenomena are due to the collective behavior of a large number of particles interacting among themselves. In many cases, the study of these phenomena does not require the exact knowledge of the state of the microscopic constituents. In fact, for example, to study the currents of a watercourse, it is not necessary to know the velocity of all the water molecules. It is not important to know the microscopic states of a system since they correspond to a single state on the macroscopic level.

CA are essentially based on these ideas. For this reason, they offer a new approach to the simulation of complex systems closest to physics. CA provide some useful and efficient tools to study and simulate many physics problems through the use of high-performance calculation systems. Some significant problems in physics that have been investigated through CA are, for example, ferromagnetism, fluid dynamics, the phenomena of diffusion, molecular

dynamics, wave propagation, etc. In this section, problems regarding fluid dynamics will be particularly addressed.

Lattice Gas

The basic idea of lattice gas is to model a fluid through a system of particles, each of which must move, at a constant velocity, only along the directions of a discrete lattice. Local laws are defined to ensure the invariance of the number of particles (conservation of mass) and the conservation of momentum. The first to propose an approach of this type were Hardy, Pomeau, and Pazzis, in 1976 [66]. The HPP model (from the initials of the three researchers) is based on a boxed grid in which each node is connected to four neighborhoods (von Neumann neighborhoods).

Each node may contain a minimum of zero and a maximum of four particles of unitary mass, each of which may move only along one direction of the lattice at a constant velocity, equal to 1 (that is, each particle may move in one step of the CA from its cell to an adjacent cell). Since it is assumed that both mass and velocity are unitary, the momentum of a particle can be defined simply by the direction (the directions allowed are South (S), West (W), North (N), and East (E)). Therefore, the possible configurations for each node of the HPP are $2^4 = 16$. For example, the configuration 0000 indicates the absence of particles, the configuration 0001 indicates the presence of a particle moving to the East, the configuration 0010 indicates the presence of a particle moving to the North, and so on. When two particles of opposite velocities are found in the same cell (configurations 0101 and 1010), an impact or collision occurs, and the particles deviate at a right angle (see Fig. 2.14). The collision phase truly involves the automata's art of 'mimicry'[147]. In the collision phase, in fact, site after site, the arrows that represent velocities must undergo rotations intended to simulate the exchange of the momentum and energy that occurs in a real fluid.

In all other cases, including cases where paths cross (for example, in configuration 1111), the particles follow their path without deviation. Hence, a CA capable of obeying the principles of conservation that characterize fluid motion.

When the number of particles is sufficiently large, on the macroscopic scale, the impression is that of a continuous fluid. HPP CA was shown to be capable of correctly modeling fluid dynamics phenomena such as the propagation of a wave, but its behavior was not very realistic in the simulation of turbulent fluids. The principal problem was due to the lattice constraint. In fact, this last is responsible for the so-called spurious invariants (or symmetries) [146], that is, invariants that have no correspondents in the continuum. In practice, the HPP, in addition to conserving mass and momentum, also conserves motion along the lines and columns of the lattice, as can easily be deduced from analyzing the transition rules.

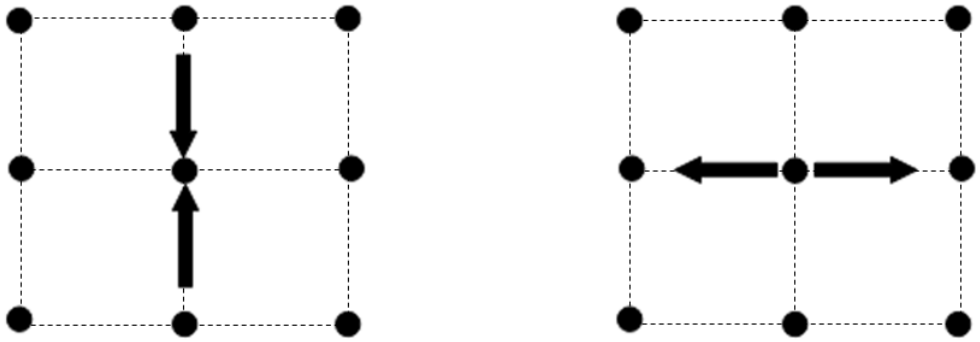

Fig. 2.14 Collisions in the HPP automata. The particles revolve its speed of ninety degrees. In this case the number and amount of motion of the particles does not change as a result of the collision.

Due to this excess of invariants, the motion of the particles is strongly anisotropic (isotropy is the symmetry connected to spatial rotations; one example is the effect of a rock thrown into a pool, generating concentric circles, which means that the crest of the wave propagates at the same velocity along all directions away from the point of the splash) and the fluid is insufficiently free to move and diffuse its momentum in all directions.

The fluids, furthermore, are under normal conditions, isotropic means, for which the chaotic motion of the molecules cancels each preferential direction. Therefore, the HPP automata truly act like a real liquid only for a restricted number of phenomena; this model, therefore, needs to be perfected. One problem with the HPP automaton is the lack of sufficient symmetry to guarantee the isotropy of the terms that regulate the transport of quantities of motions in a fluid. In reality, what it is required to do with CA is to stack the deck to pretend that the automata are in a continuum, while instead, by definition, they operate discretely. It is, therefore, plausible that it works as long as simple things are required, but when it is moved to more complicated phenomena like turbulence, problems arise because the automaton puts its antennae out a little further and understands that it is in a discrete space.

Another problem with the HPP automaton, also connected to the lack of symmetry, is the existence of a very high number of conserved quantities.

In a fluid, the quantities that are conserved are mass, momentum, and energy, while in the HPP model, there are 2^N other invariants, with N being the number of lines (columns) of the lattice, and precisely horizontal momentum on each line and vertical momentum on each column. Due to this excess of invariants, the fluid is like a lion in a cage that prevents it from moving with the freedom necessary to diffuse the momentum in all directions [147].

At this point, with a simple intuition, Frish, Hasslacher, and Pomeau in 1986 understood that the isotropic anomaly could be treated with a very simple medicine: it was sufficient to move from a square lattice to a hexagonal one [147] [149]. Therefore, they intuited that the use of a regular hexagonal mesh lattice instead of a square mesh lattice could be enough to reestablish the lost isotropy.

In the FHP model (again from the initials of the three researchers), each cell is connected to the six neighboring cells at 60-degree angles. Since the particles can move along three directions instead of two, the number of possible states of the cell changes from 2^4 to 2^6, though the transition laws remain substantially equivalent to those of the HPP model, with the difference being that in the FHP model, impacts involving three cells simultaneously are also possible, which is very important for purposes of simulating the practices of fluids.

Now the functioning of the FHP models will be examine deeply. $n_i\left(\overrightarrow{\mathbf{r}};t\right)$ is the number of particles (0 or 1) entering the cell, identified by the vector $\overrightarrow{\mathbf{r}}$ at step t along the direction $\overrightarrow{\mathbf{c}_i}$ $(i = 1,2,\ldots,6)$ (see Fig. 2.15). τ is also the time corresponding to one calculation step of the FHP model and λ is the distance between the two neighboring cells of the hexagonal lattice. The velocity $\overrightarrow{\mathbf{v}_i}$ of the particles along the directions are defined as follows:

$$\overrightarrow{\mathbf{v}_i} = \frac{\lambda}{\tau}\overrightarrow{\mathbf{c}_i} \tag{2.10}$$

The transition function of the cell can be deduced from the collision rules, illustrated in Fig. 2.15, considering the case in which there are no impacts and two cases in which, on the contrary, there are collisions between two or three particles:

- **No collision**. If there is no collision, the particles follow their path along the original lattice direction, without any deviation. Therefore, the following updated rules apply:

$$n_i\left(\overrightarrow{\mathbf{r}} + \lambda\,\overrightarrow{\mathbf{c}_i};t+\tau\right) = n_i\left(\overrightarrow{\mathbf{r}};t\right) \tag{2.11}$$

  namely, each particle that at time t is in the cell identified by the vector $\overrightarrow{\mathbf{r}}$, at the next step, $t+\tau$, will be in the adjacent cell, along the same direction, identified by the vector $\overrightarrow{\mathbf{r}} + \lambda\,\overrightarrow{\mathbf{c}_i}$.

- **Collision between two particles**. If only n_i and n_{i+3} have the value 1 in the cell $\overrightarrow{\mathbf{r}}$, as illustrated in Figures 2.15a and 2.15b, a collision occurs. The condition

$$D_i = n_i\,n_{i+3}\,(1-n_{i+1})\,(1-n_{i+2})\,(1-n_{i+4})\,(1-n_{i+5}) = 1 \tag{2.12}$$

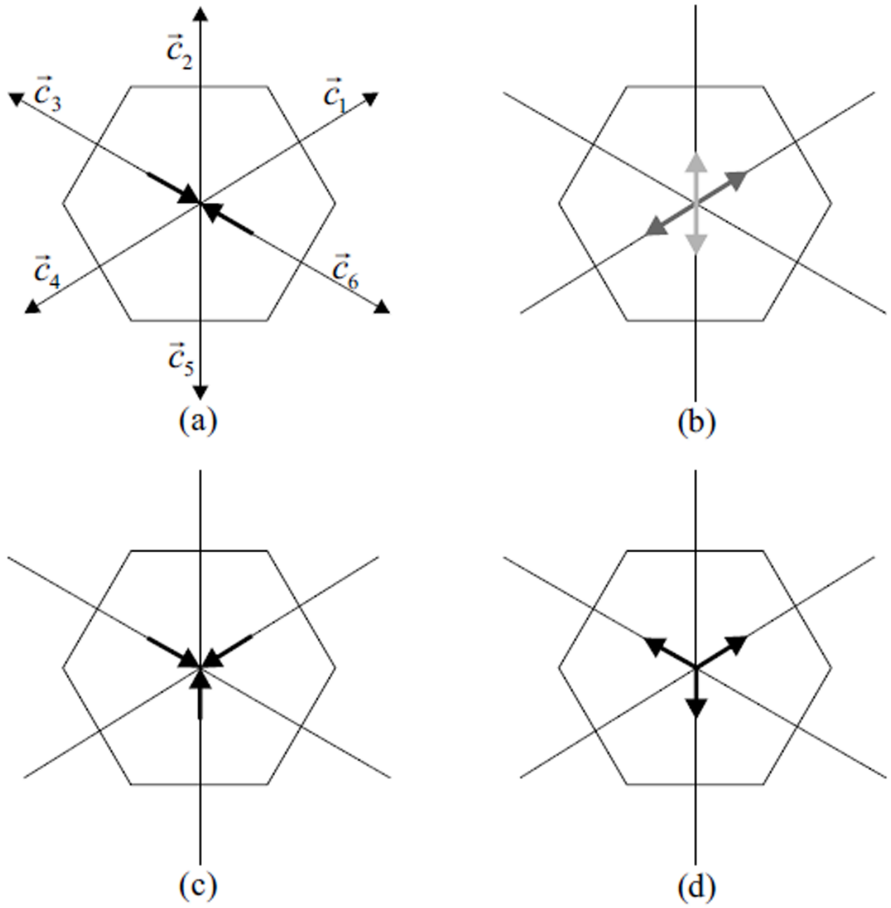

Fig. 2.15 Collision rules in the FHP model. (a) and (b) describe, respectively, the configuration of the cell before and after impact in the case of two particles; in this case, the transition rule is probabilistic: that is, the particles can deviate to the right (configuration in light gray) or left (configuration in dark gray) with the same probability. (c) and (d) describe, respectively, the configuration of the cell before and after impact in the case of three particles. The six possible directions of the particles, $c_1, c_2, \ldots, c_6$ are highlighted in (a).

identifies such impact. Therefore, the number of particles that remain along the direction $\overrightarrow{\mathbf{c}_i}$ after the impact is given by: $n_i - D$

However, a new particle can appear in the direction $\overrightarrow{\mathbf{c}_i}$ due to the collisions between n_{i-1} and n_{i+2} or between n_{i+1} and n_{i+4}. The number of particles created in the direction $\overrightarrow{\mathbf{c}_i}$ can therefore be deduced from the following formula:

$$qD_{i-1} + (1-q)D_{i+1} \tag{2.13}$$

let $q = q\left(\overrightarrow{\mathbf{r}};t\right)$ a random Boolean variable worth 0 if, after the impact, the particles deviate to the left, and 1 if they deviate to the right. Therefore, the total number of particles along $\overrightarrow{\mathbf{c}_i}$ is given by:

$$n_i - D_i + qD_{i-1} + (1-q)\,D_{i+1} \tag{2.14}$$

- **Collision among three particles**. The condition T_i identifies one impact among three particles (Figures 2.15c and 2.15d). The effect is that of the particles deviate at an angle of 180 degrees. Therefore, the number of particles that remain along the direction $\overrightarrow{\mathbf{c}_i}$ after the impact is given by $n_i - T_i$.

  However, an impact between the particles n_{i+1}, n_{i+3} and n_{i+5} determines the appearance of a new particle along the direction $\overrightarrow{\mathbf{c}_i}$, a condition that is expressed as follows T_{i+3}.

  The total number of particles in the direction $\overrightarrow{\mathbf{c}_i}$ due to collision among three particles is therefore given by $n_i - T_i + T_{i+3}$.

Therefore, the dynamics of the FHP model along each direction of the lattice is defined by the following law:

$$n_i\left(\overrightarrow{\mathbf{r}} + \lambda\,\overrightarrow{\mathbf{c}_i}, t+\tau\right) = n_i\left(\overrightarrow{\mathbf{r}}, t\right) + \Omega_i\left(\overrightarrow{\mathbf{r}}, t\right) \tag{2.15}$$

in which the term:

$$\Omega_i\left(\overrightarrow{\mathbf{r}}, t\right) = -D_i + qD_{i-1} + (1-q)D_{i+1} - T_i + T_{i+3} \tag{2.16}$$

represents the effects of the collisions among the particles; Ω_i is, in fact, the so-called collision term. With these few and simple modifications (the introduction of the hexagonal lattice and the new collision rules), the FHP solved the problem of spurious invariants and showed itself capable of correctly reproducing complex fluid dynamics phenomena, for which the problem of invariants is now largely solved thanks, on the one hand, to the possibility of triple impacts, and on the other hand to the fact that the particles can also move diagonally.

Furthermore, Chopard and Droz [18] showed that the introduction of particles with null velocity in subsequent versions of the FHP model [44] allows derivation of the Navier-Stokes equations for incompressible fluids from the collision rules. Fig. 2.16 illustrates an application of the FHP model.

Isotropy, that is, the equivalence of all the directions of the lattice, therefore plays an extremely important role in modeling the behavior of the fluid particle. This aspect constitutes

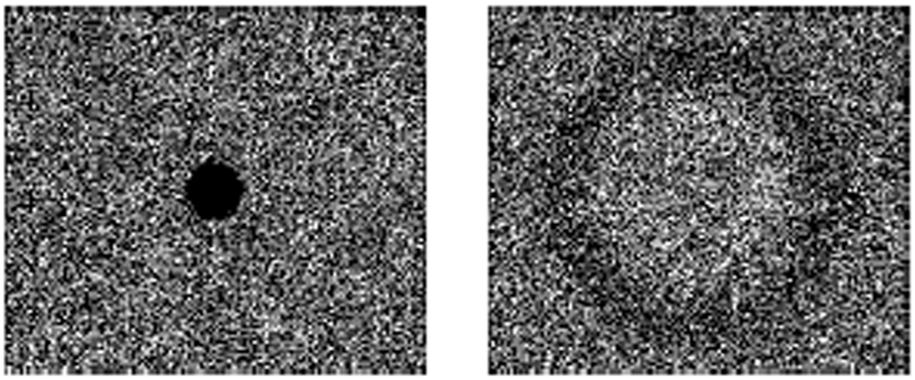

Fig. 2.16 Dynamics of a wave (b) in the FHP model due to the diffusion of a concentration of particles in the central zone of the lattice (a).

an apparently insurmountable problem in moving to the third dimension, mostly of interest for practical applications. Indeed, there is no solid primitive capable of congruently filling the space (that is, without holes) while simultaneously ensuring isotropy [146].

In 1987, Frish, d'Humières, and Lallemand noticed that a solid with the required properties already existed in the four-dimensional space. This was a face-centered hypercube (the generalization of a cube), the basis for the construction of the FCHC (Face-Centered Hyper Cube) lattice [53]. The move to the third dimension, although theoretically flawless, nevertheless poses significant problems in computational terms. There are 12 possible directions in the FCHC, and as a consequence, the number of possible states becomes 2^{24} (more than 16 million). Therefore, the transition table that defines the result of all possible configurations of the cell ends up being more than 48 megabytes. Leaving aside the fact that such a quantity was considered quite large in 1987, the more pressing problem was that a transition table so large required unacceptable access times, and therefore many studies focused on reducing its size.

Lattice Boltzmann Models

Simultaneously with the research on reduced collision tables, an alternative solution was developed, known today as the lattice Boltzmann method, first proposed by McNamara and Zanetti [99] of the University of Chicago, and simultaneously by Higuera and Jiménez of Madrid Polytechnic [69]. One advantage of the lattice Boltzmann models compared to Lattice Gas that is not to be overlooked is the much higher computational efficiency, given that in the latter, the quantities of interest are no longer individual particles, but their density.

Thus, the number of system components is substantially reduced and the phase of calculating the space-time averages is no longer necessary to determine the physical quantities of interest in the system: the density of fluid, ρ, and the momentum, ρu, are noted in every cell of the lattice. In its simplest form [120] [17], the dynamics of a lattice Boltzmann model can be described as follows:

$$f_i(\overrightarrow{\mathbf{r}} + \tau\overrightarrow{\mathbf{v}_i}, t+\tau) - f_i(\overrightarrow{\mathbf{r}}, t) = \Omega_i(f_i(\overrightarrow{\mathbf{r}}, t)) = \frac{1}{\xi}(f_i^{(eq)}(\overrightarrow{\mathbf{r}}, t) - f_i(\overrightarrow{\mathbf{r}}, t)) \tag{2.17}$$

Here $f_i(\overrightarrow{\mathbf{r}}, t)$ represents the density of the particles that at time t are found in the cell $\overrightarrow{\mathbf{r}}$ with velocity $\overrightarrow{\mathbf{v}_i}$; $f_i^{(eq)}(\overrightarrow{\mathbf{r}}, t)$ represents the so-called local *equilibrium distribution*; ξ, the so-called relaxation term, represents the number of calculation steps necessary to reach equilibrium in the local context of the neighborhood.

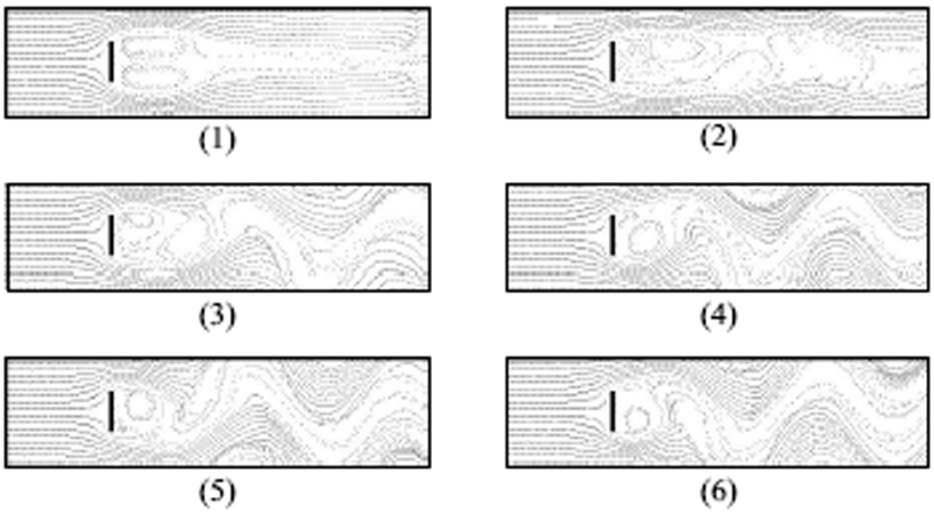

Fig. 2.17 Simulation of a flow around a plane in a lattice Boltzmann model of 512×128 cells and $\xi = 1$. Cases 1 through 6 illustrate the evolution of the system.

The laws that determine the dynamics of the lattice Boltzmann models therefore reduce conditions of non-equilibrium in the local context of the neighborhood. The function $f_i^{(eq)}(\overrightarrow{\mathbf{r}}, t)$ specifies the conditions of local equilibrium of the system as a function of density, $\rho = \sum f_i$ and momentum, $\rho\,\overrightarrow{\mathbf{u}} = \sum f_i\overrightarrow{\mathbf{v}_i}$, of the fluid in the cell. The parameter ξ expresses the dependence of the system on the viscosity, ν, of the fluid. In fact, the following relation applies: $\nu = K(\xi - \frac{1}{2})$ where K is a constant that depends on the geometry of the lattice [19]. In this way, viscosity becomes an explicit parameter of the model, unlike what occurs with

Lattice Gas, which implicitly depends on the specification of the laws that regulate impacts among particles.

The lattice Boltzmann models therefore involve quantities that are no longer expressible as whole numbers (as with individual particles in lattice gas), but as real numbers. If, on the one hand, this may represent a problem from the point of view of numerical stability (understood as propagation of error, typical of models based on the processing of floating-point values), on the other hand, it offers greater flexibility in calibrating the model, given that it is possible to make explicit, as with viscosity, some important parameters of the system. Furthermore, as for the FHP model, for lattice Boltzmann models as well, equivalence with Navier-Stokes equations for incompressible fluids was demonstrated [18]. Fig. 2.17 illustrates the dynamics of the BKG model [120] in the simulation of a flow around a plane.

Theoretical studies and applications of lattice gas and the lattice Boltzmann method are described in Rothman and Zaleski [125], in Luo [84], in Chopard and Masselto [20], in Bernaschi et al. [98], in Succi [149], and in Wolfram [168].

Chapter 3

Modeling Complex Macroscopic Phenomena with Cellular Automata

"La chiave di volta per affrontare questi problemi (di estrema complessità) con gli Automi Cellulari (AC) è la possibilità di una descrizione del fenomeno in termini di interazioni locali di unità elementari;...dobbiamo considerare (però) il ruolo, che assume la rappresentazione del nostro sistema:... rappresentazioni, che sono inefficienti in termini di calcolo sequenziale, risultano eccezionalmente vantaggiose in termini di calcolo parallelo."

Salvatore Di Gregorio da "Automi Cellulari: Genesi di un Paradigma"

3.1 Introduction

Cellular Automata have received significant attention over the past few years, not only as an emergent model of Parallel Computation, but also as an effective tool for modeling and simulation in the field of complex phenomena. They represent one of the most important paradigms for the study of complex systems and together with neural nets and genetic algorithms, today constitute a set of methods and supports to scientific investigation, which

have drawn their inspiration from biology and that are, in some aspects, alternatives to the classic approaches based on the use of differential equation systems.

The laws of physics are ultimately founded on the principles of conservation, such as conservation of mass, momentum, and energy [18]. In the past, until the advent of electronic processors, the ability to describe phenomena in terms of differential equations, whose analytical solutions provided the state of the system at each point of the space-time continuum, has marked the difference between strong science (highly predictive) and weak science (purely descriptive). Unfortunately, however, as in the case of Navier-Stokes equations in fluid dynamics, for many systems, the analytic solution does not exist except trivial cases and the usage of approximated numerical methods involves usually severe limits in obtaining reliable solutions [147].

Attempts at quantitative modeling of complex natural phenomena through approximative numerical methods (commonly based on discretization in space and time) have principally been developed due to growth in the power of electronic calculators. These methods (for example, the analysis of slope stability [162]) have allowed the extension of the class of problems that can be solved in terms of systems of differential equations. However, some of them are still difficult to address, others not addressed at all.

To study and resolve such problems, the international scientific community had to overcome the difficulties involved in solving differential equation systems through various technical alternatives [153]. Simultaneously with the development of approximative methods for the numerical solution of differential equation systems [121], new numerical methods were in fact developed and consolidated, founded on the principles of parallel calculation. But both approaches, the one based on differential equations and the one based on new parallel calculation models, are based on common concepts of modeling and simulation.

Fortunately, the common belief that very complex phenomena require necessarily sophisticated models has been shown to be erroneous: complexity can emerge in a model even if governed by very simple rules (cf. e.g. Wolfram, [168]). Among these approaches Cellular Automata represents a simple, attractive and alternative modeling technique respect to traditional numerical models that solve differential equations to describe complex phenomena [153].

3.2 Modeling with Cellular Automata

Cellular Automata have introduced a radically new approach in the modeling of complex phenomena that evolve based on local laws. The previous chapter presented the Gas Reticular

and models of lattice Boltzmann, who first highlighted the potentialities in the AC in the modeling and simulation of complex physical systems.

However, while Lattice Gases have always been considered CA for all intents and purposes (that is, they are composed of a discrete lattice, a finite number of states per cell, a transition function expressible in terms of a look-up table, etc.), the lattice Boltzmann models were seen for some time as 'quasi-automata'[147]. In fact, in the lattice Boltzmann models, the state of the cell represents the density of the particles in the corresponding region of space and can therefore change in a continuous range of values. However, continuity is a problem only from a formal point of view. In practical cases, real variables have a finite number of significant digits and, as a consequence, a finite set of permitted values (in other words, the set of permitted values can be extremely large but is, in any case, finite).

Therefore, the lattice Boltzmann model can be considered CA for all intents and purposes. The applications of these models generally include phenomena that evolve on a purely microscopic scale, since they identify the elementary components of the system in the parts of the fluid, or, at most, in their density in regions that are extremely limited. Their sphere of applicability did not generally include macroscopic phenomena that evolve in necessarily three-dimensional contexts, like lava or debris flows.

However, in the past several decades, numerous empirical models based on CA have been proposed for the simulation of complex macroscopic phenomena. Among the most recent, Smith [143], Murray, and Paola [103] [104] proposed models for the simulation of soil erosion; Miyamoto and Sasaki proposed models for the simulation of lava flows [100]; Sassa [128], Segre, and Deangeli [133], Malamud and Turcotte [93], Clerici and Perego [21], have proposed models for the simulation of debris flows.

In the early 1980s, the EMPEDOCLES interdisciplinary research group (that is, the first group), based on some of the intuitions of Prof. Salvatore Di Gregorio of the Department of Mathematics and Computer Science, proposed a CA-based alternative semi-empirical method for modeling and simulating complex macroscopic phenomena, initially applied to the simulation of lava flows [29] [28] [10] [9]. Up until that time, the models applied to fluid dynamics had been difficult to manage for macroscopic phenomena that evolved on a large spatial scale, like lava flows. This need therefore pushed the group's researchers to try a different approach, considering the macroscopic characteristics of an event. Boltzmann's Gas had not yet been conceived when in 1982 Prof. Salvatore Di Gregorio, together with Prof. Gino M. Crisci of the Department of Biology, Ecology, Earth Science (currently rector of the University of Calabria), constructed a simple, three-dimensional CA model to simulate a lava flow event on the island of Pantelleria about ten thousand years ago. This model led to innovations for application of CA to some problems of fluid dynamics, particularly

for surface flows. The evolution of a complex system originating from the interaction of elements that are in themselves macroscopic, giving rise to emergent phenomena, neglecting other characteristics irrelevant to the evolution of the system.

3.2.1 Criteria for CA for the Modeling of Macroscopic Phenomena

The applications of CA to fluid dynamics have generated two important computational paradigms: the Lattice Gas models [54], and from there, the more robust Lattice Boltzmann method [18] [148]. However, many complex macroscopic phenomena seem to be difficult to model with these types of CA, since they occur on a very broad spatial scale. Consequently, a macroscopic level of description must be used, which implies, however the management of a large quantity of data, e.g., morphological data.

It is hence unthinkable to work at the microscopic level, where evaluation factors such as data quality would make no sense. The move to the macroscopic also means a greater number of states, which could also lead to complicated transition functions that can no longer be practically identified with a lookup table, as in the microscopic one.

The classical CA definition is not sufficient for modeling spatially extended natural macroscopic phenomena [1]. This extension in its completeness does not formally alter the classic notion of CA as developed by von Neumann, but renders it capable of modeling and dealing with the complex macroscopic phenomena to be simulated. A very high number of states are needed for macroscopic phenomena, because they must contain all the information related to the portion of space corresponding to the cell, with all the specifications needed to model the evolution of the phenomenon of interest. This gives rise to a very high number of states, which can be formally represented in terms of sub-states (i.e., the Cartesian product of the sets of all the sub-states constitutes the set of the states). In this way, a sub-state specifies important characteristics (e.g., altitude, temperature, etc.) to be attributed to the state of the cell and necessary to determine the evolution of the CA.

The extended definition of CA for modeling macroscopic phenomena descends from the need to correlate the evolution of the phenomenon with the evolution of the simulation; it is necessary also to consider, those simple, non-local specifications (the parameters) related to the phenomenon or its representation in terms of CA (Etnean lava solidification temperature, cell dimension, etc.).

A CA is formally defined as a septuplet:

$$\langle R,\ G,\ X,\ S,\ P, \tau, \gamma \rangle \tag{3.1}$$

Its components are specified in following paragraphs.

3.2.2 Global Parameters

First requirement: The abstract CA must be uniquely related to the real macroscopic phenomena with regard to time and space.

Some global parameters must be considered at least:

- The cell dimensions, for instance the distance between the centers of two neighboring cells p_d.
- The time (clock) corresponding to one step of the transition function p_t

These are defined as 'global parameters', as their values are equal for all the cellular space. They constitute the finite set, $P = \{p_d, p_t, \dots\}$, with other global parameters that affect the transition function.

With regard to dimensions of the cell size and clock, the choice of the value of the parameters cell size and clock is dependent on the elementary processes.

3.2.3 Space

The cell normally corresponds to a portion of space, therefore the cellular space should be three-dimensional:

$$R = \left\{(x,y,z)/x,y,z \in \mathbb{N}, 0 \le x \le l_x - 1, 0 \le y \le l_y - 1, 0 \le z \le l_z - 1\right\} \tag{3.2}$$

Here is the set of coordinated integer points that define the finite region of the space where the phenomenon evolves. $\mathbb{N}$ is the set of natural numbers.

If there are legitimate simplifications, it is easy to reduce the formula to 1-2 dimensions.

In a finite region, the cells at the edges do not have complete neighborhoods. To solve this, a variation of the definition of the function V is considered: $X = \{\xi_0, \xi_1, \dots, \xi_{m-1}\}$ the neighborhood relationship (or index) is a finite set of three-dimensional vectors that defines the set $V(X,i,l)$ of generic cell neighborhoods $i = \langle i_x, i_y, i_z \rangle$, with $l = \langle l_x, l_y, l_z \rangle$, as follows through the function W: let $m = \#X$, then $V(X,i,l) = \{W(i,\xi_0,l), W(i,\xi_1,l), \dots, W(i,\xi_{m-1},l)\}$ with ξ_0 the null vector and $V\left(i,\xi_j,l\right) = \left\langle \left(i_x + \xi_{jx}\right) mod\ l_x, \left(i_y + \xi_{jy}\right) mod\ l_y, \left(i_z + \xi_{jz}\right) mod\ l_z \right\rangle$, $0 \le j \le m-1$.

3.2.4 Sub-States

Second requirement: The macroscopic part of the phenomenon may imply heterogeneity. Each characteristic significant to the evolution of the system and related to the portion of

space corresponding to the cell is identified as a sub-state; the Cartesian product of the sets of sub-states expresses the finite set S of the states:

$$S = S_1 \times S_2 \times \cdots \times S_n \tag{3.3}$$

The value of a sub-state is approximated to a unique value in the space occupied by the cell (e.g., the temperature). When a characteristic (e.g., a physical quantity) is expressed as a continuous variable, then a finite but sufficient number of meaningful digits are used so that the set of possible values can be arbitrarily large but finite. The sub-state value is considered always constant inside of the each cell (e.g., altitude).

The cellular space should be three-dimensional, but a reduction to two dimensions is permitted if the quantities related to the third dimension (the height) can be represented as sub-states of the cell: this is the case with surface flows, which include debris flows, mud-flow, granular flows and lahars.

3.2.5 'Elementary' Processes

Third requirement: Just as the state of the cell can be broken down into sub-states, also the transition function τ can be subdivided into 'elementary' processes, defined by the functions $\sigma_1, \sigma_2, \ldots, \sigma_k$ with k being the number of elementary processes.

The elementary processes are applied sequentially according to a defined order. Different elementary processes can result in a different neighborhood; the union of all neighborhoods associated with each elementary process specifies the CA neighborhood. Each elementary process updates the states of the CA.

3.2.6 Neighborhood

The neighborhood of the CA is specified by the union of all neighborhoods associated with each elementary process, k is the number of elementary processes, then for the j-th process, $1 \leq j \leq k$, it has:

$$\sigma_j = Q_j^{m_j} \longrightarrow Q_j^{'} \tag{3.4}$$

Here Q_j and $Q_j^{'}$ are the Cartesian products of the elements of the subsets of Q, with $Q = \{S_1, S_2, \ldots, S_n\}$, with m_j being the number of cells in the neighborhood X_j, part of the elementary process j; Q_j identifies the sub-states in the neighborhood, which affect the variation of value of the sub-states and $Q_j^{'}$ identifies the sub-states of the cell that change in value.

$X = \{\xi_0, \xi_1, \ldots, \xi_{m-1}\}$, the neighborhood relationship (or index) of the CA is defined as follows: $X = \{X_1 \cup X_2 \cup \cdots \cup X_k\}$, where X_j, $1 \leq j \leq k$, refers to the elementary process j-th.

3.2.7 External Influences

Fourth requirement: Sometimes, a sort of input from the 'external world' on the cells of the CA must be considered; these account for external influences that cannot be described in terms of the local rules (e.g., the rainfall) for simulating on the base of real or probabilistic data. Therefore, special and/or additional functions (γ) must be specified for that type of cell (G). Note: γ and G do not need always be specified in the CA.

$G = \{G_1 \cup G_2 \cup \cdots \cup G_n\}$ is the set of cells that are affected by the 'external world'; here are considered n external influences, each defining a sub-region G_i $1 \leq i \leq n$ of the cellular space, with $G \subseteq R$.

$\gamma : N \times G \longrightarrow S$ expresses the external influences for the cells of G in the cellular space; this determines the variation of the state S for the cells in G. N, the set of natural numbers, here refers to the steps of the CA.

γ is specified by the sequential application of n functions:

$$\gamma_1 : N \times G_1 \longrightarrow Q_1, \gamma_2 : N \times G_2 \longrightarrow Q_2, \ldots, \gamma_v : N \times G_n \longrightarrow Q_n$$

where $Q_1, Q_2, .., Q_n$ are Cartesian products of elements of the subsets of Q, $Q = \{S_1, S_2, .., S_n\}$

3.3 Algorithm of Minimization of Differences

Many complex systems evolve locally toward conditions of maximum possible equilibrium: essentially in terms of CA, the system tends to minimize, within the neighborhood, differences related to a certain amount of matter, giving rise to flows from central cell to the other neighbor cells [42] [5].

In the context of CA, this means that sub-states 'outflow' have to be calculated for the generic cell c from the 'distributable' quantity q_d. Values of such outflows correspond to values of the sub-states 'inflow' for c neighbors in the next step. τ is applied simultaneously on each cell in R and flows, potentially from each cell toward neighborhood cells, give rise to the evolution of the system.

A simple and intuitive example can be a fluid (e.g., debris, lahar, etc.) on a morphology. A sub-state 'altitude' is attributed to each of the cells along with a sub-state 'fluid thickness'. The property or quantity to be minimized is the 'height' h, whose value is given in this case by the sum of altitude and fluid thickness. The process of minimization is constituted for each

cell by outflows from the central cell to the other neighbors, so that the differences in height are reduced to the minimum between the cells of the neighborhood following the outflows.

Let n = # X be the number of cells in the neighborhood; the minimization algorithm is based on the following assumptions:

1. The content of the central cell to which the neighborhood refers, which here is identified by the index 0, is divided into two quantities: the immovable part (e.g. the altitude) q_0, and the distributable part (e.g. lahar, expressed in terms of lahar thickness in the cell) q_d.

2. The quantity q_i (i = 1, 2, ..., n - 1) for the other neighborhood cells is considered immovable due to the fact that the application of the transition function to a cell allows the modification only of its state, not that of other cells in its neighborhood, cells that will be hereinafter called adjacent cells. (It is obvious that in CA, each cell changes its state in the context in which the transition function is applied to the cell, and this occurs in parallel for each cell).

3. Only q_d can be distributed to the adjacent cells

$$q_d = \sum_{i=0}^{n-1} f_i \tag{3.5}$$

where the notation f_i represents the flow that moves from the central cell to the adjacent cell i , f_0 will indicate, on the other hand, the part of q_d that is not distributed and remains in the central cell. We note that this definition ensures the principle of conservation of mass.

4. $q_i^{'} = q_i + f_i$ (i = 1, 2, ..., n - 1) represents the quantity contained in the neighborhood cells after the flow distribution.

Algorithm of Minimization of the Differences is so specified:

Initialization:

Step 1. All the neighboring cells are considered 'admissible' to receive flows from the central cell, A is the set of admissible cells.

Cycle:

Step 2. The 'average q' ($\overline{q}$) is found for the set A of admissible cells:

$$\overline{q} = \frac{q_d + \sum_{\{i/(0 \le i < n) \wedge (i \in A)\}} q_i}{\#A} \tag{3.6}$$

Step 3. Each cell x with $q_x \ge \overline{q}$ is eliminated from the set A. It implies that 'average q' does not increase, because:

$$\overline{q} = \frac{q_d + \sum_{i=0}^{n-1} q_i}{\#A} = \frac{q_d + \sum_{i=0}^{n-1} q_i - \overline{q}}{\#A - 1} \ge \frac{q_d + \sum_{i=0}^{n-1} q_i - q_x}{\#A - 1} \tag{3.7}$$

End of cycle:

Step 4. Go to step 2 until no cell is eliminated.

Result:

Step 5.

$$f_i = \overline{q} - q_i \quad \text{for} \quad i \in A \quad \text{if} \quad q_i < \overline{q}$$

$$f_i = 0 \quad \text{for} \quad i \notin A \quad \text{if} \quad q_i \ge \overline{q}$$

Conservation bound:

$$\sum_{i=0}^{n-1} f_i = \sum_{i=0}^{n-1} (\overline{q} - q_i) = \#A\left(\frac{q_d + \sum_{i=0}^{n-1} q_i}{\#A}\right) - \sum_{i=0}^{n-1} q_i = q_d \tag{3.8}$$

Properties:

P 1. $q_i^{'} = f_i + q_i = \overline{q} - q_i + q_i = \overline{q}$ for $i \in A$

P 2. $q_i^{'} = q_i$ because $f_i = 0$ for $i \notin A$

Fig. 3.1 illustrates an example of application of the algorithm of minimization of the differences in the case of a two-dimensional AC with square cells and neighborhood von Neumann. In (a) the north, west, east and south cells are identified by numbers 1, 2, 3 and 4 respectively; by convection the central cell is identified as cell 0. Continuing with the Fig. 3.1 it is assumed that $q_d = 9, q_0 = 81, q_1 = 100, q_2 = 76, q_3 = 83, q_4 = 71$. (b) $\overline{q} = 450/5 = 84$ cell 1 is eliminated; (c) $\overline{q} = 320/4 = 80$ cells 0 and 3 are eliminated; (d) $\overline{q} = 156/2 = 78$ no cell is eliminated; (e) $f_2 = 2;; f_4 = 7; f_0 = f_1 = f_3 = 0$

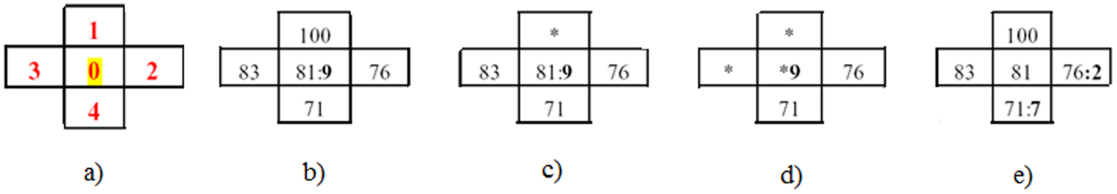

Fig. 3.1 Example of application of the Algorithm of Minimization of the Differences.

3.3.1 A Fundamental Theorem about AMD

Theorem 3.1 *The Algorithm of Minimization of the Differences (AMD or shortly minimization algorithm) computes values of* f_h, $0 \leq h < n$, *such that*

$$\sum_{\{(i,j)/0\leq i<j<n\}} |q'_i - q'_j| \text{ is minimized.} \tag{3.9}$$

Proof. It is demonstrated that any distribution f'_h $0 \leq h < n$, $\sum_{0\leq h<n} f'_h = q_d$, different from the minimization algorithm one, with $q''_h = f'_h + q_h$ involves that

$$\sum_{\{(i,j)/0\leq i<j<n\}} |q''_i - q''_j| > \sum_{\{(i,j)/0\leq i<j<n\}} |q'_i - q'_j| \tag{3.10}$$

Differences $\Delta_h = q''_h - q'_h$ $(0 \leq h < n)$ imply $\sum_{0\leq h<n} \Delta_h = 0$. A different distribution f'_h $(0 \leq h < n)$ implies the existence of at least one $\Delta_x > 0$ counterbalanced by at least one $\Delta_y > 0$.

A different distribution involves that $\Delta_i \geq 0$ for $i \notin A$ because $f_i = 0$ and $f'_i \geq 0$; $\Delta_i > 0$ for $i \in A$ implies $q''_i > \overline{q}$; the value $\Delta_i < 0$ can be assumed only for cells $i \in A$ because $f_i > 0$ and $f'_i \geq 0$ permits cases with $f_i > f'_i$.

Consider then

$$C = \{r/(\Delta_r = 0) \wedge (0 \leq r < n)\}$$

$$C' = \{s/(\Delta_s = 0) \wedge (0 \leq s < n)\}$$

$$C'' = \{t/(\Delta_t = 0) \wedge (0 \leq t < n)\}$$

and $D = \sum_{s\in C'} \Delta_s$; $\sum_{s\in C'} \Delta_s + \sum_{t\in C''} \Delta_t = 0$, $\sum_{s\in C'} \Delta_s = -\sum_{t\in C''} \Delta_t$, $D = -\sum_{t\in C''} \Delta_t$. Note that $C'' \subseteq A$.

Step by step may be changed from the minimization distribution to another distribution by a consecutive q-shift $c_{j,i} = -\frac{\Delta_j \Delta_i}{D}$ from each cell j of C'' to each cell i of C', so that each shift is proportional both to Δ_i and Δ_j. $\sum_{i\in C'} c_{j,i} = -\sum_{i\in C'} \frac{\Delta_j \Delta_i}{D} = -\Delta_j$ and $\sum_{j\in C''} c_{j,i} = -\sum_{j\in C''} \frac{\Delta_j \Delta_i}{D} = -\Delta_i$.

Let $c_{u,v}$ be a shift with $u \in C''$, $v \in C'$, q_h^b, q_h^a quantities in the cell h $(0 \le h < n)$ respectively before (^{b}) and after (^{a}) the shift $c_{u,v}$.

Note that

$$\begin{array}{rcl} q_i^b \ge \overline{q}, \quad i \in C' \quad \text{then} \quad q_v^b & \ge & \overline{q}; \\ q_j^b \ge \overline{q}, \quad j \in C'' \quad \text{then} \quad q_u^b & \ge & \overline{q}; \\ q_k^b & \ge & \overline{q}, \quad k \in C. \end{array}$$

For v and u:

$$\begin{array}{rcl} |q_v^a - q_u^a| & = & |(q_v^b + c_{u,v}) - (q_u^b - c_{u,v})| \\ & = & |q_v^b - q_u^b + 2c_{u,v}| > |q_v^b - q_u^b| \quad \text{because} \quad q_v^b \ge q_u^b; \end{array}$$

$\{t/t \in C''\}$:

$$|q_v^a - q_t^a| = |q_v^b + c_{u,v} - q_t^b)| = (|q_v^b - q_t^b| + c_{u,v}) \quad \text{because} \quad q_v^b \ge q_t^b;$$

$$|q_u^a - q_t^a| = |q_u^b - c_{u,v} - q_t^b)| \ge (|q_u^b - q_t^b| - c_{u,v}); \text{ minimum value of } |q_u^a - q_t^a|$$
$$\text{when } q_u^b = c_{u,v} + q_t^b \text{ therefore } (|q_v^a - q_t^a| + |q_u^a - q_t^a|) \ge (|q_v^b - q_t^b| + |q_u^b - q_t^b|)$$

$\{t/t \in C' \vee t \in C\}$:

$$|q_u^a - q_t^a| = |q_u^b - c_{u,v} - q_t^b)| = (|q_u^b - q_t^b| + c_{u,v}) \quad \text{because} \quad q_t^b \ge q_u^b;$$

$$|q_v^a - q_t^a| = |q_v^b + c_{u,v} - q_t^b)| \ge (|q_v^b - q_t^b| - c_{u,v}); \text{ minimum value of } |q_u^a - q_t^a|$$
$$\text{when } q_t^b = c_{u,v} + q_v^b \text{ therefore } (|q_v^a - q_t^a| + |q_u^a - q_t^a|) \ge (|q_v^b - q_t^b| + |q_u^b - q_t^b|)$$

$\{(u,t)/u \ne v, t \ne u\}$:

$$|q_u^a - q_t^a \quad | = \quad |q_u^b - q_t^b|$$

therefore

$$\sum_{\{(i,j)/0 \leqslant i < j < n\}} (|q_i^a - q_j^a|) > \sum_{\{(i,j)/0 \leqslant i < j < n\}} (|q_i^b - q_j^b|)$$

A distribution is obtained q_i'' $(0 \le i \le n)$ by consecutive applications of all the shifts $c_{j,i}$, $j \in C''$ and $i \in C'$, starting from distribution q_i' $(0 \le i \le n)$; then (3.10) is proved.

This theorem demonstrates how the properties of the minimization algorithm are far broader than those demonstrated in Di Gregorio & Serra [42], where the minimization of the differences was demonstrated only in relation to the differences between the neighborhood cells and the minimum value, but not among all the cells of the neighborhood. This results from a broader perspective in bringing some phenomenologies into the context of CA and the possibility of more accurately and efficiently formulating their transition functions, in particular with regard to the evolution of the current version of LLUNPIY.

The algorithm of minimization of differences calculates flows minimizing the differences in height, but is rarely applicable in this extremely simple form, as the effect is to bring the neighborhood into a situation of hydrostatic equilibrium, thus minimizing the altimetric differences between the various cells.

The minimization algorithm is based on the average value for the 'height' of the cells, but in certain CA this specification is not obvious and can be misleading, e.g., for a cell whose physical correspondent is a portion of a building and a portion of a road. In such cases, an average value would falsify the simulation of a debris flow between the houses, resulting in a single intermediate portion in the cell that would correspond to a small non-existent building occupying the entire cell.

This situation can be resolved by an appropriate extension of the minimization algorithm.

3.4 Method of Conversion of Digital Geographical Data for Hexagonal Cells

Digital topographical maps (DEM, Digital Elevation Models) are represented through two-dimensional grids in which each 'cell' (each component of the matrix) contains the average altitude of the region of space that it represents. When a digital map contains information on many characteristics of the terrain, e.g., altitude, average erosion, etc., Digital Terrain Models (DTM) are being explained.

In this case, we are dealing with a set of square tessellation matrices, one for each characteristic (sub-state). The numeric values of the magnitudes considered (altitude, depth of soil erosion, depth of lava, etc.) are represented mathematically in the form of matrices, digitally in the form of two-dimensional arrays. This makes quite natural the management, and possibly manipulation, of DTM by the two-dimensional CA on matrices with square cells: indeed, it is sufficient to set the parameter p_c equal to the distance between two successive points on the DTM grid (map detail) to create a bi-unique correspondence between the CA cells and the points on the digital terrain model. In other words, for example, in the case of

topography, this makes the map of the sub-state 'altitude' of the CA and the DEM of the digital terrain map perfectly super-imposable. The same discussion does not apply, however, for CA with regular hexagonal tessellation.

One possible solution lies in the 'hexagonalization' of the DTM, i.e., carrying out a transformation that maps the square matrices of the DTM onto the grids of regular hexagonal cells. A method for the hexagonalization of digital terrain maps was proposed by D'Ambrosio et. al. [37]. The method maps a generic square cell matrix into a regular hexagonal cell matrix with a hexagonal apothem of $l/2$, with l being the side of the square (Fig. 3.2). For a DEM, the method consists in assigning to each hexagon of the new map the average altitude of the squares partially covered by the hexagon in question, weighted on the respective areal portions.

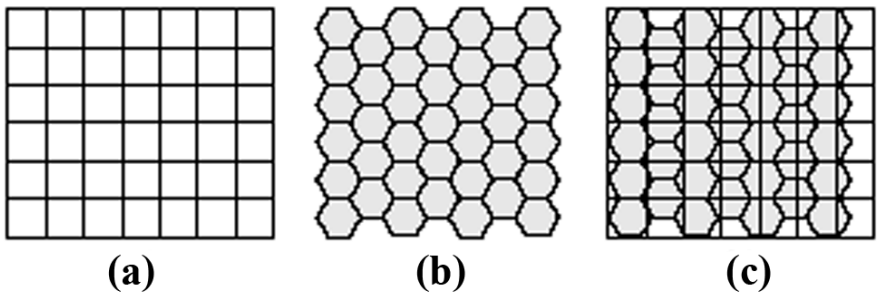

Fig. 3.2 Method of converting a matrix with square cells into a regular hexagonal cells matrix. (a) represents a generic matrix with square cells; (b) a matrix of regular hexagonal cells with an apothem of the hexagon equal to $a = l/2$, l is the side of the square of the first matrix; (c) the effects of overlapping matrices.

Fig. 3.3 illustrates a particular case of application of the method of hexagonalization. The same applies, obviously, for any other DTM information, such as an erosion map or a map of vegetation density in a given area.

3.5 Validation Phase of MCA Models

Two main phases are involved for verifying the reliability of MCA simulation models: the calibration phase identifies an optimal set of parameters capable of adequately reproduce the observed event and the validation phase, in which the model is tested on a sufficient (and different) number of cases similar in terms of physical and geomorphological properties. Once the optimal set of parameters is calibrated, the model can be considered applicable in

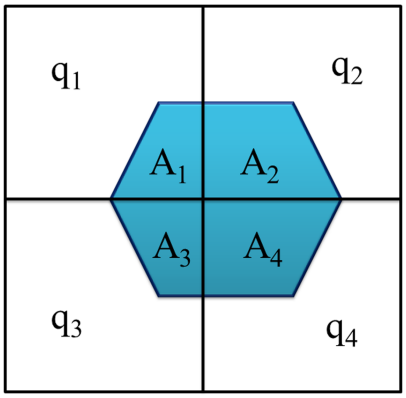

Fig. 3.3 A special case of hexagonalization procedure of the DTM: $q_1,..,q_4$ represent the altitudes of the cells of square cells matrix; $A_1,...,A_4$ the measure of the areas resulting from the intersection between the hexagon and the four squares involved in the process. The altitude of the hexagon, $q_{hexagon}$, is calculated using the following weighted average: $q_{hexagon} = \frac{\sum q_i A_i}{\sum A_i}$ with $i = 1,...,4$.

the same homogeneous geological context in which the parameters are derived, enabling a predictive analysis of surface flow hazard.

The likelihood between the cells involved by the real event and the cells involved in the simulation can be measured by the fitness function in relation to the dimensions d of cellular space:

$$f(R,S) = \sqrt[d]{\frac{R \cap S}{R \cup S}} \tag{3.11}$$

where R is the set of cells involved in the real event and S is the set of cells involved in the simulated event. This function ranges from 0 (completely wrong simulation) to 1 (perfect match between real and simulated events); values greater than 0.7 may be considered acceptable for two dimensions.

Chapter 4

Approaches to Modeling the Lahar Dynamics

"In all natural disasters through time, man needs to attach meaning to tragedy, no matter how random and inexplicable the event is"

Nathaniel Philbrick

4.1 Introduction to Lahar Phenomenology

Lahar is an Indonesian word originally used by Escher for a hot volcanic mudflow that had been generated by an eruption through a crater lake [47]. This expression specifically applied to the 1919 volcanic mudflows originating from the crater lake of Mt Kelut on Java, which inundated over 130 km^2 of the surrounding lowlands, causing approximately 5,000 casualties [61]. Escher proposed to classify volcanic mudflows according to whether: a) there had been an eruption through a crater lake producing a hot mudflow (a true lahar), b) there was ice-cap melting that producing a jökulhlaup (an Icelandic term signifying flooding resulting from the melted ice following a volcanic eruption) or c) there had been a cold mudflow generated by heavy rains on loose volcanic materials [47]. The terms Lahar was introduced into the volcanological literature through the work of Schimdt [131] and van Bemmelen [13], and is widely used in literature as a synonym of "volcanic mudflow or debris flow" [27] [50] [115] [139].

Lahars are one of the most dangerous and destructive natural events to communities located near volcanoes. As the flows of sediment and water travel down the volcano's

flanks, they incorporate a large quantity of sediment and rock fragments, making lahars very destructive. In fact, along the path on volcanic flanks, its size and speed are constantly changing. The initial flow can incorporate water from melting of snow or glaciers (if present), river or rainfall water, and erode rocks and tephra (volcanic debris of previous volcanic activities) increasing easily to more than 10 times their initial size. As it moves away from the volcano and with decreasing of slope, the lahar begins to lose its heavy load of sediment and decrease in size.

During motion, a lahar looks like a mass of dense mud that carries rock debris ranging in size from clay to boulders more than 10 m in diameter. This represents, together with debris origin, the principal difference with debris flows that range in size from 104 m^3 to 107 m^3 [155]. They are capable of moving up to 60-70 m/s and may travel for hundreds of kilometers. In particular small lahars less than a few meters wide and several centimeters deep may flow a few meters per second, large lahars hundreds of meters wide and tens of meters deep can flow several tens of meters per second.

Lahars almost always occur on or near stratovolcanoes because these volcanoes tend to erupt explosively and theirs steep cones are often snow covered, topped with a crater lake, constructed of weakly consolidated rock debris that is easily eroded, or again internally weakened by hot hydrothermal fluids.

Eruptions may trigger one or more lahars directly by quickly melting snow and ice on a volcano or ejecting water from a crater lake. More often, lahars are formed by intense rainfall during or after an eruption, in fact rainwater can easily erode loose volcanic rock and soil on hillsides and in river valleys.

These gravity flows descend valleys, but their large volume enables them to overflow their and invade lateral areas of at low gradient. Lahars racing down river valleys and spreading across flood plains tens of kilometers downstream from a volcano. The direct impact of a lahar's turbulent flow front or from the boulders and logs carried by the lahar can easily crush, abrade, or shear off at ground level just about anything in the path of a lahar. Buildings and land may become partially or completely buried by one or more layers of volcanic debris. This result in distal communities being unexpectedly inundated, sometimes with catastrophic consequences, often cause serious economic and environmental damage.

This chapter reviews characteristics and fundamentals of lahar generation, as well as approaches that have been adopted for modeling lahar behavior, which are variously informed by theoretical analysis and assesses their strengths and weaknesses.

4.2 Lahar Triggering Mechanism

According Manville [97], initiation mechanism can greatly influence lahar volumes, compositions, flow behavior and hazards. Lahars may be broadly subdivided into two categories based on their initiation: *primary lahars* that are originated by direct volcanic eruptive activity (e.g., the 1985 Nevado del Ruiz event in Colombia [113]), for instance, when lava or pyroclastic flows melt snow and glacier and/or mix with wet soil; another cause during an eruption can be the breakout of crater lake or expulsion of crater lake waters [97][116].

In contrast, *secondary lahars* may occur in post-eruptive events or quiescent periods (e.g., the 1991 eruption of Mt. Pinatubo, Philippines [123]), when heavy rainfalls–rainwater can easily erode loose volcanic rock and soil on hillsides and in river valleys, typhoons or lake breakout mobilize ash and other volcanic debris of previous volcanic activities.

Lahar genesis requires certain preconditions, including: (1) an adequate water source; (2) abundant unconsolidated volcanic debris (tephra); (3) steep slope with high gravitational potential; and (4) a triggering mechanism [154].

The scenarios listed below illustrate most of the mechanisms by which lahars are generated.

4.2.1 Primary Lahars Triggering

Lahars Triggered by Melting Snow and Ice

Many of the largest and most destructive historical lahars were accompanied by volcanic eruptions of volcanoes covered by a substantial mantle of snow and ice, such as:

1. Pyroclastic flows which are the most common volcanic events that generate lahars. For instance, the lahars that occurred at Mount St. Helens during its catastrophic eruption on May 18, 1980 [110]. A similar event occurred in the Nevado del Ruiz volcano (Colombia) in 1985 [113]. These lahars were triggered by the sudden melting of snow and ice from hot volcanic rocks ejected by the initial explosive activity and subsequent pyroclastic flows [92].

2. Lava flows which moving slowly across snow usually do not melt snow and ice rapidly enough to form large lahars but the eruption of lava beneath a glacier can result in substantial ponding of water. It happened in the Llaima volcano (Chile) in 1979 and Villarrica volcano (Chile) in 1984 when incandescent lava flows crossed the glacier surface, generating lahars that flowed down the slopes of volcanoes [92].

3. Snowmelt triggered by basal heating of a glacier. This process has been observed in Iceland. An example is what happened in the Katla volcano in 1918. The largest historic lahars in terms of discharge (volume of material per second) have occurred in Iceland, where these glacial outburst floods are called Jökulhlaups [92].

Lahars Caused by Collapse of Crater Lake

During an eruption, if crater lake is present, are possible lahars caused by breakout of crater lake or expulsion of crater lake waters. This phenomenon was observed in the New Zealand's worst volcanic disaster, the 1953 Tangiwai lahar, causing 151 casualties, was generated by partial failure of the rim of Mt Ruapehu's Crater Lake after the 1945 eruption. Most recently, post 1996 refilling of the lake behind a barrier of unconsolidated tephra laid down during the 1995/96 eruption sequence culminated in breaching and failure of the dam on 2007, resulting in the release of 1.3 million m^3 of water and generation of the largest historic lahar at the volcano [95].

Lahars Triggered by Phreatic Explosions

A volcanic eruption caused by the interaction of hot magma with groundwater is named phreatic eruption. The water that surrounding the magma is heated and transformed into steam. When the steam expanding exceeds the confining pressure produces a phreatic eruption, not necessarily accompanied by volcanic eruption. The release of large amounts of water combined with volcanoclastic detrital, accumulated along the volcano flanks, is able to generate lahars. Is this the case of some lahars generated by Mount St. Helens eruption of 1980 [75].

4.2.2 Secondary Lahars

Torrential Rain after Volcanic Activity

After a volcanic eruption, the erosion of new loose volcanic deposits in the river valleys or along slopes can lead to severe flooding and extremely high rates of sedimentation in areas far downstream from a volcano. Common triggers include mobilization of ash and other volcanoclastic debris by flowing water, due chiefly to rainfall runoff [97]. These events can bury entire towns and agricultural land downstream. Also, although if no lahars occur, the erosion can lead to frequent floods because of the deposition of sediment along the river channels.

Events as the rain-triggered lahars at Mount Pinatubo (Philippines) after the enormous eruption on June 15, 1991, destroyed roads and bridges, buried farmland and towns with sediment. Thousands of lahars have occurred since 1991, and nearly all were triggered by intense rainfall [114].

Similar cases have been observed in volcanoes Mayon (Philippines), Unzen (Philippines) and Merapi (Indonesia) [151].

Lahars Caused by Lake Breakouts

High-altitude lakes tend to form in volcanic craters – where they are called crater lakes – or in valleys dammed as the result of earthquakes or glacial or volcanic deposition. Lake breakouts commonly occur weeks to months after that river or one of its tributaries become blocked by a landslide or other volcanic deposits, especially pyroclastic flows and lahars.

The most frequent cause of a lake breakout is the overflow of water across the newly formed dam and subsequent erosion and rapid downcutting into the loose rock debris. As more water rushes outwards from the lake, the initial channel grows deeper and wider, further increasing the flow. By eroding the blockage and flowing out river channel downstream, the initial surge of water will incorporate a tremendous volume of sediment and increase in volume two to four times or even more. This produces violent floods and lahars with devastating effects for any settlements in their path.

4.3 Lahar Phenomenology

It is necessary to detail some of the features of lahar types and behavior, before a discussion of lahar modeling. The term ‘lahar’ has evolved in such a way to include both mudflows and debris flows, and later hyperconcetrated flows, on the flanks of a volcano. Although the term has sometimes been used to refer to the deposits of such flows, Smith and Fritz (1989) dismiss this meaning stating that "lahar is an event that can refer to one or more distinct processes, but does not refer to a deposit" [141]. This has led to the more generally accepted definition: Lahars are highly mobile mixtures of material of volcanic origin and water occurring on and around volcanoes [154], other than normal streamflow [142]. This definition describes the flow but not the resultant deposit.

Independently of the causes that generate lahars, these, once triggered, can undergo multiple and reversible spatial and temporal transformations in flow behavior, for example, from hyperconcentrated flow to debris flow and vice versa, which is explained by the increase (bulking) and loss (debulking) of water or material along of its travel. [154].

Bulking, in both the types of lahar, occurs by soil erosion and/or incorporation of water, along streams. Unconsolidated pyroclastic material, where the redistribution of volcanic sediment can continue for months to years after an eruption [91][96], it can be easily eroded by superficial water forming dilute sediment-laden flows that can bulk-up to debris flows whose magnitude will depend upon the volume of both the water and remobilized material [11]. For both types of lahar, flowing matter is modeled to be produced by two main mechanisms: (1) a mobilization process of tephra (pyroclastic stratum that could contain some exotic material) is caused by percolation of an adequate water quantity on abundant unconsolidated sediment, and (2) an erosion process that depends of the impact of lahar with high kinetic energy on the soil (that could contain more pyroclastic matter than exotic material or vice versa), where such an erosion could be facilitated (but not caused) by rainfall water percolation. Flood evolves along the volcano steep slopes with high gravitational potential energy, contemporary possible bulking by water inclusion along watercourses or lakes, and water extrusion and deposit formation process occurs in flat zones of the final phase (see Fig. 4.1).

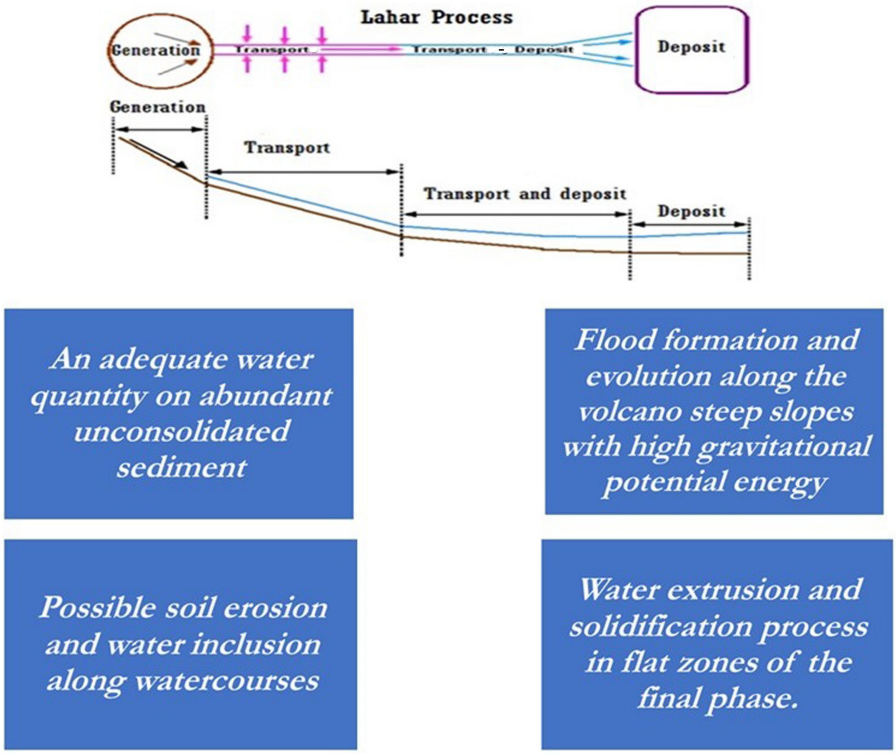

Fig. 4.1 Lahar phenomenology process.

As mentioned above, they hyperconcentrated flows and debris flows can form different types of lahar, which are classified on the base of their percentage of water and sediment. Because the estimate of this parameter should be made during the development of lahar process, its measurement is dangerous; likewise, it is essential to be in the moment in which the event occurs, which is not always possible. An alternative way to differentiate the various lahar flows is the characterization of their rheological, hydraulic, geomorphological and sedimentological properties [25], which are described below.

Rheology is the study of the flow of matter, primarily in a liquid state, but also as 'soft solids' or solids under conditions in which they respond with plastic flow rather than deforming elastically in response to an applied force [132] [107]. In the lahars, this force is normally gravity. For a fluid flowing between two parallel plates, the force per unit area required to produce the motion is known as the 'shear stress', and the rate at which a shear is applied is the 'shear rate'; for simple shear, the shear rate can be considered a gradient of velocity that is established in the fluid. Different types of fluids behave differently under stress.

The fluids are divided into two types: Newtonian and non-Newtonian. A Newtonian fluid, such as water, has a viscosity (colloquially referred to as 'resistance to flow') proportionately constant between the shear stress and the shear rate. A non-Newtonian fluid is defined as one for which the gradient of stress-strain-rate relationship (known as dynamic viscosity) is not constant. There are several types of non-Newtonian flow behavior, characterized by the way a fluid's viscosity changes in response to variations in shear rate (see Fig. 4.2).

Strictly lahars are non-Newtonian fluids; their flow (rheological behavior) is dependent upon lahar composition, scale, time and shear-rate [111]. The rheological differences of lahar flows are:

- *Normal stream flows* are typically multiphase (water and sediment) and behave as Newtonian fluids, provided sediment concentrations are low enough so that the dispersed particles do not interact [111].

- *Hyperconcentrated flows*, water and solids behave as separate phases; the fluid starts to acquire yield strength and becomes non-Newtonian [111]. Flow is intermediate between dilute, fully turbulent, normal stream-flow and viscous generally non-turbulent debris-flow [140]. Fluid is the transporting medium, with clasts supported by turbulence, buoyancy and, to a lesser extent, particle-particle interactions [111].

- *Debris flows* are denser than hyperconcentrated flows, and flow starts to behave as a coherent, plastic single-phase mass driven by inertial forces [48]. The physics of debris flows are comprehensively discussed by Iverson (1997) [73].

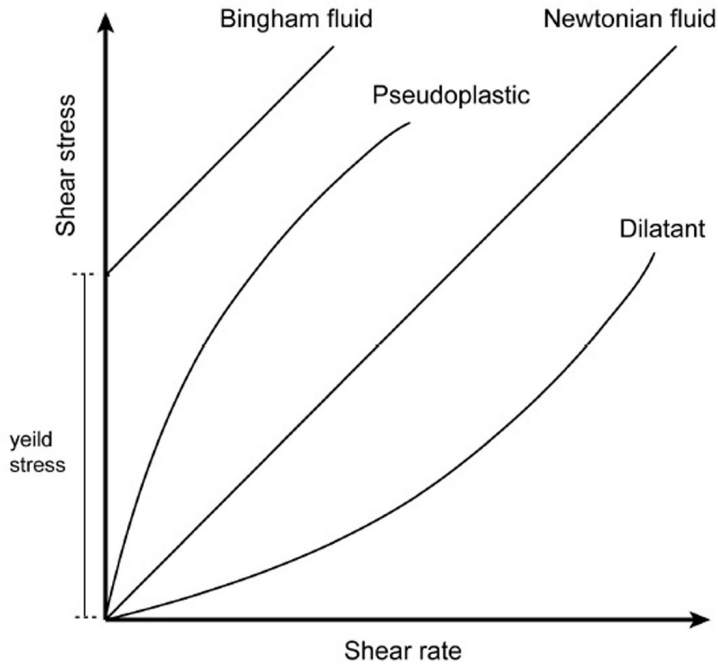

Fig. 4.2 Relationship between shear strees and shear rate for different models of flow behavior [105].

The transition between 'normal' stream flow and hyperconcentrated flow occurs at the boundary between Newtonian and non-Newtonian fluid [68]. In this manner, the sediment: water ratio for different flow types depends on the ability to acquire yield strength. Stream flows have been calculated at a sediment concentration below 3 — 10 % [112] or 20 % by volume [82]; hyperconcentrated flows between 20 and 50 — 60 % by volume, and debris flows above 50 — 60 % [82].

4.4 Lahar Modeling

A variety of approaches has been used to model the behavior of lahars and the hazards posed to downstream communities [97]. In this way, lahar models available for runout analysis can be divided into different classes (empirical, analytical, simple flow routing and numerical) and operate in different spatial dimensions (one-dimensional and two-dimensional). A few of the main approaches from the literature will now be discussed.

1. *Empirical models* based on observed correlations of phenomenon among lahar parameters such as volume, flow velocity and inundation area. They predict the average behavior of future lahars without regard for the underling flow physics.

A Geographic Information System-based model, LAHARZ, was developed from statistically-based coefficients extracted from a database of numerous lahars (27 individual events). The statistics relate total-lahar-volume with inundated cross-sectional area and inundated planimetric area [130][102]. LAHARZ, calculates inundation limits of specific drainages for lahars having a range of user-specified volumes by 'filling' a DEM rendering of the valley topography. A major assumption of this model is that the deposit volume is equal to that of the lahar.

2. *Single-phase rheological models*. A range of single-phase rheological models exists to describe lahar behavior. These models developed on observations of debris-flow and deposit geometry, supplemented by rheological measurements on sub-samples of deposits reconstituted into slurries. The models all assume that a constant stress-strain-rate relationship, suitable for an idealized, homogeneous, single-phase material, adequately describes debris-flow behavior. The simplest non-Newtonian rheological model describes a Bingham viscoplastic material, with a viscosity independent of shear rate.

3. *Hydrologic flow models*. Another approach to modeling lahars is the use of conventional surface-flow as a Newtonian fluid. Hydrologic and hydraulic routing are used as main techniques. Hydrologic routing is based on mass conservation on a reach-by-reach basis. Although this model is potentially useful for roughly approximating the broad-scale evolution of a lahar hydrograph, the technique assumes that a lahar can be characterized as a Newtonian flow.

4. *Hydraulic models*. Hydraulic flow-routing simultaneously solve mass and momentum conservation equations (known as the Saint-Venant or shallow water equations) subject to an input hydrograph boundary condition, channel geometry and an energy dissipation expression. Costa [26] reviews the various simplifications that have been applied to achieve tractable solutions to the hydraulic routing of lahars. Such simplifications are necessary because of the poorly understood ways in which energy dissipation in lahars differs from that in water flows [73].

   For these reasons some authors have adopted the fully dynamic hydraulic flow routing model [26] [94], DAMBRK [51], which solves the full Saint-Venant equations to model unsteady, nonuniform flows. However, the problem remains of the differing energy dissipation mechanisms of lahars with respect to water flows. Energy losses are generally treated with an empirically determined parameter such as the Chezy coefficient, C, or the Manning coefficient, n. Furthermore, these hydraulic routing models are unable to treat volume losses or additions during transit [48].

5. *Coulomb mixture theory*. This approach use separate equations for the conservation of mass and momentum of the solid and fluid components of a flow of granular material, and coupling terms that link the momentum equations of the separate phases [73] [74].

   Titan2D [134] is a program originally developed for the dry granular flow of debris avalanches and is based on the earlier work of Savage and Hutter [129], Iverson [73], Iverson and Denlinger [74], Denlinger and Iverson [39]. Similar to the shallow water equations, the conservation equations for mass and momentum are solved, but with a Coulomb-type (dry, sliding) friction term for the interactions between grains and between the granular material and the basal surface.

   A two-phase version of Titan2D has been developed that allows fluid flow with granular flow [163] [119]. Williams et al. [163] coupled Titan2D [117] and the Pitman-Le two-phase debris-flow model [118] to enable the simulation of more types of gravitational mass flows. The new model was applied to Tungurahua (Ecuador) lahars [163] and Ruapehu (New Zealand) lahars [119].

4.5 Some Considerations

Computer models have been used intensively in the last years to evaluate and map hazards associated with lava flows, pyroclastic flows, ash fall and lahars. These models use different approaches to simulate the extension and characteristics, and sometimes the dynamics, of the flows associated with each hazard. These approaches vary from statistical–empirical data-based models with correlation parameters that do not take into account the physics of volcanic processes (e.g., LAHARZ; [130]), to very complex ones that take into account the physical and environmental variables needed to derive and solve governing equations, e.g., TITAN2D [24].

Lack of precise information (e.g., quantitative data and direct measurements of large-magnitude flows which are generally difficult to obtain) on lahar events can generate various problems for applying these methods to simulation. Nevertheless, numerical modeling remains an important tool for risk management in threatened regions. In a correct approach to lahar modeling, flow parameters with their uncertainties should be defined first and, more importantly, should be validated through the comparison between field studies and simulated inundation areas.

The previous listed mechanisms were modeled according to the methodological approach of Multicomponent (or Macroscopic) Cellular Automata (MCA) [42][1][5] for computer simulation of surface flows: water percolation (e.g., model SOIL [42] and model SCAVATU [7]); soil detachments evolving in debris, mud, granular flows (family of models SCIDDICA

[36][3] [4]) and deposit formation can be described in terms of viscosity variation by water loss (in similar equational way as viscosity variation of lava flows by cooling in SCIARA model [42][2][38]).

The CA approach is based on the definition of 'simple', but fundamental, local rules that have to observe conservation physical laws in the context of space and time discretization. Such rules have to capture the significant interacting processes. The phenomenon evolution 'emerges' by local interactions: 'simplest' rules can generate very complex realistic behaviors.

Chapter 5

The LLUNPIY MCA Model

"...in the library of mathematics, the physicist does not find solutions ready made, in constructing a mathematical relation between things he must be an artist."

Dennis Flanigan

5.1 Introduction

Due to the recent technological advances, computer simulated models have become widely used by the scientific community to predict the distribution of catastrophic events to mitigate possible damage to population located in a risk area. Volcanic eruptions can generate directly (primary lahars) or indirectly (secondary lahars) catastrophic surface flows that are a mixture of volcanic debris and water occurring on and around volcanoes.

Lahars are very complex dynamical systems, very difficult to be modeled: they can grow by soil erosion and/or incorporation of water, along watercourses. Unconsolidated pyroclastic material [91] [96], can be easily eroded by superficial water forming dilute sediment-laden flows, that can bulk-up to debris flows whose magnitude will depend upon the volume of both the water and remobilized material [11].

Surface flows are a typical application of Multicomponent (or Macroscopic) Cellular Automata [42] [1] for computer simulation: SCIARA model for lava flows [2], SCIDDICA [4] for debris flows, PYR [32] for pyroclastic flows, VALANCA [6] for snow avalanches, SCAVATU [36] for soil erosion by rainfall.

A very important characteristic of all these models is that they are based on two-dimensions CA, but they work effectively in three dimensions because the third dimension is enclosed in part of the sub-states: altitude, kinetic head, lahar thickness, depth of erodible pyroclastic stratum, and so on.

This chapter describes a model that has been well-developed for simulating lahars in terms of complex system evolving on the base of local interaction. **LLUNPIY** (**L**ahar modeling by **L**ocal rules based on an **UN**derlying **PI**ck of **Y**oked processes, from the Kichwa word llunp'iy meaning flood), is a deterministic CA model for simulating primary and secondary lahars, taking into account experience and solutions matured in the elaboration of previous models. Anyway, numerical modeling remains an important tool for hazard management in threatened regions.

5.2 LLUNPIY Main Specification

CA modeling and simulation of real complex 'macroscopic' systems implies that a time-space correspondence must be explicitly established between the model and the real world in order to compare phenomenon development with simulation progress; the cell has to correspond to a precise space portion, and the transition step has to correspond to a time interval. Moreover, cell state must account for components, which are related to various characteristics of the space portion and the *transition function* must account for a complexity of interrelating processes of similar or different nature.

Multicomponent Cellular Automata (MCA) characterize such a methodological approach for modeling complex systems, especially macroscopic phenomena, that need many components both for the *states* (sub-states) with the purpose to account for different properties of the cell and for the transition function ('elementary' processes), in order to describe local processes constituting the overall phenomenon. Besides, some *parameters* (e.g., cell dimension, temporal correspondence of a MCA step, etc.) are generally considered, which allow to 'tune' the model for reproducing different dynamical behaviors of the phenomenon, by taking into consideration their physical/empirical meaning. At the beginning of the simulation, cell states are initialized through input values (e.g., by means of matrices). Model parameters have also to be allocated in this phase. By simultaneously applying the transition function, τ, to all cells and at discrete steps, states are changed and the evolution of the phenomenon can be simulated. Sub-states permit to operate in three effective dimensions by two-dimensional MCA, if all the quantities concerning the third dimension may be expressed as sub-states; this is the case of LLUNPIY, which adopts a hexagonal tessellation, assuring the lowest

anisotropy for two-dimensions CA and minimizes the problem of spurious symmetries [161][166].

Furthermore, a MCA step is an ordered sequence of applied elementary processes and every elementary process implies the MCA state updating.

Eventually, the investigated phenomenon involves external influence which cannot be described in terms of local rules (e.g., the rain), so a kind of input from the 'external world' for some cells has to be introduced in MCA approach [42][7].

Lahars are modeled by LLUNPIY in three main phases (Fig. 5.1), explained in the following. *Generation phase*: In the case of primary lahars, these are generated from pyroclastic flows and melting of the volcano's icecap, due to interaction of eruptive products with a summit glacier. In the case of secondary lahars, heavy rainfalls mobilize abundant unconsolidated sediments in steep slopes by percolation of an adequate water quantity, that determines the collapse of cohesion forces of the soil components. *Flood phase*: lahar flows develop along the volcano steep slopes with high gravitational potential energy and turbulence with possible bulking by soil erosion and water inclusion along watercourses. *Exhaustion phase*: the lahar flow reduces its kinetic energy and velocity in flat areas; rapid decrease of turbulence causes deposit formation by water extrusion. In this latter, in some cases, lahar can partially 'be diluted' and 'disappear', if it runs into a watercourse with a water flow, sufficiently large to englobe the lahar matter.

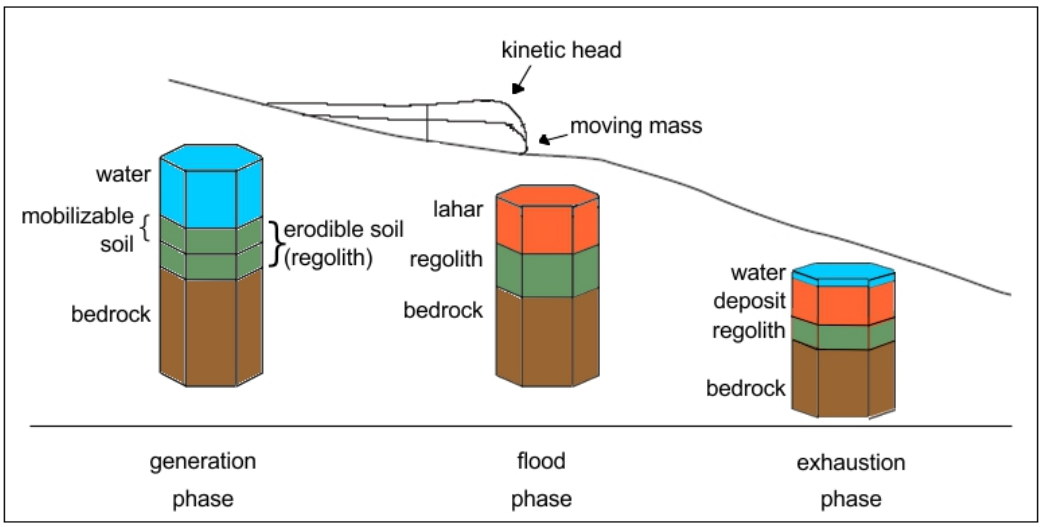

Fig. 5.1 Representation of the three phases: generation phase before the collapse of the mobilizable stratum of regolith; flood phase with the lahar; exhaustion phase with lahar deposit and extruded water.

The generation phase of the primary and secondary lahars differ only for the generation phase: Primary lahars are modeled in LLUNPIY by specifying the direct interaction between

the volcanic product and the water source; the melting of ice and snow could be produced by pyroclastic bombs or lava flows. This version of LLUNPIY specifies in a simple way such as interaction: pyroclastic bombs are generated according an opportune stochastic function that mimics the melting of ice/snow and mixing of pyroclastic matter with water. Lava flows interactions with ice/now could be easily implemented by version of SCIARA model, that has to be included in LLUNPIY. Lava flows melt ice/snow in its path and generates flows of water mixed with pyroclastic ash. Lava flows and pyroclastic bombs can fill a crater lake with water expulsion; this case was not explicitly considered in LLUNPIY, but the water modeling on a surface (the crater surface) with no possible percolation may be perfectly adopted to such a situation. Furthermore, bombs and opening of vents can destroy or distort part of crater walls, this occurrence is considered in LLUNPIY as the initial conditions.

With regard to Secondary lahars, a rainfall history is specified by real data or by stochastically produced realistic data. Pyroclastic soil cover (regolith) is represented by two soil strata with averaged physical features such that nearly saturation conditions can appear in the former one by water percolation. The two strata constitute the erodible soil, i.e., the regolith (Fig.5.1). Depths of the strata are deduced by soil tomography data [122]. The detachment/mobilization of the former stratum depends on degree of stratum saturation and cell slope. The produced lahar accounts for a percent of pyroclastic material and water content from percolation, lahar viscosity is depending on water content. Note that water content is referred only to gravitational water and excludes irreducible (immobile) water and capillary water, that is considered at the maximum value during the phenomenon evolution [43].

Another essential point on flood phase, free water from rainfall on the soil surface interacts with mobilized pyroclastic cover; the two flows mix according to a threshold of kinetic energy of lahar. The mix is specified as lahar with an increased percent of water from absorbed water. The Minimization Algorithm [42] is applied in two different versions and rules water flows and lahar flows. The lahar inside a cell is modeled as a ‘cylinder’ tangent the next edge of the hexagonal cell with mass, velocity and barycenter co-ordinates. Such ‘cylinders’ are modeled moving toward the center of adjacent cells with mass, final velocity and barycenter final co-ordinates. Three cases are possible for outflows toward adjacent cells: internal flows (cylinder remains all inside the cell after the shift), external flows (cylinder is all outside the cell after the shift) and the mixed case. Lahar momentum is determined according to velocities of inflows and outflows. Soil erosion is depending on the kinetic energy of the lahar inside the cell, eroded soil mixes with lahar. Energy loss by turbulence (that is proportional to kinetic energy) is considered.

Exhaustion phase: maximum water content in lahar is depending on its kinetic energy, water surplus is released as free water running in surface upon lahar, while lahar viscosity grows until complete deposition occurs below a threshold of water content.

5.3 Formal Definition of LLUNPIY

The LLUNPIY model is a two dimensional CA with a hexagonal tessellation and is formally defined by the septuplet:

$$\langle R, G, X, S, P, \tau, \gamma \rangle \tag{5.1}$$

where:

- $R = \{(x,y) | x,y \in \mathbb{N}, 0 \leq x \leq l_x, 0 \leq y \leq l_y\}$ is the set of points with integer co-ordinates, that individuate the regular hexagonal cells, covering the finite region, where the phenomenon evolves. $\mathbb{N}$ is the set of natural numbers.

- $G \subseteq R$ is the set of cells, where lahar is formed when pyroclastic matter melts ice (the case of primary lahars) or cells effected by rainfall (the case of secondary lahars).

- $X = \{(0,0),(1,0),(0,1),(-1,1),(-1,0),(0,-1),(-1,-1)\}$,the neighborhood index, identifies the geometrical pattern of cells (Fig. 5.2a), which influence state change of the 'central' cell: the central cell (index 0) itself and the six adjacent cells (indexes $1,...,6$). The sum of opposite indexes with reference to the central cell is always 7, in order to specify easily opposite directions with x and $7-x$ (Fig. 5.2b).

- S is the finite set of states of the finite automaton, embedded in the cell; it is equal to the Cartesian product of the sets of the considered sub-states (Table 5.1).

  Table 5.1 reports the names of the sub-states; they are individuated in the 'Sub-states'column by a shortening in the subscript of 'S', the corresponding letters to the shortening are written in bold in the 'Description' column.

- P is the set of the global physical and empirical parameters, which account for the general frame of the model and the physical characteristics of the phenomenon (Table 5.2).

  The choice of some parameters is imposed by the desired precision of simulation where possible, e.g., cell dimension; the value of some parameters is deduced by physical features of the phenomenon, e.g., turbulence dissipation, even if an acceptable value is

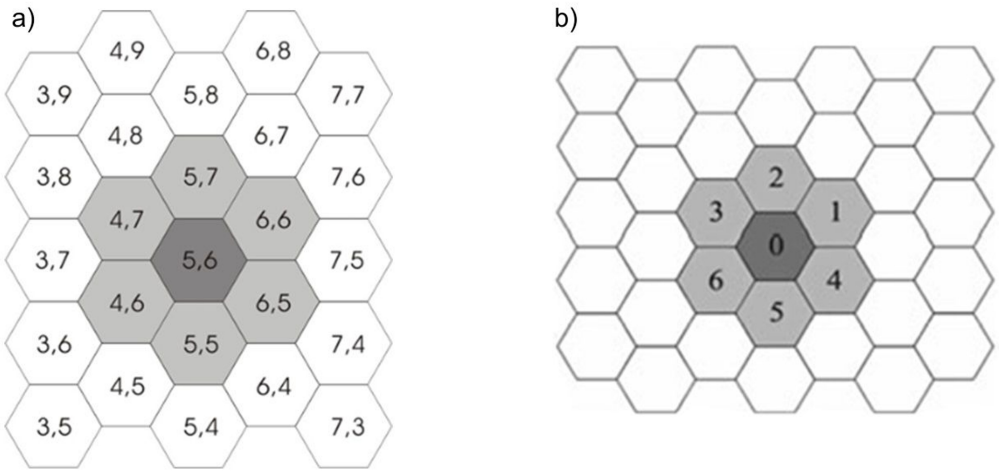

Fig. 5.2 (a) The neighborhood of the cell (5,6); (b) neighborhood indexes in LLUNPIY model.

fixed by the simulation quality by attempts, triggered by comparison of discrepancies between real event knowledge and simulation results.

- $\tau : S^7 \rightarrow S$ is the cell deterministic state transition in R, it embodies the SCIDDICA-SS2 elementary processes, furthermore introducing two new ones in order to account to characteristics of the lahar dynamics: the following main components of the phenomenon:
  * σ_{wf}, water flow
  * σ_{wp}, water percolation
  * σ_{psm}, pyroclastic stratum mobilization
  * σ_{lf}, lahar flow
  * σ_{se}, soil erosion
  * $\sigma_{\mathrm{wi\&eld}}$, water inclusion, extrusion and process of lahar complete deposition
- $\gamma_1 : N \times G_g \times S_{\mathrm{IT}} \times S_{\mathrm{A}} \times S_{\mathrm{LT}} \rightarrow S_{\mathrm{IT}} \times S_{\mathrm{A}} \times S_{\mathrm{LT}}$ for primary lahars which express the 'external influence' of the fall of the pyroclastic matter on glacier (G_g cells) and consequently ice state change in lahar with the addition of pyroclastic matter at the initial CA step. N is here referred to the step number (Fig. 5.3).
- $\gamma_2 : N \times G \times S_{\mathrm{WL}} \times S_{\mathrm{WKH}} \rightarrow S_{\mathrm{WL}} \times S_{\mathrm{WKH}}$ for secondary lahars expresses the raining water quantity to be added for G cells at each CA step. N is here referred to the step number (Fig. 5.4).

Table 5.1 Sub-states

Sub-states	Description
$S_A, S_{\mathrm{D}}, (S_{\mathrm{D1}}, S_{\mathrm{D2}})$	cell **A**ltitude, tephra stratum **D**epth, that could be divided in upper erodible stratum (D1) and lower stratum (D2) if data are available
$S_{\mathrm{SR}}, S_{\mathrm{SWC}}, S_{\mathrm{MIR}}$	mobilizable stratum: **S**tratum **R**eceptivity, **S**tratum **W**ater **C**ontent, **M**ax **I**nfiltration **R**ate
$S_{\mathrm{WL}}, S_{\mathrm{WKH}},$ $S_{\mathrm{WO}}, S_{\mathrm{WKHO}}$	**W**ater **L**evel, **W**ater **K**inetic **H**ead, **W**ater **O**utflows, **W**ater **K**inetic **H**ead of **O**utflows (6 components)
$S_{\mathrm{IT}}, S_{\mathrm{LT}}$	**I**ce **T**hickness, **L**ahar **T**hickness
$S_{\mathrm{KH}}, S_{\mathrm{LWC}}$	Lahar **K**inetic **H**ead, **L**ahar **W**ater **C**ontent
$S_{\mathrm{X}}, S_{\mathrm{Y}}$	the co-ordinates **X** and **Y** of the lahar barycenter
$S_{\mathrm{MX}}, S_{\mathrm{MY}}$	the components **x** and **y** of the lahar **M**omentum
$S_{\mathrm{E}}, S_{\mathrm{EX}}, S_{\mathrm{EY}}, S_{\mathrm{KHE}}$ (6 components)	**E**xternal flow normalized to a thickness, **E**xternal flow co-ordinates **X** and **Y**, **K**inetic **H**ead of **E**xternal flow
$S_I, S_{IX}, S_{IY}, S_{KHI}$ (6 components)	**I**nternal flow normalized to a thickness, **I**nternal flow co-ordinates **X** and **Y**, **K**inetic **H**ead of **I**nternal flow

At step 0, cells are in states that correspond to the initial conditions of the system to be simulated; the CA evolves by applying simultaneously the function γ to cells in G, and by applying simultaneously the state transition function τ to neighborhoods of all the cells. A step is given by the consecutive application of γ and τ.

5.4 The LLUNPIY Transition Function

In the formulas, a sub-state is specified by S, its right subscript is a shortening of the sub-state name in capital letters (e.g., S_A, the sub-state altitude), if the left subscript is not specified the

Table 5.2 Physical and empirical parameters

Parameters	Description
p_a, p_t	cell **a**pothem (m), **t**emporal correspondence of a CA step (s)
p_{fc}, p_{wfc}	lahar and water **f**riction **c**oefficient parameters (-)
$p_{td}, p_{ed}, p_{pe}, p_{mt}$	lahar parameters: **t**urbulence **d**issipation (-) and **e**rosion **d**issipation (-) of energy; lahar parameter of **p**rogressive **e**rosion (-), **m**obilization **t**hreshold (m),
p_{slt}, p_{wct}	**s**lope **t**hreshold ($^\circ$),**w**ater **c**ontent **t**hreshold ($\%$)
p_{khl}	**k**inetic **h**ead **l**oss (m)
$p_{dft}, p_{adh1}, p_{adh2}$	lahar complete **d**eposit **f**ormation **t**hreshold ($\%$), minimum **adh**erence (m), maximum **adh**erence (m)

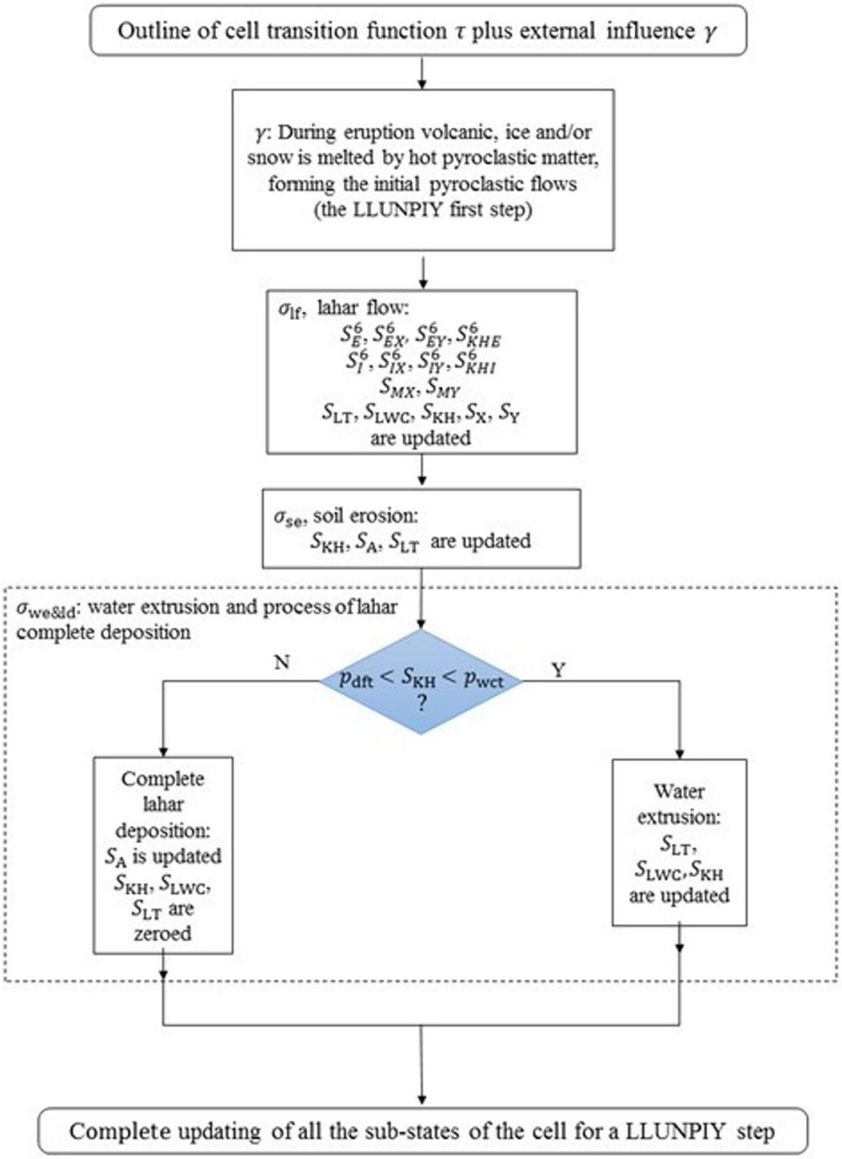

Fig. 5.3 Flow diagram for functions γ and τ for primary lahars.

sub-state is related to the central cell of the neighboring and other cells of the neighboring are not considered, otherwise the left subscript specifies the index of the neighboring cell, when other cells of the neighboring are considered (e.g., ${}_1S_A$, the sub-state altitude of the cell with index 1 in the neighboring). S'_X indicates the updated value of the generic sub-state S_X. ΔS_X means S_X value variation.

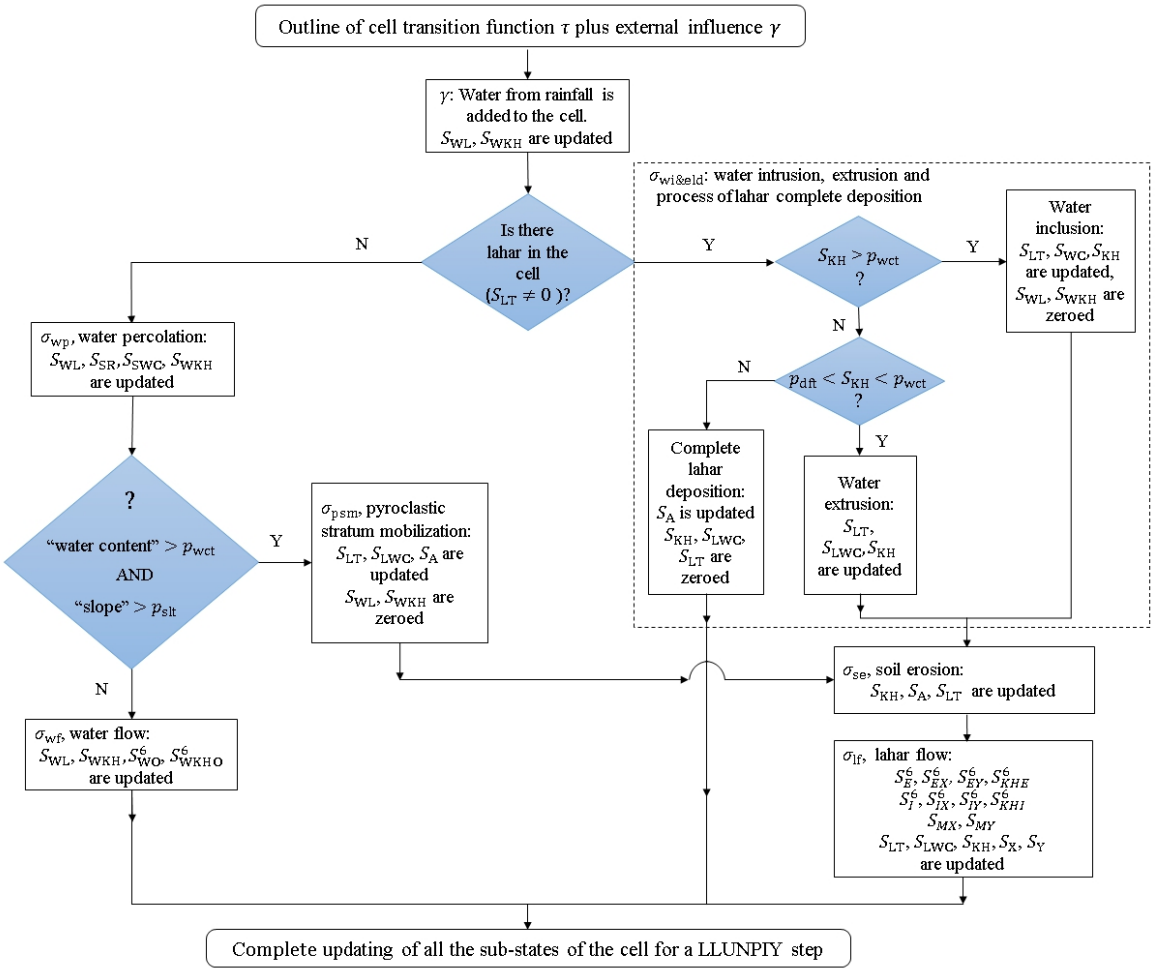

Fig. 5.4 Flow diagram for functions γ and τ for secondary lahars.

Quantities related to volumes as raining water and maximum infiltration rate in a step, stratum receptivity, stratum water content, outflows are normalized to lengths, because the cell area is constant in value.

Computations of lahar and water flows are based on two different applications of the Algorithm of the Minimization of Differences (AMD) [42][5]. The common base involves the determination of minimizing outflows f_i $(1 \leq i \leq 6)$, i.e., the flows that minimize differences in height for the cell neighborhood and the determination of outflow shifts. AMD involves different specification of 'heights' h_i $(0 \leq i \leq 6)$, the 'fixed' parts and d, the 'distributable' part. Motion equations specify a shift x and a final velocity v, in order to determine from f_i $(1 \leq i \leq 6)$ the outflows f'_i $(1 \leq i \leq 6)$ during a step. Lahar (water) kinetic head are obtained by

$$S_{KH} = \frac{v_l^2}{2g} \tag{5.2}$$

$$S_{WKH} = \frac{v_w^2}{2g} \tag{5.3}$$

where g is the gravity acceleration, the subscripts l and w mean lahar and water velocity.

If lahar is not present in the cell ($S_{LT} = 0$) the γ function effects S_{WL}:

$$S'_{WL} = S_{WL} + q_w \tag{5.4}$$

otherwise lahar encloses water, it effects S_{LT} and S_{SWC}:

$$S'_{LT} = S_{LT} + q_w \tag{5.5}$$

$$S'_{LWC} = \frac{S_{LWC} \cdot S_{LT} + q_w}{S'_{LT}} \tag{5.6}$$

where q_w is the water quantity that falls down in the cell during the particular step.

5.4.1 Water Flow

The "Algorithm of Minimization of Differences" [42][5] is applied in the following way:

$$d = {}_0S_{\mathrm{WL}} \tag{5.7}$$

$$h_0 = {}_0S_{\mathrm{A}} + {}_0S_{\mathrm{WKH}} \tag{5.8}$$

$$h_i = {}_iS_{\mathrm{A}} + {}_iS_{\mathrm{WL}} \ \ (1 \leq i \leq 6) \tag{5.9}$$

The motion equations are related to outflows from central cell toward the adjacent cell $i(1 \leq i \leq 6)$:

$$x_i = v_0 p_t + g \left[\sin(\theta_i) - p_{wfc} \cos(\theta_i)\right] \frac{p_t^2}{2} \tag{5.10}$$

$$v_i = v_0 + g \left[\sin(\theta_i) - p_{wfc} \cos(\theta_i)\right] p_t \tag{5.11}$$

where v_0 is the initial velocity (deduced by S_{WKH} (Eq. 5.3)), x_i is the shift of the outflow toward the cell i, θ_i is the slope angle between the central cell and the neighbor i $(1 \leq i \leq 6)$. Sub-states regarding outflows are computed in the same way as debris flows in SCIDDICA-SS2 [7].

$S_{\mathrm{WKHO}i}$ $(1 \leq i \leq 6)$ are deduced by Eq. 5.3. S'_{WL} and S'_{WKH} are computed by balancing equations that consider the contribute of outflows and inflows:

$$ {}_0S'_{WL} = {}_0S_{WL} + \sum_{i=1}^{6} ({}_iS_{\mathrm{WO}(7-i)} - {}_0S_{\mathrm{WO}i}) \tag{5.12} $$

where ${}_iS_{\mathrm{WO}(7-i)}$ is the outflow of neighboring cell i toward the cell 0, that is specified by component $7-i$ for the neighboring of cell i $(1 \leq i \leq 6)$. An average weight is also considered:

$$ {}_0S'_{WKH} = \frac{{}_0S_{WKH} \cdot {}_0S_{WL}}{{}_0S'_{WL}} + \frac{\sum_{i=1}^{6} ({}_iS_{\mathrm{O}(7-i)} \cdot {}_iS_{\mathrm{WKHO}(7-i)} - {}_0S_{\mathrm{O}i} \cdot {}_0S_{\mathrm{WKHO}i})}{{}_0S'_{WL}} \tag{5.13} $$

The turbulence affects the kinetic head and consequently the velocity:

$$ -\Delta S_{\mathrm{WKH}} = p_{\mathrm{hkl}} \cdot S_{\mathrm{WKH}} \tag{5.14} $$

5.4.2 Water Percolation

Only the mobilizable stratum is considered, because eventual water saturation begins at its bottom according to data of soil tomography. When soil tomography is not available, as the two events that were simulated, only a stratum is hypothesized. The surface water loss by absorption is computed according to empirical considerations [7]: The water level S_{WL} in a cell is generated by rainfall and by the balance between water inflows and outflows among the central cell and its neighborhood. Part of it infiltrates in the mobilizable stratum, which may be considered as a water reservoir of a given capacity, that is the sum of stratum water receptivity S_{SR} plus stratum water content S_{SWC}; a maximum infiltration rate (in a step) S_{MIR} is fixed according to the cell physical characteristics related to the mobilizable pyroclastic stratum and does not change until mobilization. Infiltration v_I is the minimum value among S_{WL}, S_{SR} and S_{MIR}. Sub-states are updated:

$$ S'_{WL} = S_{WL} - v_I \tag{5.15} $$

$$ S'_{SR} = S_{SR} - v_I \tag{5.16} $$

$$ S'_{SWC} = S_{SWC} + v_I \tag{5.17} $$

5.4.3 Pyroclastic Stratum Mobilization

The saturation conditions that determine lahar emergence are specified by overcoming two thresholds, that regard the percentage of S_{SWC} related to water capacity of the mobilizable stratum and a sufficient slope angle related to a certain adjacent cell i $(1 \leq i \leq 6)$ such that the slope component of gravity force is larger than the reduced cohesion forces:

$$\frac{S_{SWC}}{(S_{SWC} + S_{SR})} > p_{wct} \tag{5.18}$$

$$\arctan\left(\frac{{}_iS_A - {}_0S_A}{2p_a}\right) > p_{slt} \tag{5.19}$$

When saturation conditions occur, the mobilizable stratum liquefies after the collapse of soil cohesion forces and encloses the surface water; the following formulas are applied:

$$S'_{LT} = S_{D1} + S_{WL} - S_{SR} \tag{5.20}$$

$$S'_{LWC} = \frac{(S_{SWC} + S_{WL})}{(S_{D1} + S_{WL} - S_{SR})} \tag{5.21}$$

$$S'_{WL} = S'_{SR} = S'_{D1} = 0 \tag{5.22}$$

$$S'_A = S_A - S_{D1} \tag{5.23}$$

5.4.4 Lahar Flow

Lahar in the cell and its lahar outflows are computed similarly as debris in the cell and its debris flows in SCIDDICA-SS3 [4]. It implies an alteration of 'height' values for accounting directional effects concerning momentum, according to a height correction function $f_{corr}(S_{MX}, S_{MY})$.

The outflow path from the central cell to a neighboring cell i follows an ideal direction between two points: the lahar barycenter of the central cell and the center of the adjacent cell i accounting the slope θ_i (Fig. 5.5). Viscosity is modeled as the part of lahar thickness that cannot be movable [2] according a function $f_{visc}(S_{KH}, p_{adh1}, p_{adh2}, p_{dft}, p_{wct})$, working for $p_{dft} < S_{KH} < p_{wct}$; adherence varies between to values p_{adh1} and p_{adh2} in relations to the water content according to an inverse exponential law, which can be approximated linearly (see Fig. 5.6). M and m are respectively the maximum and minimum water content, c and

k are positive constants such that: $p_{adh1} = ce^{-kM(p_{wct})}$ and $p_{adh2} = ce^{-km(p_{wct})}$. Deposit formation of lahar is 'de facto' derived by viscosity dynamics along the path, while, at the phenomenon ending, lahar deposit is derived by the almost total water loss (Section 5.4.6).

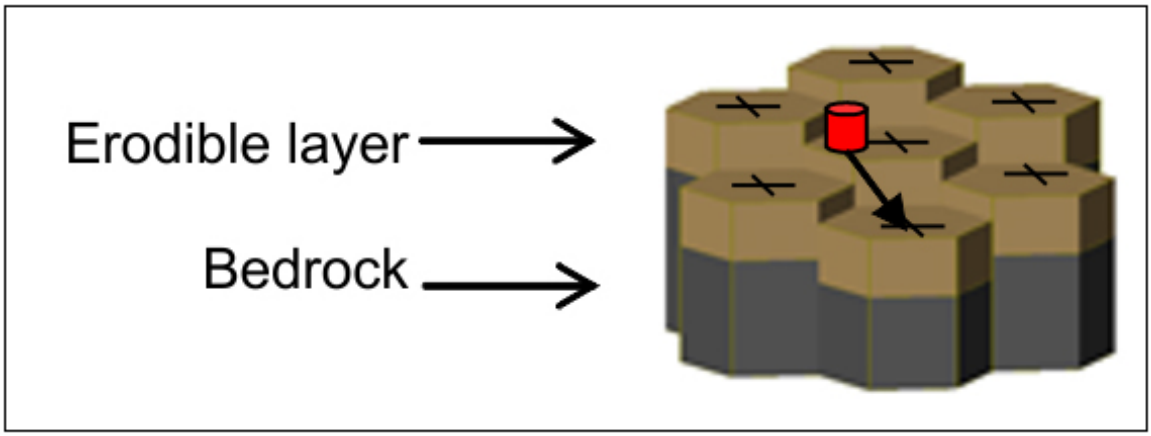

Fig. 5.5 Outflow direction from central cell to the center of an adjacent cell in 3-dimensions.

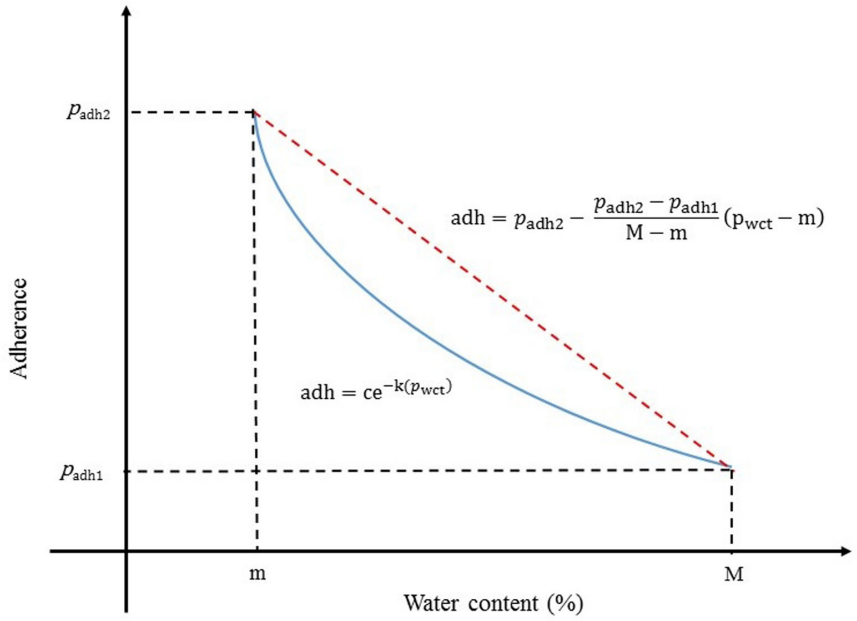

Fig. 5.6 Adherence variation according to water content.

AMD is so applied:

$$d = {}_0S_{LT} - f_{visc}(S_{KH}, p_{adh1}, p_{adh2}, p_{dft}, p_{wct}) \tag{5.24}$$

$$h_0 = {}_0S_A + {}_0S_{KH} + f_{visc}(S_{KH}, p_{adh1}, p_{adh2}, p_{dft}, p_{wct}) \tag{5.25}$$

$$h_i = {}_iS_A + {}_iS_{LT} + f_{corr}(S_{MX}, S_{MY}) \;\; (1 \leq i \leq 6) \tag{5.26}$$

The motion equations are related to outflows from central cell toward the adjacent cell i $(1 \leq i \leq 6)$:

$$x_i = v_0 p_t + g\left[\sin(\theta_i) - p_{fc}\cos(\theta_i)\right]\frac{p_t^2}{2} \tag{5.27}$$

$$v_i = v_0 + g\left[\sin(\theta_i) - p_{fc}\cos(\theta_i)\right] p_t \tag{5.28}$$

where v_0 is the initial velocity (deduced by S_{KH}), x_i is the shift of the outflow toward the neighbor i, θ_i is the slope angle between the central cell and the neighbor i $(1 \leq i \leq 6)$. Substates regarding outflows are computed in the same way as debris flows in SCIDDICA-SS3 [3].

S'_{LT}, S'_{KH}, S'_{LWC}, S'_X, S'_Y are computed by balancing equations that consider the contribute of outflows and inflows:

$${}_0S'_{\mathrm{LT}} = {}_0S_{LT} + \sum_{i=1}^{6}({}_iS_{\mathrm{E}(7-i)} - {}_0S_{\mathrm{E}i}) \tag{5.29}$$

where ${}_iS_{\mathrm{E}(7-i)}$ is the outflow of neighboring cell i toward the cell 0, that is specified by component $7-i$ for the neighboring of cell i $(1 \leq i \leq 6)$. An average weight is also considered:

$${}_0S'_{KH} = \frac{{}_0S_{KH}\cdot\ {}_0S_{LT} + \sum_{i=1}^{6}({}_iS_{\mathrm{E}(7-i)}\cdot\ {}_iS_{\mathrm{KHE}(7-i)} - {}_0S_{\mathrm{E}i}\cdot\ {}_0S_{\mathrm{KHE}i})}{{}_0S'_{\mathrm{LT}}} \tag{5.30}$$

$${}_0S'_{LWC} = \frac{{}_0S_{LWC}\cdot\ {}_0S_{LT} + \sum_{i=1}^{6}({}_iS_{\mathrm{E}(7-i)}\cdot\ {}_iS_{LWC} - {}_0S_{\mathrm{E}i}\cdot{}_0S_{LWC})}{{}_0S'_{\mathrm{LT}}} \tag{5.31}$$

$${}_0S'_X = \frac{{}_0S_X\cdot\ ({}_0S_{LT} - \sum_{i=1}^{6}{}_0S_{\mathrm{I}i} + {}_0S_{\mathrm{E}i})}{{}_0S'_{\mathrm{LT}}} + \frac{\sum_{i=1}^{6}({}_0S_{\mathrm{I}i}\cdot{}_0S_{\mathrm{IX}i} + {}_iS_{\mathrm{E}(7-i)}\cdot{}_iS_{\mathrm{EX}(7-i)})}{{}_0S'_{\mathrm{LT}}} \tag{5.32}$$

$$ {}_0S'_Y = \frac{{}_0S_Y \cdot ({}_0S_{LT} - \sum_{i=1}^{6} {}_0S_{\mathrm{I}i} + {}_0S_{\mathrm{E}i})}{{}_0S'_{\mathrm{LT}}} + \frac{\sum_{i=1}^{6} ({}_0S_{\mathrm{I}i} \cdot {}_0S_{\mathrm{IY}i} + {}_iS_{\mathrm{E}(7-i)} \cdot {}_iS_{\mathrm{EY}(7-i)})}{{}_0S'_{\mathrm{LT}}} \tag{5.33} $$

A turbulence effect is modeled by a proportional kinetic head loss at each LLUNPIY step: $-\Delta S_{\mathrm{KH}} = p_{\mathrm{khl}} \cdot S_{\mathrm{KH}}$. The turbulence affects the kinetic head and consequently the velocity. This formula implies that a velocity limit is asymptotically imposed for any value of slope.

5.4.5 Soil (Tephra) Erosion

When the kinetic head value overcomes an opportune threshold ($S_{KH} > p_{mt}$) depending on the soil features, then an erosion of the pyroclastic cover occurs proportionally to the quantity overcoming the threshold:

$$ p_{pe}(S_{KH} - p_{mt}) = \Delta S_{LT} = -\Delta S_{D1} \tag{5.34} $$

because the pyroclastic cover depth diminishes as the debris thickness increases; the kinetic head loss is:

$$ -\Delta S_{KH} = p_{ed}(S_{KH} - p_{mt}) \tag{5.35} $$

The mixing of the eroded pyroclastic cover with the earlier debris involves that the earlier debris kinetic energy becomes the kinetic energy of all the mass of debris, it implicates trivially a further kinetic head reduction:

$$ S'_{KH} = \frac{(S_{KH} - \Delta S_{KH})S_{LT}}{(S_{LT} + \Delta S_{LT})} \tag{5.36} $$

momentum variation follows from velocity reduction, it is computable by S'_{KH}, considering the increased mass.

5.4.6 Water Intrusion, Extrusion and Process of Lahar Complete Deposition

When $S_{KH} > p_{wct}$, intrusion of all the water (e.g. rainfall) into the lahar is considered: S_{LWC} and S_{LT} increase proportionally to intruded water. When $p_{dft} < S_{KH} < p_{wct}$, water extrusion occurs, according the empirical approximate function 'water loss':

$$ \Delta S_{LWC} = f_{wl}(S_{KH}, p_{dft}, p_{wct}), $$

f_{wl} accounts for water extrusion in lahar and expresses linearly water content loss between two values of kinetic head p_{dft} and p_{wct}, considering that gravitational water content at p_{dft} is approximated to 0. When $S_{KH} \leq p_{dft}$ lahar stops and complete deposition occurs: $\Delta S_A = S_{LT}$; $S'_{LT} = 0$; $S'_{LWC} = 0$.

Chapter 6

LLUNPIY for Simulating Primary and Secondary Lahars

"... el 26 de Junio del presente año á las diez del día, un ruido espantoso llamó la atención de los moradores de Latacunga y del valle de Chillo, el volcán se hallaba oscuro y la proyección de ceniza y fuego era visible. Por la parte del Norte del volcán; en el valle de Chillo se observó el desprendimiento de una masa enorme de agua, alta como una torre y ancha como un mar, que se desprendía en forma de avalancha líquida de la base del volcán, levantando sobre la superficie de sus agua a manera de un corcho, las casas, fábricas, hombres, animales, árboles y sembrados que se hallaban á su paso. "

Periódico "El Ocho de Septiembre",
Quito, 14 de julio de 1877

6.1 Introduction

In mainland Ecuador exist 84 volcanoes, 27 of these volcanoes are considered potentially active with some type of activity in the last 10,000 years. From the list of active volcanoes,

seven have shown historic activity since 1534. According to the Instituto Geofísico de la Escuela Politécnica Nacional of Ecuador (Geophysical Institute) (IG) who is officially responsible for volcanic and seismic monitoring as well as issueing alerts in event of volcanic activity, there are three of the most feared active volcanoes in the highlands of Ecuador named Tungurahua, Pichincha, and Cotopaxi. Around 35% of Ecuadorians (4.4 million) live on the flanks of volcanic hazard areas.

This chapter shows a preliminary version of LLUNPIY, which was applied together with simulation of 2005 secondary lahar of Vascún Valley of Tungurahua Volcano, Ecuador [88]. Furthermore, the model was applied for simulating the 2008 secondary lahar of Vascún Valley [89]. The model is extended in this research, accounting for the possibility of acquiring data from soil tomography [122], permits an improvement to the model for forecasting future probable lahar events. This extension was not applied obviously for the simulated events because tomography data are non-existent for 2005 and 2008 events.

An optimal simulation of part of the 2005 secondary lahar of Vascún Valley, was performed by Titan2D [163]; such a simulation represents a touchstone for our research.

On the other hand, LLUNPIY model is applied to Cotopaxi event of 1877 primary lahars, after the successful simulation of some secondary lahars of Tungurahua volcano [87]. Such an extension permits simulations with different initial hypotheses: the preliminary simulations agree in outline with field studies about the event evolution, LLUNPIY allows even a broader approach to overall phenomenon in comparison with other tools [90].

6.2 Model Implementation

Necessary input data for simulation of primary and secondary lahars with LLUNPIY are:

- DEM (Digital Elevation Model) with adequate cell-size.

- Source areas: extension of glaciers, whose melting originates lahars, or extension of ponds/lakes, whose destruction by volcanic matter releases enough water to generate lahars, only for primary lahars, while the extension of detachment areas in the case of secondary lahars.

- Initial values of sub-states concern the pre-event morphology (DEM), the depth of volcanic deposit, the depth of erodible soil, the free water basin (if involved in lahar) or rate of river flow or percentage of water inside deposit (deduced or computed e.g., melting glacier).

- Specifications of volcanic activity (eruption duration, strength and range of action) that effects glacier melting and/or destruction of ponds/lakes.

At each CA step, it is possible for each cell to obtain values (output data) of: altitude, lahar thickness, velocity, kinetic energy, erosion depth, outflow thickness and erodible cover depth.

At end of the simulation, the area affected by lahar with the new morphology accounts for erosion and deposits.

It is possible to introduce alterations to morphology in order to consider possible human interventions (embankments, canals, etc.).

In order to calibrate model parameters it is fundamental to identify the lahar path and invaded area of real phenomenon in order to measure the simulation 'goodness'.

Simulations were performed by desktop pc with Processor Intel(R) core i7, CPU 2.8 GHz and NVIDIA Quadro FX 580 video card.

The adopted programming language is C++, the model is implemented in a 'skeleton' fashion, developed for MCA, where the transition function is divided into the 'elementary processes' of LLUNPIY. Such elementary processes are executed sequentially in the same order as in section 5.4. Parallelism was not explicitly activated and the simulation average time is now 5 days, because the implementation of LLUNPIY is not optimized; an optimization is in progress, it will speed simulations up to 2 days. A parallel version for GPGPU will be developed when the model will be completed for both primary and secondary lahars, in the same way as Spataro et al. (2008).

6.3 The 2005 and 2008 Vascún Valley Lahars: Evaluation of the LLUNPIY Model using Actual Events

6.3.1 Background

Tungurahua volcano is located in the Cordillera Oriental of Andes of central Ecuador (latitude $01°28'S$; longitude $78°27'W$), 140 km south of the capital Quito (Fig. 6.1). It rises above the small thermal springs town of Baños de Agua Santa, which is located at its foot 8 km to the north. Other nearby towns are Ambato (30 km to the northwest) and Riobamba (30 km to the southwest). Tungurahua is part of the Sangay National Park.

With its elevation of 5,023 m.a.s.l., the volcano has tremendous relief over the surrounding landscape. The city of Baños is located on the northern flank of the volcano at an elevation of 1800 m, some 3,200 m below the summit crater. The eruptive history of Tungurahua has been described in detail by Le Pennec et al., [83] who showed that over the last 2,000 years,

eruptions have occurred on an average of once per century. Its numerous eruptions, particularly from 1999 until 2014 are characterized by several Strombolian episodes [101], with widespread ash deposition around the crater, and by the frequent generation of pyroclastic flows and rain-induced lahars. Tungurahua is considered to be a dangerous volcano which threatens the tourist town of Baños, as well as some small villages. A few kilometers east of Baños, the large Pastaza river is contained by the Agoyan dam and used for hydroelectric power generation.

In the last 15 years around 900 rain-induced lahars were generated. Thanks to the Instituto Geofísico of the Escuela Politécnica Nacional (IGEPN) that uses Acoustic Flow Monitor (AFM) station to detect and register secondary lahar activity, most lahars were detected, and others were observed by Tungurahua Volcano Observatory (OVT) located 13 km north-northwest from the crater and also by vigias (local volunteer volcano observes). Tungurahua's top is snow-covered with a small summit glacier which melted away after the increase of volcanic activity in 1999. Consequently the only way to generate lahars, with such magnitude and frequency, depends upon rainfall characteristics and the quantity of fresh material available within the principal ravines (quebradas), which flow down the Rio Vascún, Juive Grande-La Pampa Valley, Achupashal Quebrada and among others less important. Nearly all of the lahars remain within the canyons and flow into the Pastaza river [101].

6.3.2 The 2005 and 2008 Secondary Lahars of Vascún Valley

The Vascún Valley is located on the NE flank of Tungurahua and leads directly to the Rio Pastaza; the slopes in the upper 3 km of the valley are steep, being higher than $35-40°$, while in the lower 2-3 km the slopes are much gentler ranging from $6-20°$. The channel of the Rio Vascún is very sinuous in the first 1-2 km, passing though a series of tight $90°$ bends. The thermal structure 'El Salado Baths' lies along the banks of the river, while the town of Baños is located in the depositional area (Fig. 6.1).

On February 12, 2005, heavy rainfalls caused the remobilization of ash fall deposits, generating lahars in the Rio Vascún. The mean velocities of flows were estimated on the base of records of alert instrumentation. They varied between 7 m/s and 3 m/s, depending on the cross sections [163]. The lahar volume, measured by staff of Acoustic Flow Monitor station, was approximately estimated at 70,000 m^3, while a subsequent investigation, carried out by IGEPN [70], estimates it 55,000 m^3. The lahar ran through the valley approximately for 10 km and flooded El Salado Baths during the passage of the flows, then reached the Pastaza river. Note that the above event chronicle is taken from the work of Williams et al. [163], where authors performed simulations of part of the event (about 2 km) with Titan2D with start point at 2005 m a.s.l. and final point approximately at the end of Las Ilusiones. Their

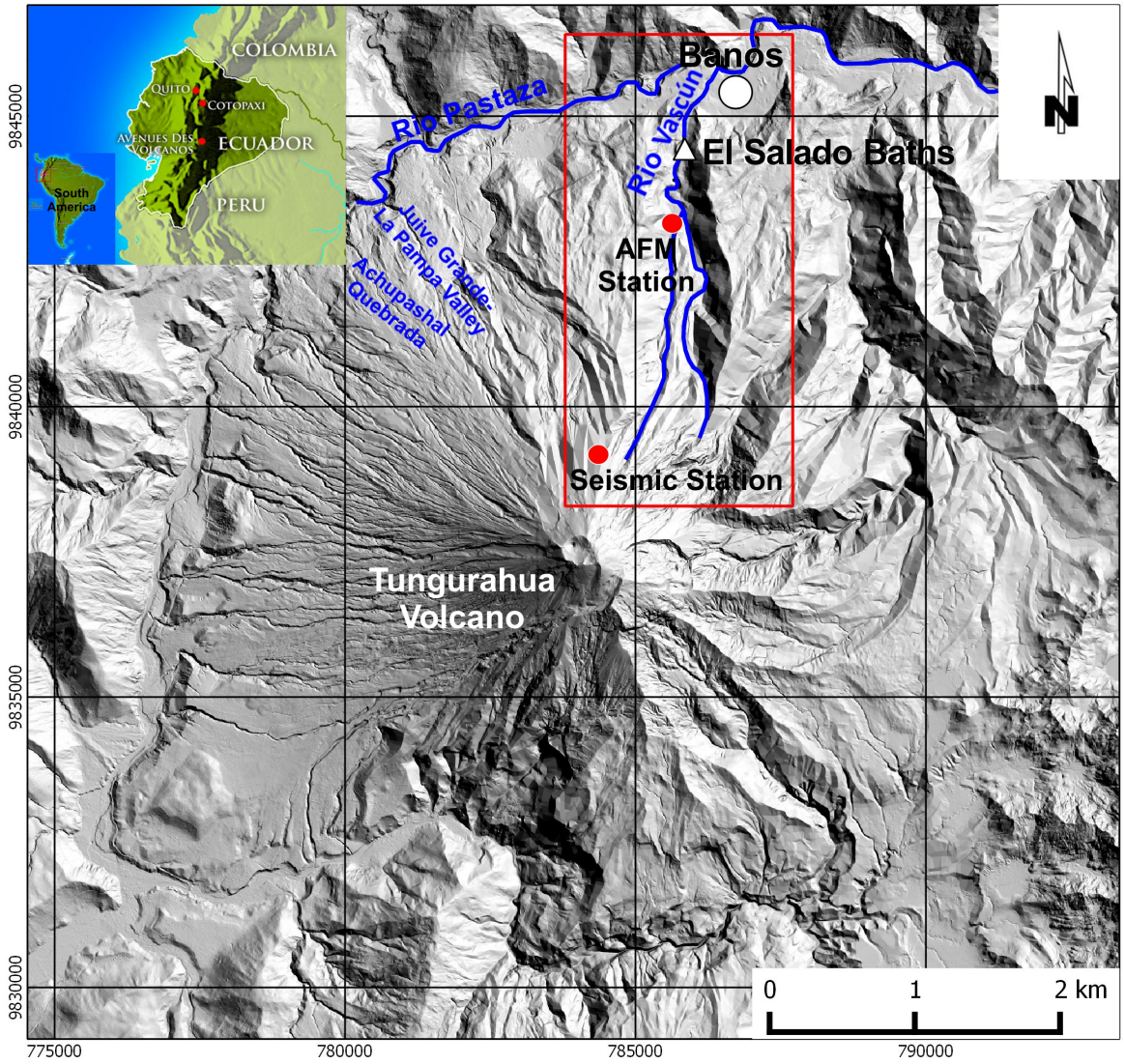

Fig. 6.1 Tungurahua Volcano. The Vascún Valley is inside box.

data and simulations were referred for comparison with LLUNPIY simulation because they were able to collect data.

On August 2008, the Vascún Valley was interested by frequent and mostly heavy rainfall [71]. On August 13, a 13 mm rainfall in three hours caused a small landslide that generated a natural barrier along Rio Vascún at an altitude approximately of 2,200 m a.s.l. The barrier created at upstream a pond 3 m deep, 20 m wide and with a length 100 m. On August 22, the collapse of barrier generated a lahar in the almost saturated soil by the previous rainfall [71]. Such a lahar may be considered secondary because is not directly generated by a volcanic event, e.g. by pyroclastic or lava flows. The documentation does not report any information about lahar volume.

The estimated velocity of the flow is 15 m/s with an average height of 4 m and a flow rate of 1,120 m^3/s [71], that is 10 times higher than that recorded in the 2005 lahar. The lahar reached the thermal spa of El Salado in 5 min, destroying the pools, and further downstream some houses in the village of Las Ilusiones.

6.3.3 Simulations of the 2005 and 2008 Lahars of Vascún Valley

The simulation of 2005 event is based on a DEM with 1m cell size with vertical accuracy from 0.6 m to 1.3 m (supplied to us by Dr. Gustavo Cordoba). It was integrated (in QGIS software) for the last 500 m by a DEM with 5m cell size (supplied by IGEPN), this one also used for the 2008 lahar simulation. In addition, a uniform thickness of 5 m was imposed for detrital cover, because detailed surveys were not available. All this introduces a series of approximations, that affects simulations. Simulations regard the flood phase of the events (elementary processes: 'soil erosion', 'lahar thickness and outflows') with an appropriate simplification about the moment computation, that shorted computation times.

First simulations were limited by the partial information on the 2005 Lahar of Vascún Valley. The work had carried out on a set of data, that did not include all the lahar extension. A stretch of about 2.3 km had been considered, from elevation 2,150 m a.s.l. (about 850 m upstream of El Salado Bath) to elevation 1,900 m a.s.l. (in correspondence of Pastaza river). The area, where the simulation starts, does not concern the detachment phase: the primary detachment phase occurs 8 Km upriver. A kind of detachment, where an initial velocity of 7 m/s was imposed to lahar, was considered in order to express the first arrival of lahar. An equivalent fluid approach was adopted, because precise data about water flows are not available. Therefore, bulking must account not only for erodible layer, but for water inclusion. The total mass is inclusive of the water mass. This generates a discrepancy between the lahar volume, measured on the deposit and 'fluid' lahar volume including water to be loss in the event last part.

Fig. 6.2 shows the simulation of a part of 2005 lahar with LLUNPIY. In particular, the maximum debris thickness values, which were reached by the lahar in simulation, are reported in Fig. 6.2a. Maximum velocities, reached by simulated flows (Fig. 6.2b), are high in steeper areas (the expected result) and decrease gradually at the outlet in downstream. A velocity increase occurs at south of Baños, probably because of the higher gradient of the river bed. Erosion has a trend similar to that of the velocity (Fig. 6.2c).

Table 6.2 synthesizes values of Fig. 6.2 and compares such data with field data of IGEPN reported in [70] and with simulation performed by Titan2D [163]. Such field data are obviously partial for the complete development of catastrophic phenomenon, but extremely precious by comparison with LLUNPIY simulations. Observation data are not sufficient to

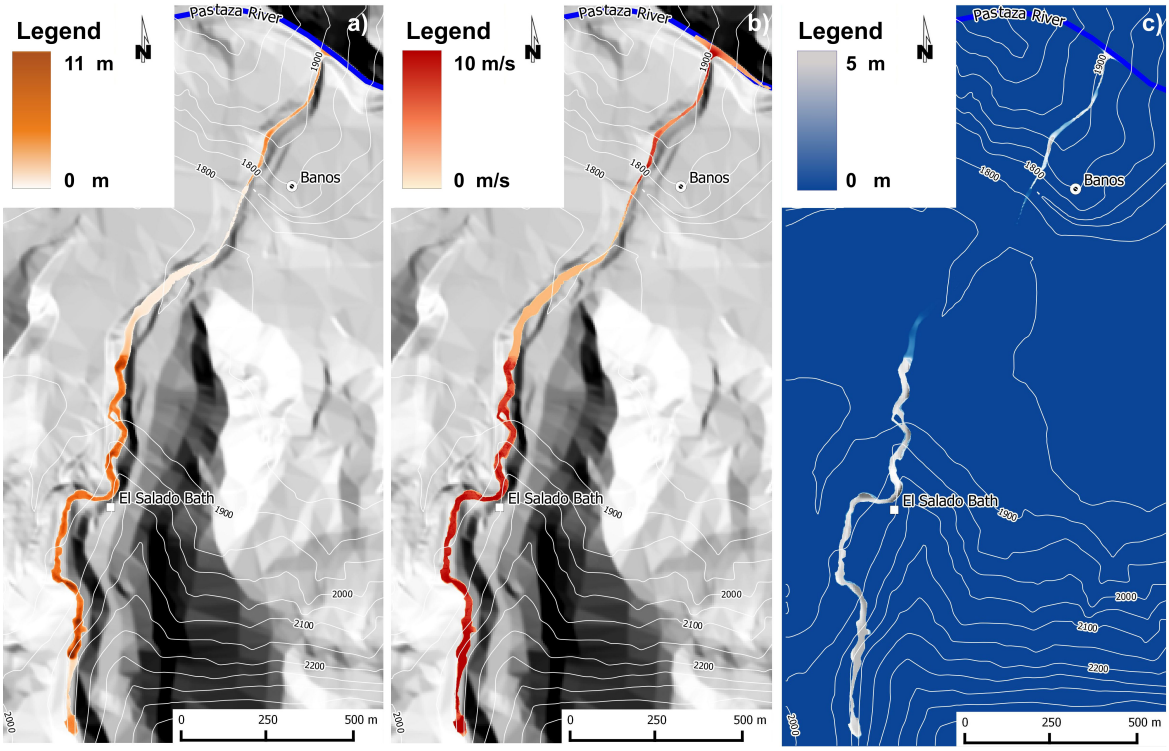

Fig. 6.2 a) Maximum thickness, b) Maximum velocity, and c) erosion depth, in 2005 simulated event.

a precise comparison with the simulation paths that are partial because limited field data. Furthermore, the lahar starts with null velocity in the simulation of William et al. [163], while LLUNPIY simulations start with 7 m/s velocities. The difference for total eroded mass rises from the lost water volume that was not possible to be considered in measurements.

Fig. 6.3 shows the 2008 lahar simulation: the flow velocity reaches, in many areas of the valley, 20 m/s (Fig.6.3b) with a total of eroded material of about 970,000 m^3. Table 6.3 reports the comparison between field data, collected by IGEPN [71], and LLUNPIY simulation data.

The parameters used for simulations of the 2005 and 2008 Lahars of Vascún Valley are based on the values reported in the Table 6.1. The lahar parameters of progressive erosion (p_{pe}) are different in the two cases, because of difference of water percent in the soil at the moment of erosion. The 2005 event was triggered by almost contemporary detachment in higher zone of Rio Vascún according to the combined effect of the slope and amounting of rainfall water inside the soil. The 2008 event was triggered mainly by breaking temporary pool that created a strong initial conditions with a water percent in the moving mass that is larger than 2005 with also a larger turbulence. Such a larger turbulence was modeled by a higher value of the lahar parameters of progressive erosion (p_{pe}).

Table 6.1 Used global parameters for simulations of the 2005 and 2008 Lahars of Vascún Valley

Parameters	Simulation 2005 lahar	Simulation 2008 lahar	Unit
cell apothem (p_a)	0.5	2.5	m
temporal correspondence of a CA step (p_t)	6.5×10^{-2}	5.5×10^{-2}	s
mobilization threshold (p_{mt})	5.0×10^{-1}	5.0×10^{-1}	m
turbulence dissipation (p_{td})	5.0×10^{-5}	5.0×10^{-5}	-
lahar friction coefficient (p_{fc})	8.0×10^{-2}	8.0×10^{-2}	-
erosion dissipation of energy (p_{ed})	3.0×10^{-1}	3.0×10^{-1}	-
lahar parameter of progressive erosion (p_{pe})	1.0×10^{-3}	1.0×10^{-2}	-

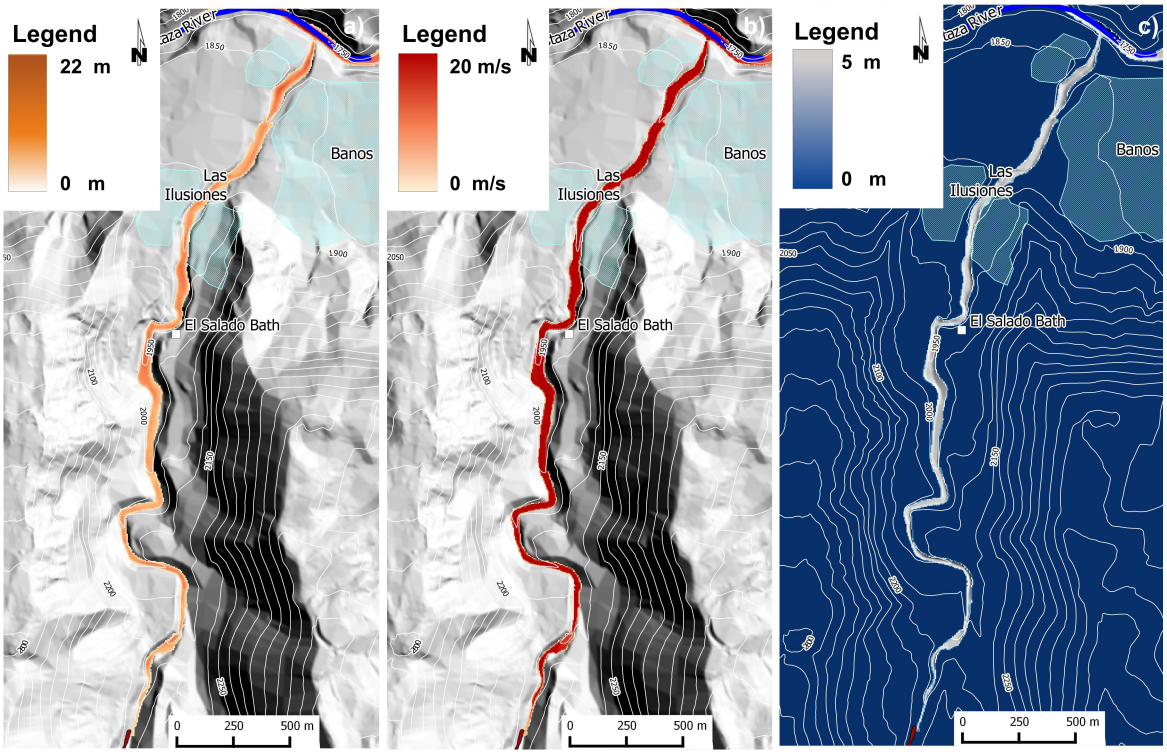

Fig. 6.3 (a) Maximum thickness, (b) Maximum velocity, and (c) erosion depth, in 2008 simulated event.

A partial simulation of the first phase of the event (only detachment) was performed by a reduced two-dimensional CA 'ad hoc' in order to compare experimental scarce data about triggering areas, which we adopted in the simulation, and data, that are obtained by application of the combined elementary processes: water percolation, water flow, pyroclastic stratum mobilization. The Vascún Valley may be considered a canyon for the lahars, so linearizing the path in only two dimensions does not involve serious problems of approximation

Table 6.2 Comparison among field data, Titan2D and LLUNPIY simulation data

	Field data	Titan2D simulation outputs	LLUNPIY simulation outputs
Mean velocity between Retu Seismic Station and AFM (m/s)	7	-	-
Mean Velocity between AFM and El Salado (m/s)	3.10	-	-
Velocity at El Salado (m/s)	3.1	5.8 - 8.9	3.1
Velocity at final point (Las Ilusiones) (m/s)	-	1.1 – 2.6	3
Time between AFM station and El Salado	16 min	-	-
Time between start point and El Salado	-	-	6 - 7 min
Time between El Salado and Las Ilusiones	-	-	14 min
Total time between start point and Las Ilusiones	-	8-14 min	20 min
Eroded debris between start point and El Salado (m^3)	-	-	38,000
Eroded debris between El Salado and Las Ilusiones (m^3)	-	-	71,000
Total lahar volume between start point and Las Ilusiones (m^3)	55,000/70,000	50,000/70,000	109,000

Table 6.3 Comparison between field data and LLUNPIY simulation data

	Field data	LLUNPIY simulation outputs
Maximum velocity	15 m/s	20 m/s
Velocity at El Salado	4.7 m/s	6 m/s
Time between start point and El Salado	5 min	4 min 50 s
Maximum flow between start point and El Salado	640 m^3/s	633 m^3/s
Total time between start point and Rio Pastaza	-	9 min
Total eroded debris	-	970,000 m^3

in order to implement the partial CA. The soil (tephra) data were considered almost homogeneous in terms of composition; such an assumption is critical, because soil tomography data [122] show heterogeneity that we averaged. In spite of this weak point, triggering areas of simulation agree with experimental data. In simulation we consider two meters of saturable tephra with voids content of 35%. Fig. 6.4 reports the elevation profile of the lahar path as a colored band of constant thickness, whose color represents the degree of water content. The overlying blue and brown zones represent the water and lahar thickness (not in scale). Green zones interposed to brown zones in Fig. 6.4b represent collapsed tephra together the water inside. Fig.6.4a show water accumulation points (blue peaks), along the Vascún Valley, after 14 hours of and intense rainfalls (28.8 mm/h). Soil saturation is maximum after 19 hours. Triggering of lahars (green zones in Fig. 6.4b) occurs in many points after about 20 hours of continue rain with the same intensity, where soil conditions allow (e.g., saturation, slope angle, etc.). Note the correspondence between the source areas of the events occurred in 2005 and in 2008, respectively at elevation of 4,090 m a.s.l. and 2,200 m a.s.l.

6.3.4 Evaluating LLUNPIY Simulations: Secondary Lahars

LLUNPIY development is following the approach of MCA and more precisely enclosed modelling solutions, which are adopted in SCIDDICA [4] and SCIARA [2]. The further extension of LLUNPIY (primary lahars) will be based on the method of incremental improvement (refining upon the transition function, introduction of new sub-states and elementary processes) in order to account for a more precise description of the phenomenon.

LLUNPIY was applied for the flood phase of 2005 and 2008 lahars of Vascún Valley because available data, although incomplete, permitted us reliable simulations of the flood phase of the two events. An accurate analysis was performed in order to compare data of different sources and to obtain the most faithful reconstruction for a part of the event and extended zones under study in [163] [71] [89].

Simulation results demonstrate that the applied part of LLUNPIY is working well if we consider the partial, sometime rough data concerning the event, pre-event, post-event besides the unavoidable errors in event records. This part of model is reliable, while further specifications must be considered for extending and testing it. The simulations were satisfying in terms of reproducing the global dynamic of the events, such as velocity, height of detrital flow and times; the good correspondence between real and simulated lahar path would be easily obtained by many approaches because the flow is channeled by steep faces.

Soil data was acquired in January 2015 in four points of Vascún Valley [122] by soil tomography. This data cannot be applied to past events, but can contribute to improve the previous model by introducing two strata for the pyroclastic cover (regolith). Hypothetical

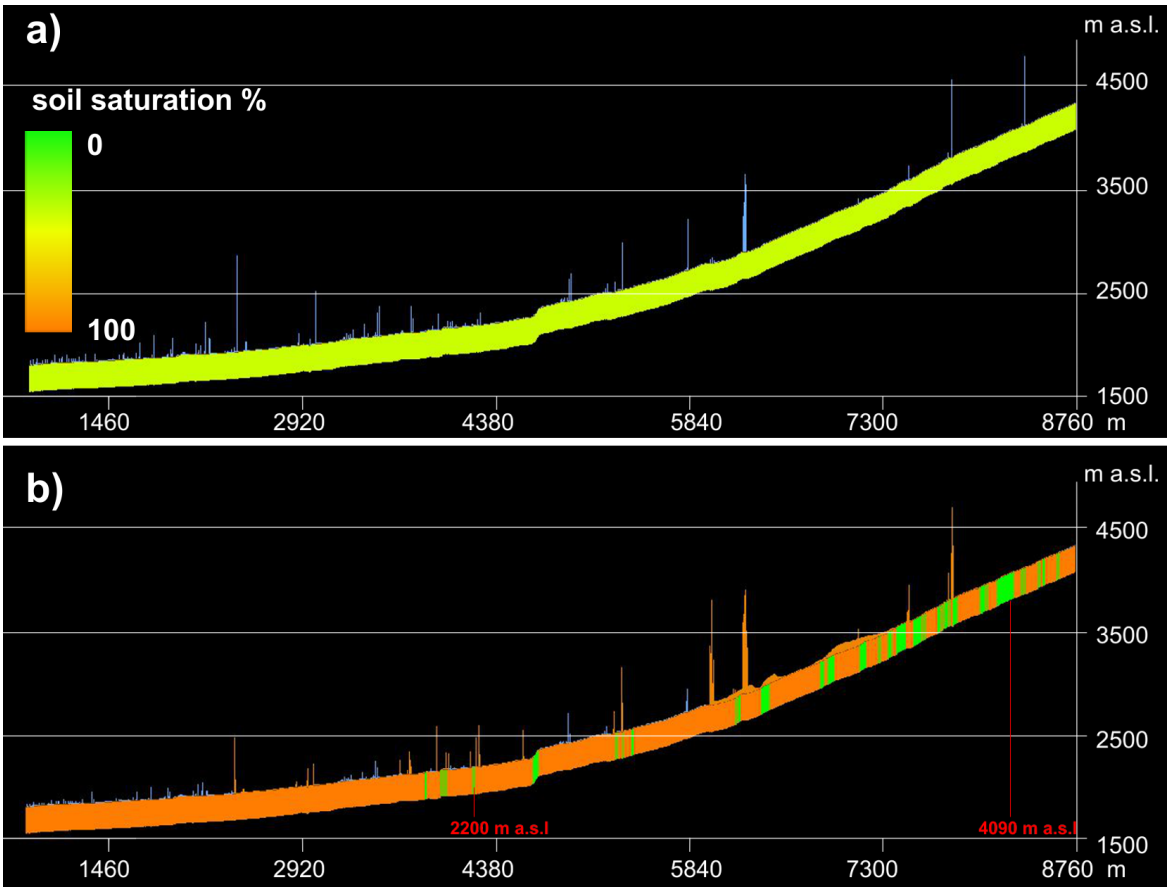

Fig. 6.4 A two-dimensional CA for determination of possible triggering points. (a) Blue peaks represent water accumulation points, (b) green zones are possible triggering points of lahars, brown peaks are points of detrital accumulation. Red altitudes evidence the triggering points of real past events that coincide with some green bands.

data about soil features before the 2005 and 2008 events were used for simulations of the generation phase and results agree with the poor knowledge of the first part of the phenomenon. Such results are indicative of the model improvement, but we cannot demonstrate their correctness. The exhaustion phase of the model was not simulated because both reported lahar floods disappeared into in the Pastaza river. Other cases will hopefully test this part of the model.

6.4 Primary Lahars: 1877 Cotopaxi Volcano Case Study

This study will concentrate on a portion of the Río Cutuchi drainage system on the south flanks of Volcán Cotopaxi, Ecuador. This area contains many communities, some of which are situated on terraces formed by lahars in recent geological history. Potential lahars

are simulated using LLUNPIY model to create a study of inundation areas for the city of Latacunga, Ecuador [90] [85].

6.4.1 Background on Cotopaxi Volcano

Cotopaxi volcano is situated in the Eastern Cordillera of the Ecuadorian Andes (Fig. 6.5) about 60 km south of Quito. It is a very hazardous active stratovolcano.

With an altitude of 5,897 m a.s.l. the summit of the volcano is currently covered with a thick layer of ice that ranges between 30 and 120 m [16]. Cáceres et al. [16] estimated that the glacier volume was approximately 1,000 million m^3 in 1976, considering an average thickness of 50 m. Such a volume since reduced to 732 million m^3 in 1997, because of a progressive melting, probably generated by climate change.

The main drainage lines are in north sector there is the Pita-Guayallabamba River and the west slopes are crossed by several tributaries of the Napo River, while waters of several streams, often encased in narrow valleys, coming from the cone of volcano, converge into the Rìo Cutuchi, that flows toward South-Southwest in the wide valley of Latacunga.

The area around the volcano is densely populated, in fact, the city of Quito is located in north. In the Cutuchi valley besides several villages, there are the towns of Latacunga and Salcedo, respectively 45 km and 50 km in South of Cotopaxi. In addition, industries and agriculture are intensively developed in these areas.

Since 1738 Cotopaxi has erupted more than 50 times. The most violent historical eruptions were in 1744, 1768, 1877, and 1904 with generation of disastrous lahars in many cases.

6.4.2 1877 Lahars

The presence of glacier on summit of Cotopaxi is one of principal causes, together with volcanic eruptions (lava or pyroclastic flows), of primary lahars. In fact, the Cotopaxi has often produced catastrophic lahars during eruptions because of ice and snow melting.

The 1877 eruption, described by Sodiro [144] and Wolf [164], produced very destructive and large lahars. These chronicles report times and extension of lahar floods next to inhabitant centers: some later observations estimated the glacier melting to 1/10 of total volume [164]. Water, which originates from melting glacier, had been mixed with pyroclastic material erupted and with pre-existing volcanoclastic materials outcropping along slopes, so many lahars flows had been generated. These flows, channeled in drainage network, destroyed population centers and everything on the path. Fig. 6.6 shows the partial reconstruction of this event performed by Mothes et al. [101].

Fig. 6.5 Cotopaxi volcano and its surrounding region.

On the western slope of volcano, three main flows are generated, coming down with a conjectured speed from about 30 m/s to about 10 m/s (depending on the slope) and reaching Latacunga, a village, at that time, in about one hour [101].

6.4.3 Simulations of 1877 Event

For 1877 event simulation a DEM with 30 m cell size with vertical accuracy from 0.6 m to 1.3 m (supplied to us by Instituto Geofísico of the Escuela Politécnica Nacional - IGEPN) is

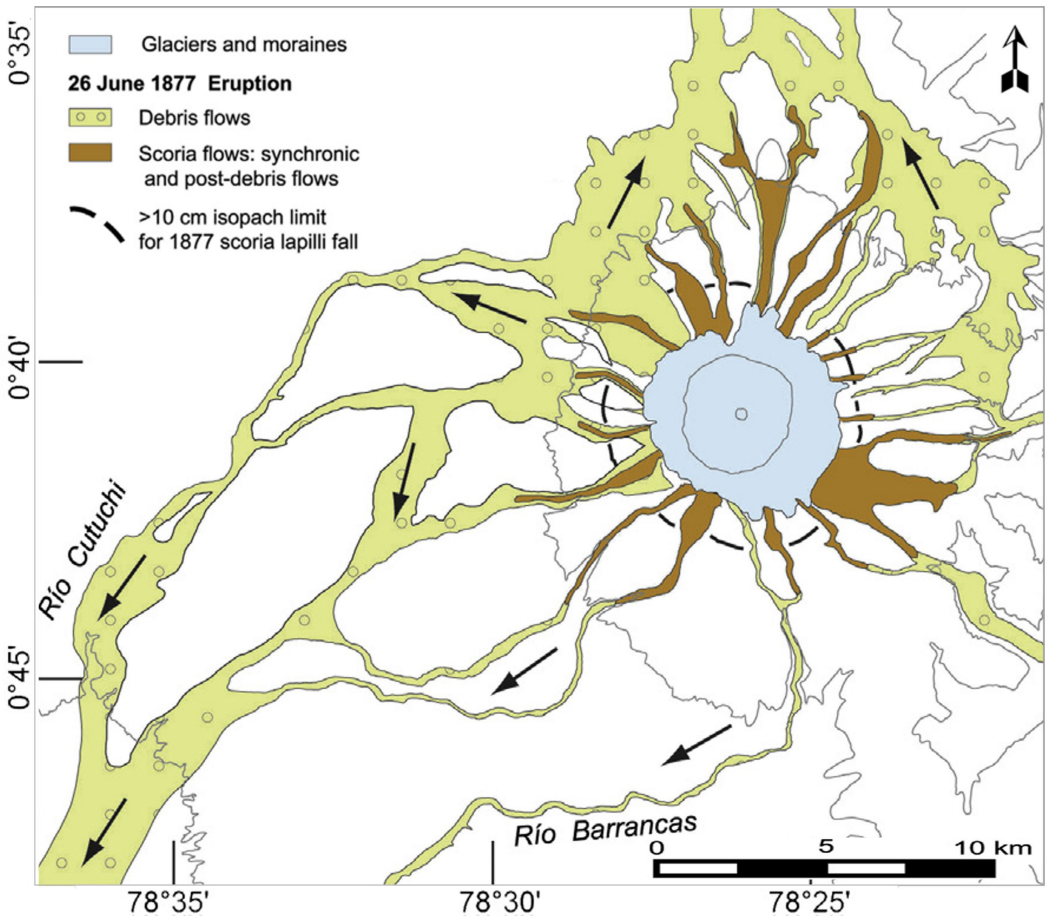

Fig. 6.6 Reconstruction of 1877 lahar path [101].

used, which is a very large size but considering the magnitude and extent of the phenomenon was considered acceptable, if changes in the time are also considered. Erodible detrital cover was considered a uniform layer of 5 m thick because field data are not available in all the simulation area.

Simulations, shown below, provide three different hypothesis:

- 'Many Sources' Hypothesis
- 'Immediate Glacier Melting (pyroclastic flows)' Hypothesis
- 'Gradual Glacier Melting (pyroclastic bombs)' Hypothesis

'Many Sources' Hypothesis

LLUNPIY model was applied to Cotopaxi 1877 event of primary lahars [101], after the successful simulation of some secondary lahars of Tungurahua volcano [87] [90]. It is

followed, as first hypothesis, the 'many sources' simplification proposed in Pistolesi et al. [116] that the main event could be equivalently generated, considering the initial positions of lahars sources in the three principal streams (Fig. 6.7): Río Cutuchi, Río Sasqìmala and Río Barrancas-Alaques. In each of these three streams, it has been placed, respectively, $18.5 \times [10]^6\ m^3$, $9.5 \times [10]^6\ m^3$ and $10 \times [10]^6\ m^3$ of lahar matter.

The parameters used for many sources simulated event are based on the values reported in the Table 6.4.

Table 6.4 Used global parameters for 'Many Sources' LLUNPIY simulations

Parameters	Value	Units
cell apothem (p_a)	15	m
temporal correspondence of a CA step (p_t)	6.5×10^{-2}	s
mobilization threshold (p_{mt})	5.0×10^{-1}	m
turbulence dissipation (p_{td})	5.0×10^{-5}	-
lahar friction coefficient (p_{fc})	8.0×10^{-2}	-
erosion dissipation of energy (p_{ed})	3.0×10^{-1}	-
lahar parameter of progressive erosion (p_{pe})	1.0×10^{-3}	-

The resultant simulations are shown in Fig. 6.7. These results are comparable with simulations performed by the model LAHARZ [116], that considered larger quantities of initial lahars ($120 \times [10]^6\ m^3$ sum of: $60 \times [10]^6\ m^3$ in Río Cutuchi, $30 \times [10]^6\ m^3$ in Río Sasqímala and $30 \times [10]^6\ m^3$ in Río Barrancas-Alaques). The width of LLUNPIY simulation is smaller in the area next to 'spurious' sources, but LAHARZ simulation is larger (Fig. 6.7). The two results are very similar in the final sector (Latacunga area), because, at the end, the addition of eroded material in LLUNPIY balances the two approaches.

'Immediate Glacier Melting (Pyroclastic Flows)' Hypothesis

The previous hypothesis involves the limit of initial quantity of lahar at the sources, because overflows can distort the effective evolution of the phenomenon. This did not permit to overcome an initial lahar quantity at the beginning in the previous simulation. For this purpose, a new CA 'elementary process' of glacier melting was introduced. The ice layer is supposed to enclose pyroclastic matter and to melt immediately (the LLUNPIY first step) the glacier. That is more realistic the 'Immediate Glacier Melting' Hypothesis than sources approach, if the rapid evolution of eruption is considered. The simulations of icecap melting are based on data, which correspond to 1976 glacier extension [16] with average glacier thickness of 50 m.

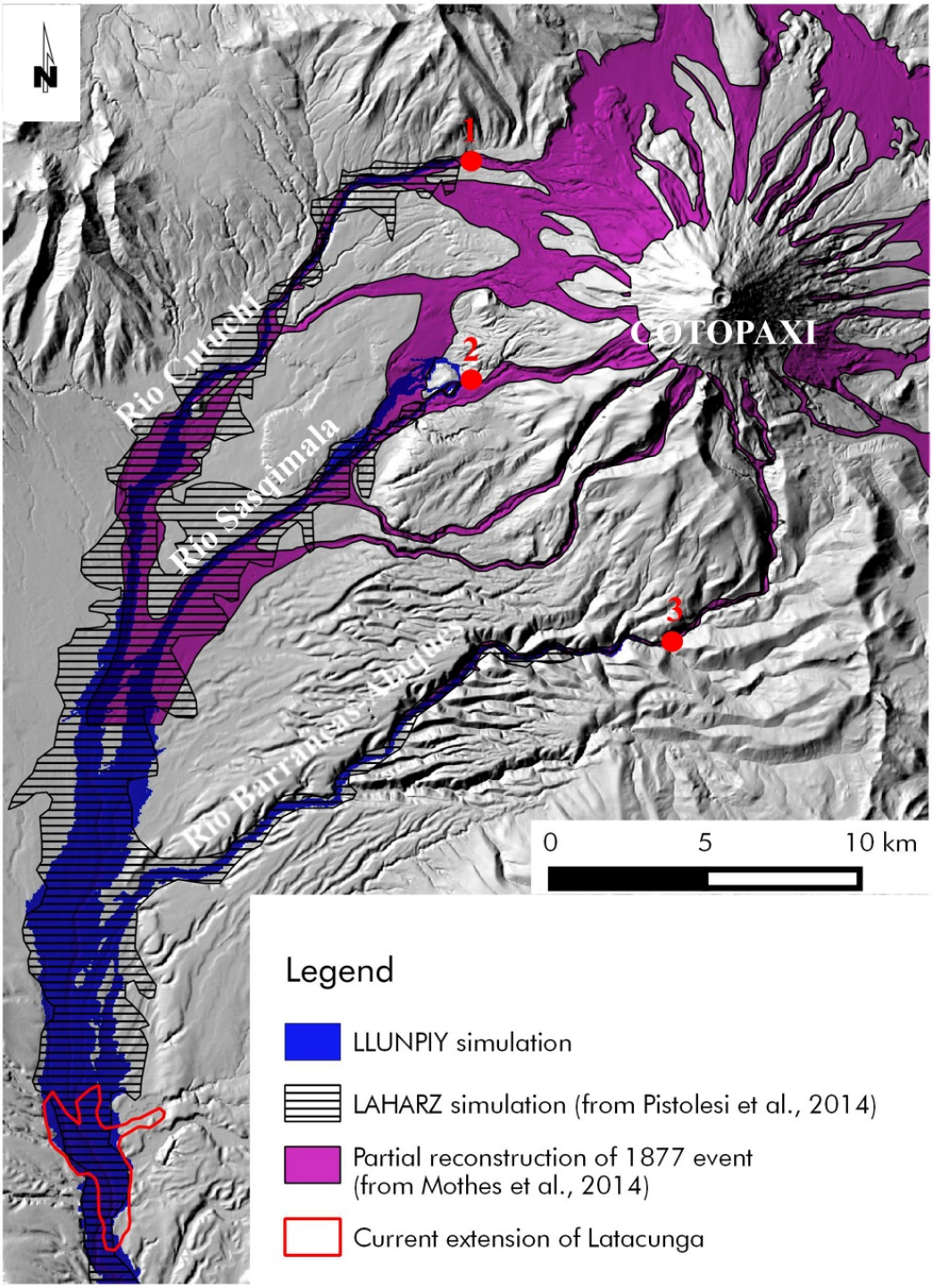

Fig. 6.7 LLUNPIY 'Many Sources' simulation of 1877 lahars and comparison with LAHARZ simulation and field data reconstruction.

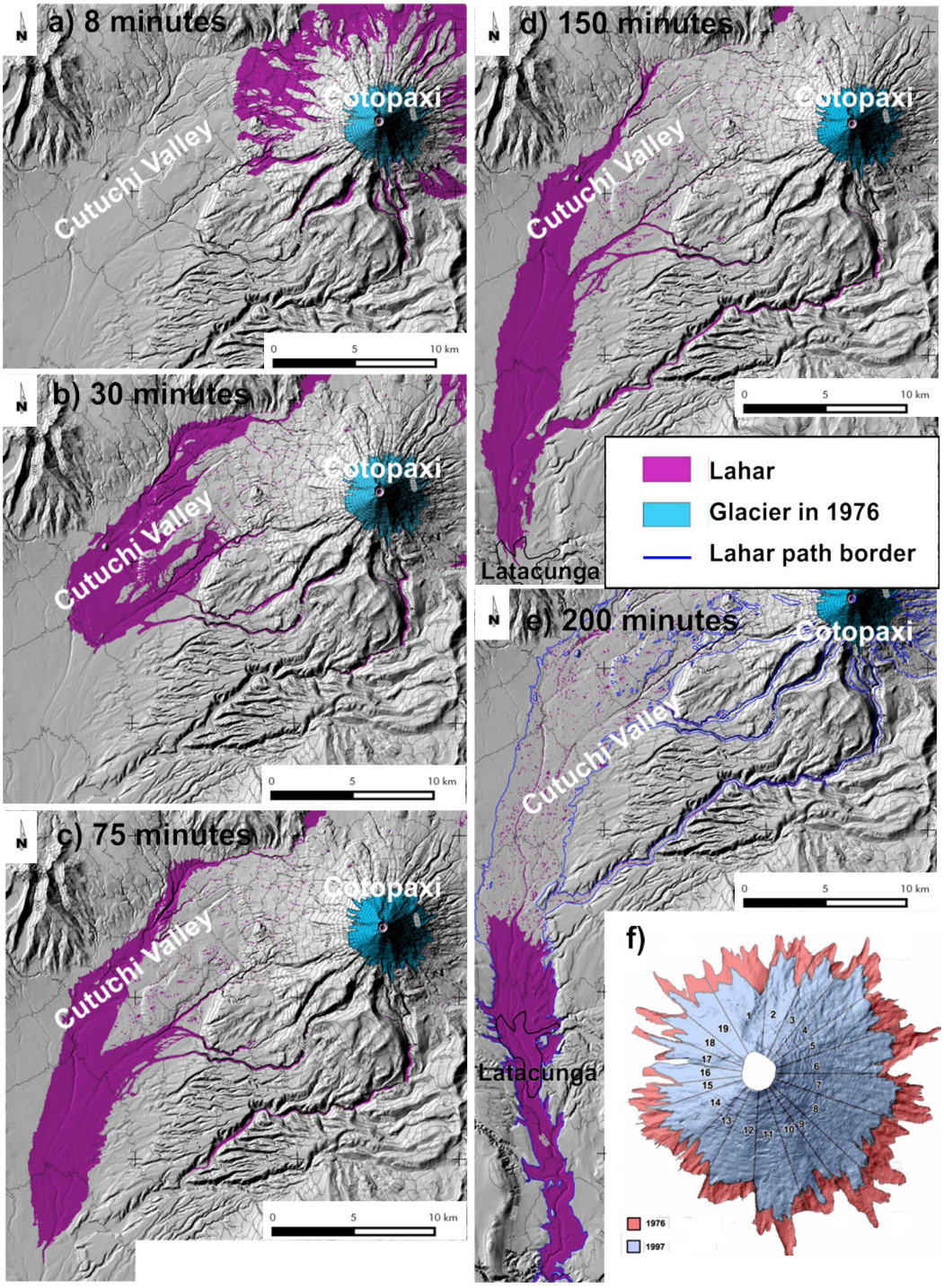

Fig. 6.8 LLUNPIY scenario 1 considering 10 m of icecap melting.

In the simulations, two possible scenarios have been considered. The first case involves the melting of only 10 m of glacier [85]. Fig. 6.8 shows the results of simulated event in various times. Results of simulation agree with partial data of the chronicles of that time [164]. A second scenario (Fig. 6.9), more catastrophic, involves the complete melting of ice cap. In this case the flows enlarge, covering a more extensive area in larger times. In both cases the paths are the same of 'many source' simulation, but in the cases of 'glacier melting' widths are obviously larger. These simulations could be considered possible scenarios for a future eruption of Cotopaxi because current DEM was used together with measures of glacier extension.

The parameters used for immediate glacier melting (pyroclastic flows) simulated event are based on the values reported in the Table 6.5, both for LLUNPIY scenario 1 (10 m of icecap melting) and for LLUNPIY scenario 2 (50 m of ice cap melting).

Table 6.5 Used global parameters for 'Immediate Glacier Melting (pyroclastic flows)' LLUNPIY simulations

Parameters	Value	Units
cell apothem (p_a)	15	m
temporal correspondence of a CA step (p_t)	6.5×10^{-2}	s
mobilization threshold (p_{mt})	5.0×10^{-1}	m
turbulence dissipation (p_{td})	1.0×10^{-5}	-
lahar friction coefficient (p_{fc})	4.0×10^{-2}	-
erosion dissipation of energy (p_{ed})	3.0×10^{-1}	-
lahar parameter of progressive erosion (p_{pe})	1.0×10^{-3}	-

'Gradual Glacier Melting (Pyroclastic Bombs)' Hypothesis

Another hypothesis of glacier melting could agree with Wolf's report [164]; the glacier melting could have been gradual because of the effect of pyroclastic bombs with a certain frequency and time length.

The simulations of gradual icecap melting by the effect of pyroclastic bombs are based on the parameters reported in the Table 6.6. Difference with 'Immediate Glacier Melting' parameters consists in a increasing the mobilization threshold (p_{mt}) and contemporary a reduction of turbulence dissipation (p_{td}). The reason was that a better simulation could be obtained by reducing the width of lahar in downstream. Initially, only mobilization threshold was increased, but the flows were decreased too much because the erosion contribution began minimum. Then, the turbulence dissipation was lowered, permitting again a larger erosion. The combined effect of these two conflicting variation improved the simulation.

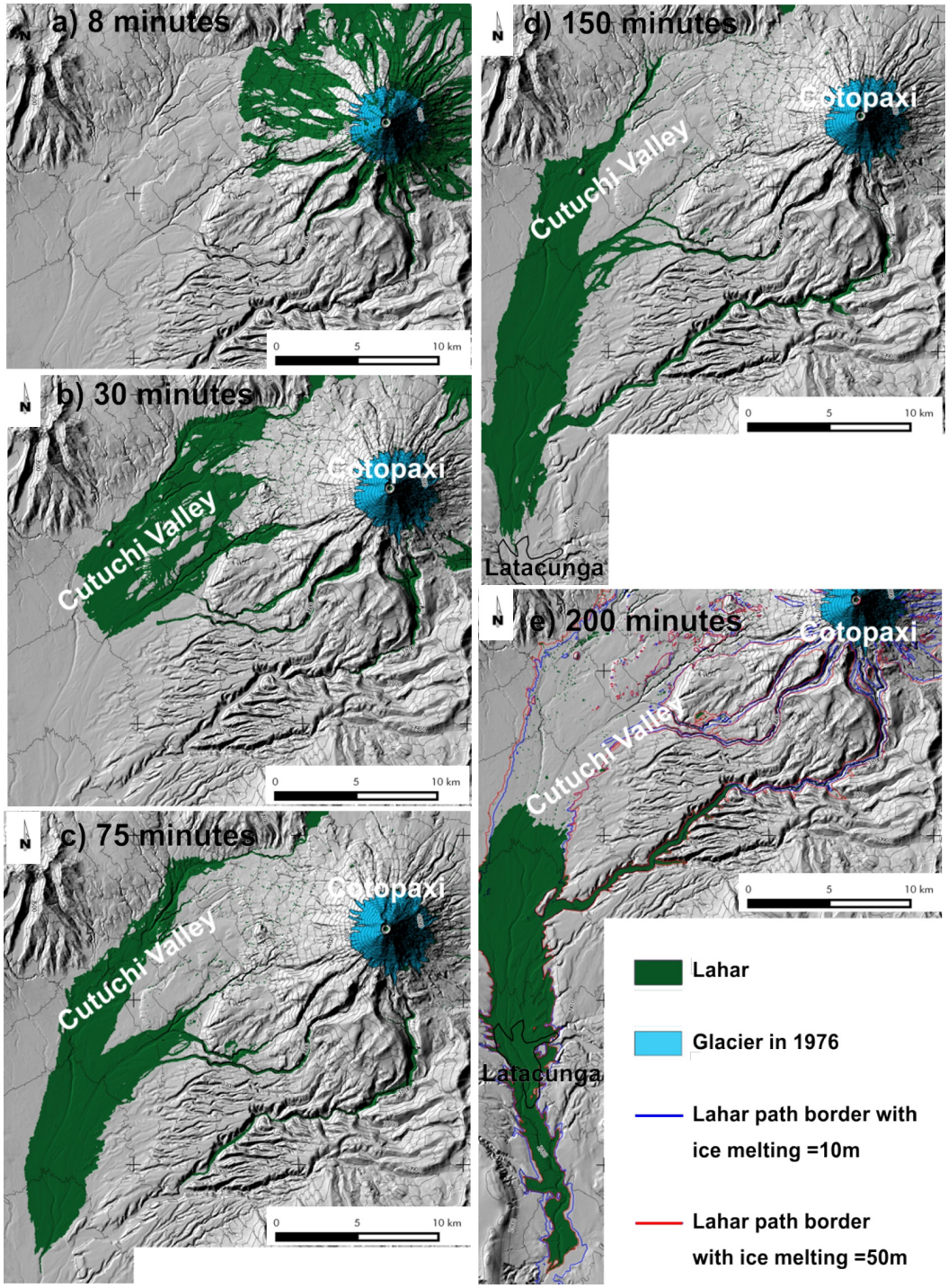

Fig. 6.9 LLUNPIY scenario 2 considering 50 m of ice cap melting.

Table 6.6 Used parameters for 'Gradual Glacier Melting (pyroclastic bombs)' LLUNPIY simulations

Parameters	Value	Units
cell apothem (p_a)	15	m
temporal correspondence of a CA step (p_t)	6.5×10^{-2}	s
mobilization threshold (p_{mt})	1.2×10^{2}	m
turbulence dissipation (p_{td})	1.75×10^{-8}	-
lahar friction coefficient (p_{fc})	4.0×10^{-2}	-
erosion dissipation of energy (p_{ed})	3.0×10^{-1}	-
lahar parameter of progressive erosion (p_{pe})	1.0×10^{-3}	-
pyroclastic bombs number for each step	50	-
pyroclastic bombs time length (steps)	1.0×10^{4}	-

Pyroclastic bombs fall on the ice surface and melt the ice in this case. This event has obviously stochastic features as illustrate in Fig. 6.10. In the simulation, it is simplified in such a way: 50 bombs pyroclastic are generated in each step for the first 10,000 steps. Each bomb has an equiprobability to fall on whatever cell of the glacier. Effect is equal for each bomb: 15 m of ice are melted.

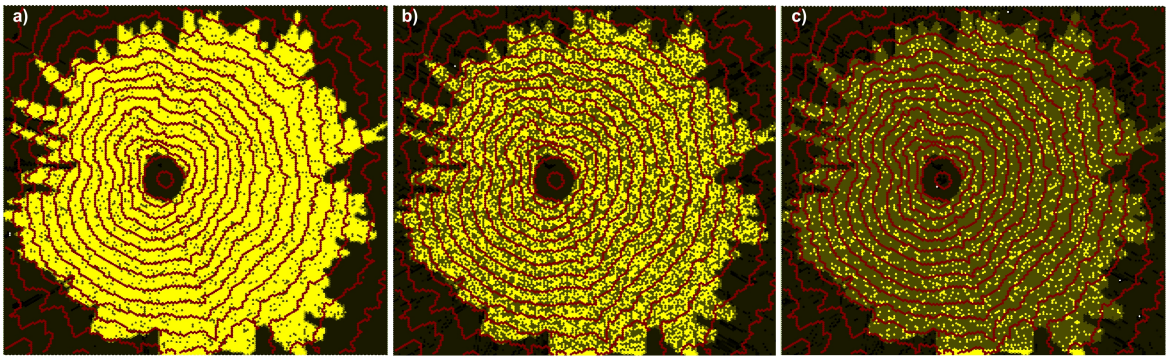

Fig. 6.10 Effects of pyroclastic bombs: yellow cells no pyroclastic bombs affected cell, gray cells, at least one pyroclastic bomb fell on the cell. Time steps of glacier melting simulation: (a) 2,500 , (b) 5,000 and (c) 7,500 steps.

Fig. 6.11 shows the results of simulated event in various times of the maximum debris thickness values, which were reached by the lahar in simulation. The maximum thickness of the flow is reached in the upper valley of the Rio Barrancas-Alaques with 150 m. In this area, in fact, the river is embanked between narrow and high rock walls. Along Cutuchi valley lahar thickness ranges from 0 to 20 - 25 m.

The LLUNPIY program contains the 'pseudo' sub-state 'maximum velocity' that registers the maximum value of the flow velocity in the cell.

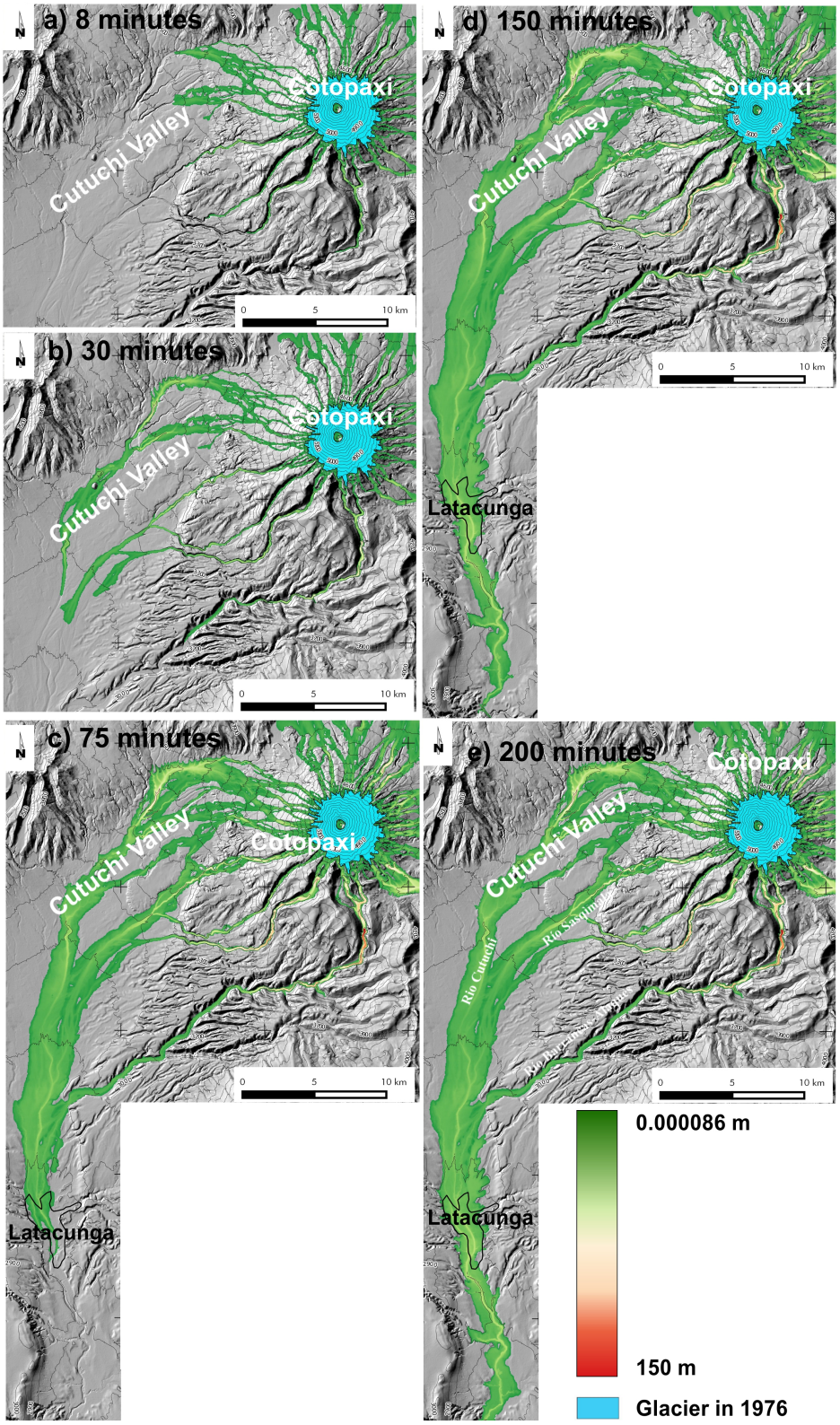

Fig. 6.11 Results of simulated event 'Gradual Glacier Melting (pyroclastic bombs)' in various times of the maximum debris thickness values.

At the end of simulation the maximum velocity of outflows in the cell is saved.

The values of the parameters, which rule the energy dissipation effect the lahar velocities.

Maximum velocities, reached by simulated flows according to the parameters adopted, are high in steep areas (the expected result), however the velocity decreases at the margin of the channels by friction effect (see Fig. 6.12 and Fig. 6.13).

The value of the maximum velocity of the flows in the cell does not mean that such a value is constant in the time.

In Fig. 6.14 is reported the erosion values at the beginning of the event (8,000 steps), when pyroclastic bombs ceased and lahars come out the glacier with hight kinetic energy because the steep slopes; and Fig. 6.15 is reported the erosion values at the end of simulation. It is possible to note how the erosion is maximum at the center of the riverbed, while it is lower along the edges of the river and in front of the lahar (Fig. 6.14b).

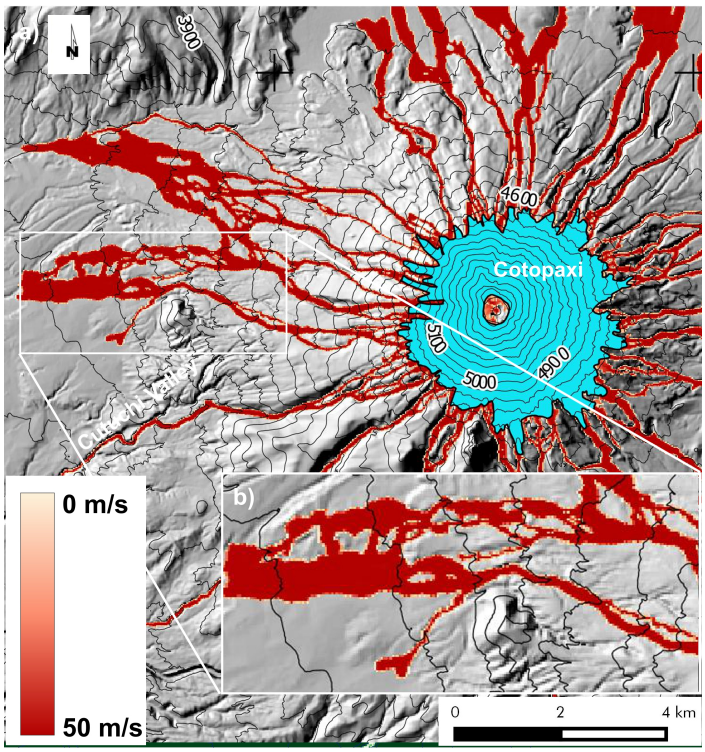

Fig. 6.12 Maximum velocities reached by flows at step 8,000 in 'Gradual Glacier Melting (pyroclastic bombs)'. The box (b) represents an enlargement of the corresponding area in the small up left box.

The intersection between real (reconstruction of 1877 lahar path [101]) and corresponding sector of simulated event (Fig. 6.16) returns a fitness value $e1 = \sqrt{\frac{R \cap S}{R \cup S}} = 0.75$ (Table 6.7), where R is the extension of real event and S is the extension of simulated event. This comparison was used for the LLUNPIY validation.

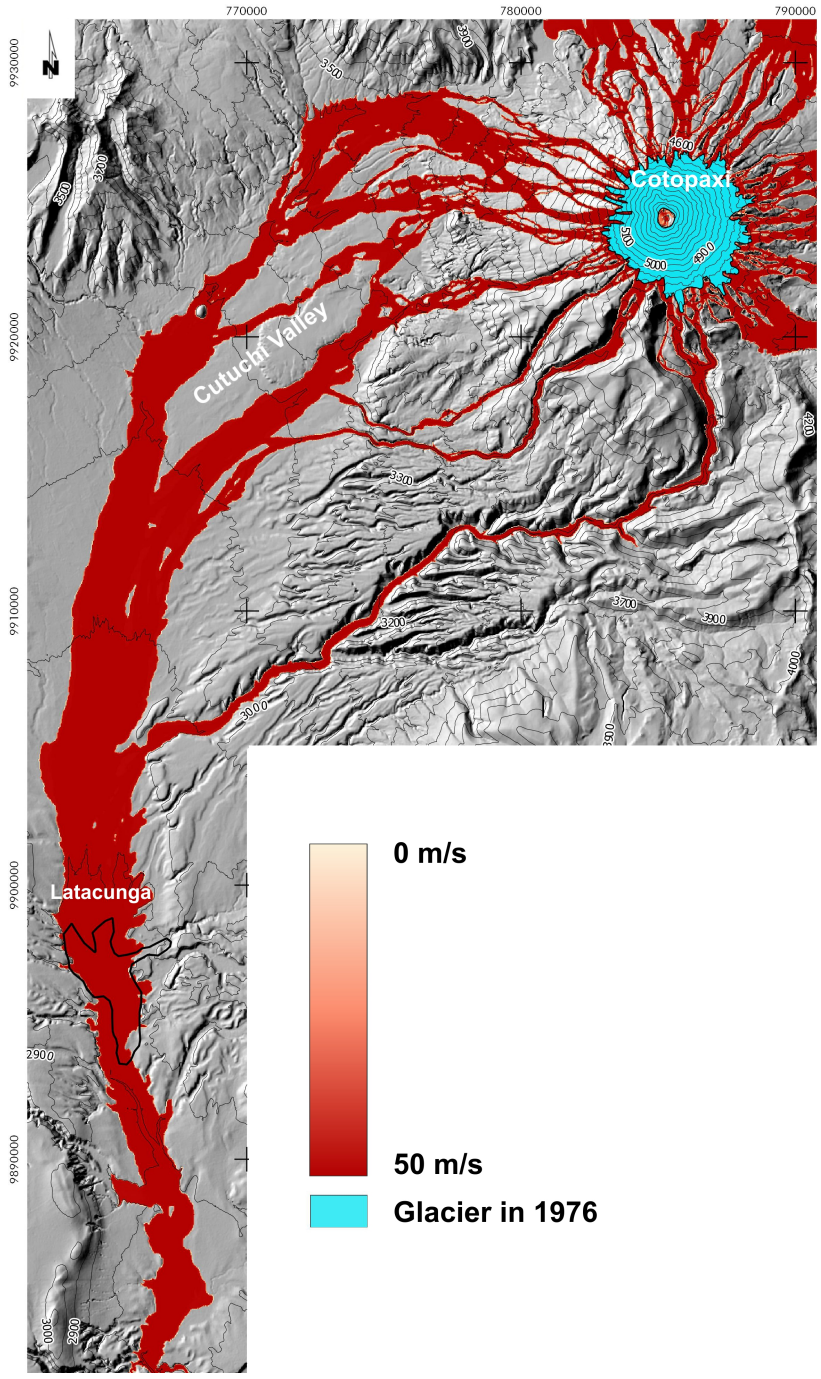

Fig. 6.13 Maximum velocities reached by flows at the end of simulation event 'Gradual Glacier Melting (pyroclastic bombs)' (steps 230,000).

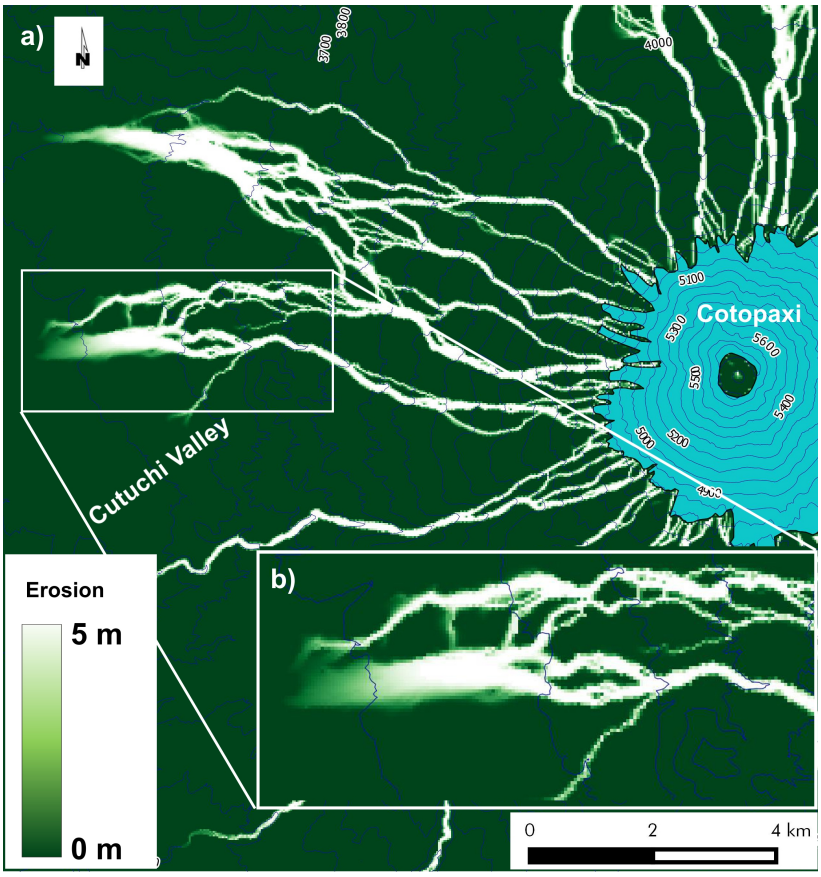

Fig. 6.14 Erosion at step 8,000. The box (b) represents an enlargement of the corresponding area in the small up left box.

Table 6.7 Invaded area values of the real (R) and simulated (S) event.

R ($\times 10^6 m^2$)	S ($\times 10^6 m^2$)	e1
100.9	166.37	0.75

The lahar reaches Latacunga in 62 minutes, remember that chronicles of the time report the flows have invaded the city in one hour. Then this simulation as well as having a good correspondence with the path of lahar are also respected travel times. This conditions was not verified in simulation with 'Many Sources' case and 'Immediate Glacier Melting' case.

6.4.4 Evaluating LLUNPIY Simulations: Primary Lahars

LLUNPIY, a CA model, was applied in order to attempt simulations of 1877 primary lahars occurred in Cutuchi Valley, south west sector of Cotopaxi volcano. A careful analysis was performed in order to obtain the most faithful reconstruction of such a catastrophic event.

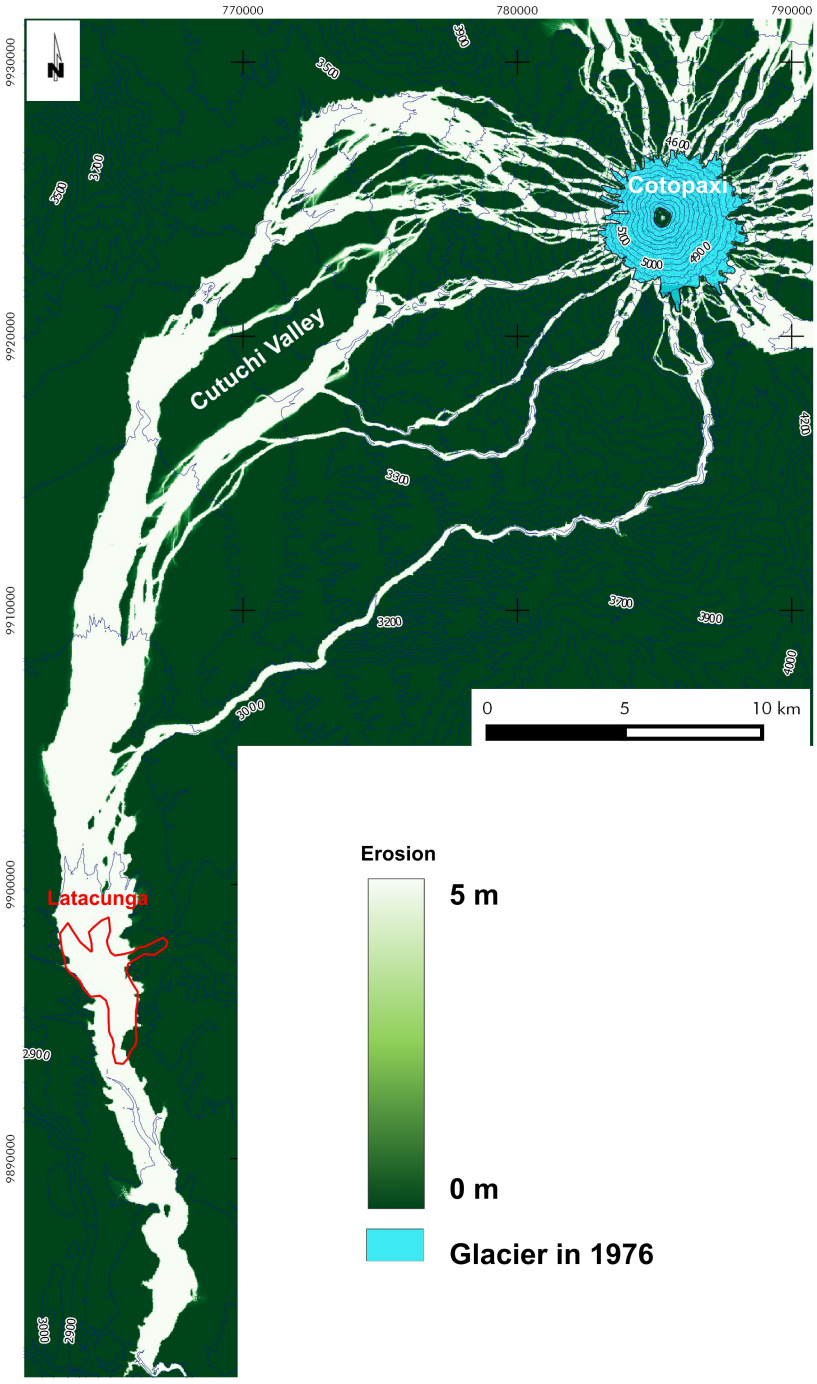

Fig. 6.15 Erosion value at the end of 'Gradual Glacier Melting (pyroclastic bombs)' simulation (steps 230,000).

Some points, which can be improved in the future research work, have to be considered: Operating on the current morphology; some corrections have to be produced in order to approach the pre-event morphology and to tune better the parameters of LLUNPIY.

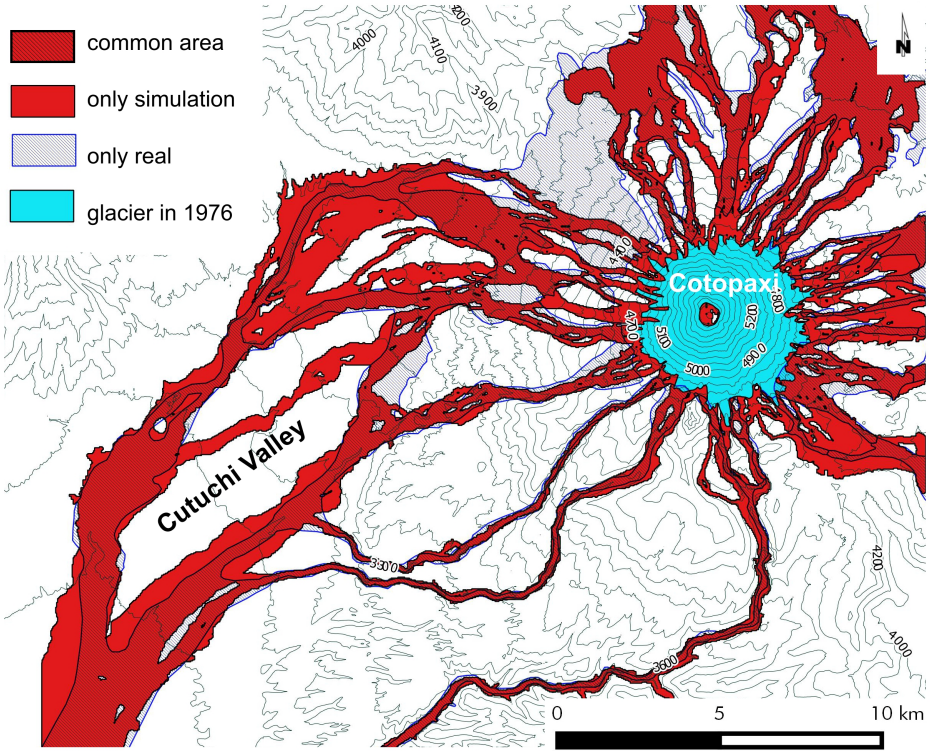

Fig. 6.16 Intersection between real event (reconstruction of 1877 lahar path [101]) and corresponding sector of 'Gradual Glacier Melting (pyroclastic bombs)' simulated event.

Initial velocity of the lahars in the case of 'many sources simulations' is null; such simulations can be repeated, starting with an opportune velocity by varying the model and introducing a 'lahar source'.

The immediate melting of the Cotopaxi icecap descends from the worst hypothesis among the possible ones, regarding the first phase of the phenomenon; it is important to test the other hypotheses.

Anyway, the results of these preliminary simulations demonstrate that the CA model LLUNPIY is working appropriately, considering a partial application, sometimes rough data concerning the event [101] and its possible improvements.

The simulations were acceptable in terms of reproducing the global dynamics of the events, such as velocity and height of detrital flow. Simulated lahar path and invaded area agree with real (partially reconstructed) one.

Times are not respected: in simulations, lahars reached Latacunga about 10 minutes later than reported in the chronicles of the time [164]. This discrepancy could depend on some imprecision of chronicles or on the increased length of paths in the simulation because of space discretization or both; such a problem will investigate considering these different viewpoints.

6.5 Sensitivity analysis

The sensitivity analysis (SA) [127] returns an assessment of the model reliability from a numerical stability viewpoint. It studies the variations of the model output due to different causes, to assess the confidence level of the model itself. Originally, it was proposed for the analysis of output variations regarding the variations in the model parameters. Afterwards, it has been extended to the study of the generic inputs variations.

The aim of this analysis is to assess the impact that measurement errors have on the simulation's results and hence to identify the critical parameters, information that is important in applications to scenario forecasting during lahars events, providing suggestions for more modeling research.

SA in this research is focused on global parameters (physical and empirical). These parameters are imposed by the precision desired of the simulation, where it is possible (e.g., cell dimension). The values of some parameters are deduced from phenomenon's physical features (e.g., turbulence dissipation), even if the simulation quality fixes an acceptable value by attempts, triggered by comparison of discrepancies between real event knowledge and simulation results.

Real events, which are considered in this thesis, have problems for sensitivity analysis, because of that morphology is particular: e.g., lahar path is channeled between steepest and very narrow walls, except the final part. The width variation of the path, related to parameter variation is, of course, meaningless for simulating such real events.

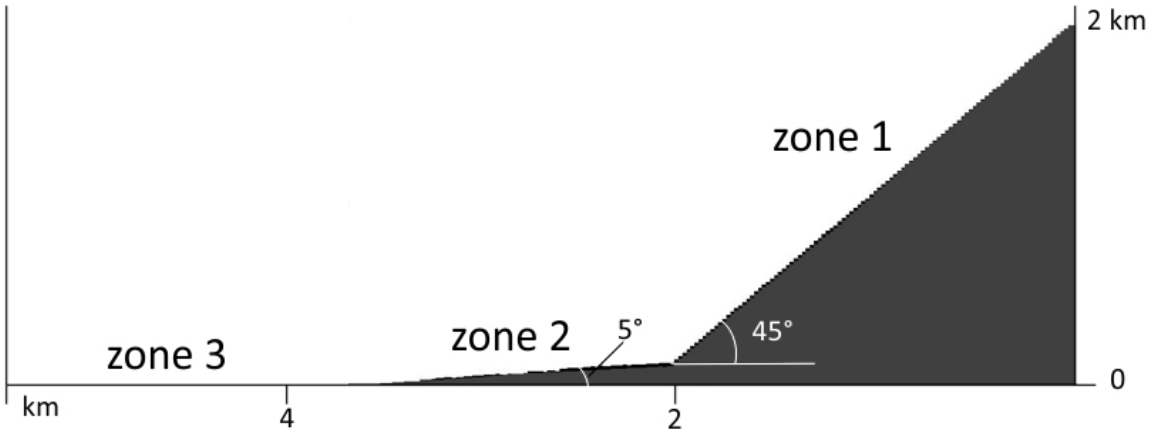

Fig. 6.17 The three zones of the ideal surface.

In order to analyze the significant sensitivity in the parameters, an ideal surface was considered: a plane, 2 km wide, divided into three zones (Fig. 6.17): 1) a sector, 2 km long and 45° of inclination (it represents the inclination in the lahar generation area), 2) the second

sector, 2 km long and 5° (representative of inclination in the area 'after lahar generation'), 3) in the third sector, 2 km long and 0°, where lahar stops by complete loss of energy.

A 'cylinder' of lahar, 10 m high with radius 22.5 m was 'placed' at the center in the top of the first sector. Only the most significant parameters are tested, by varying the parameters used in the best simulation of Cotopaxi 'Gradual Glacier Melting' (Table 6.6, Table 6.8 reference value). A series of simulations were performed by variation of a single parameter in the set of significant parameters. These were varied symmetrically in relation to the reference value.

Table 6.8 Used parameters for sensitivity analysis

Parameters	Value				
	Case c	Case a	Reference	Case b	Case d
p_{mt}	1.175×10^2	1.1625×10^2	1.2×10^2	1.2125×10^2	1.225×10^2
p_{td}		1.0×10^{-9}	1.75×10^{-8}	1.0×10^{-7}	
p_{fc}		3.0×10^{-2}	4.0×10^{-2}	5.0×10^{-2}	
p_{ed}		2.0×10^{-1}	3.0×10^{-1}	4.0×10^{-1}	
p_{pe}		1.0×10^{-4}	1.0×10^{-3}	1.0×10^{-2}	

The most relevant results of the performed tests are reported (Figs. 6.18 – 6.23, Tables 6.8 and 6.9). In the figures, the zones are specified according to Fig. 6.17; where, brown lines represent 'contour lines'. Regolith depth (initially 5 m) is represented in the top figure; the yellow degrading to black color means, depth from maximum to minimum value while white means complete erosion. Lahar thickness is represented in the lower figure; yellow degrading to black means thickness from maximum to a minimum value. The left figures are referred to a lahar that overrun the zone 1, the right figures refer to a lahar that overrun the zone 2 and the lahar accumulated at the begin of the sector 3, with null slope, because of complete energy lack.

The most sensitive parameters are the mobilization threshold (p_{mt}) and the progressive erosion parameter (p_{pe}). Figures 6.20 and 6.22 shown the variation of erosion depth and the lahar thickness together with the final volume of eroded matter (see Tables 6.8 and 6.9). Such behavior of the model is very important, if it is considered that the other simulation models do not take into account erosion [101] [116] [163], a crucial element of the phenomenon. Tables 6.8 and 6.9 report data concerning to the other parameters.

Table 6.9 Final volume of eroded matter

Parameters	Total erosion debris ($\times 10^6 m^3$)				
	Case c	Case a	Reference	Case b	Case d
p_{mt}	22.02	23.24	20.31	17.44	15.47
p_{td}		20.19	20.31	20,40	
p_{fc}		20.54	20.31	20.36	
p_{ed}		20.41	20.31	20,31	
p_{pe}		2.79	20.31	26.74	

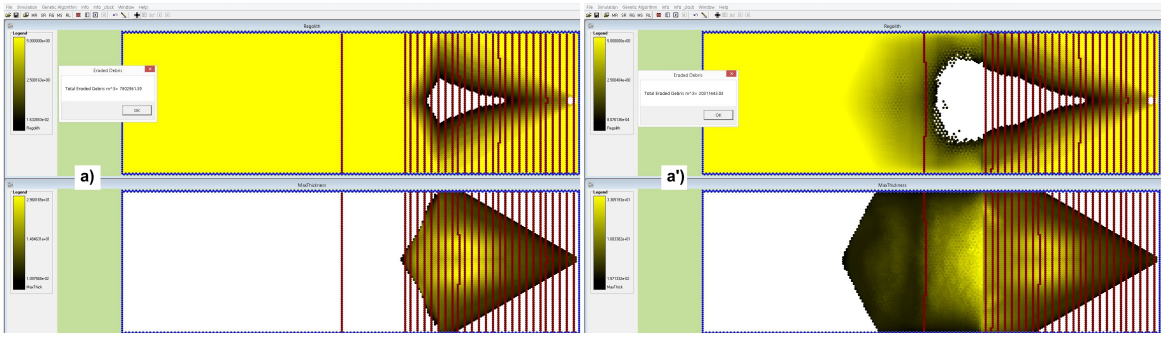

Fig. 6.18 Simulation with the reference parameters.

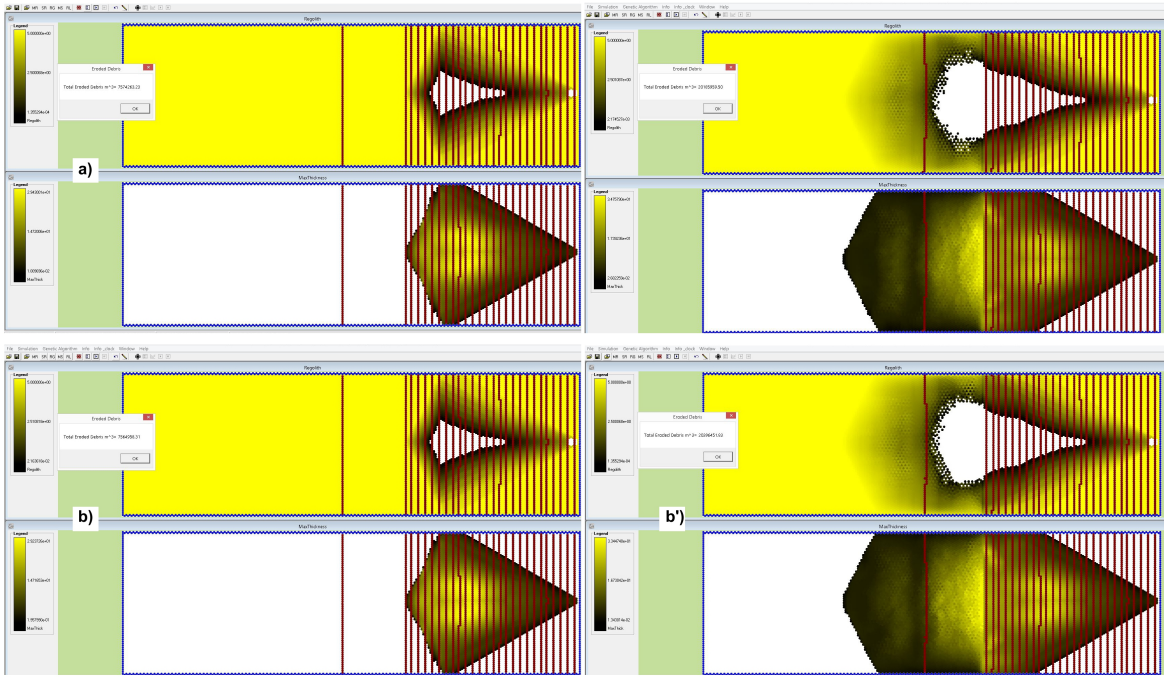

Fig. 6.19 Simulations with variation of the turbulence dissipation (p_{td}) value.

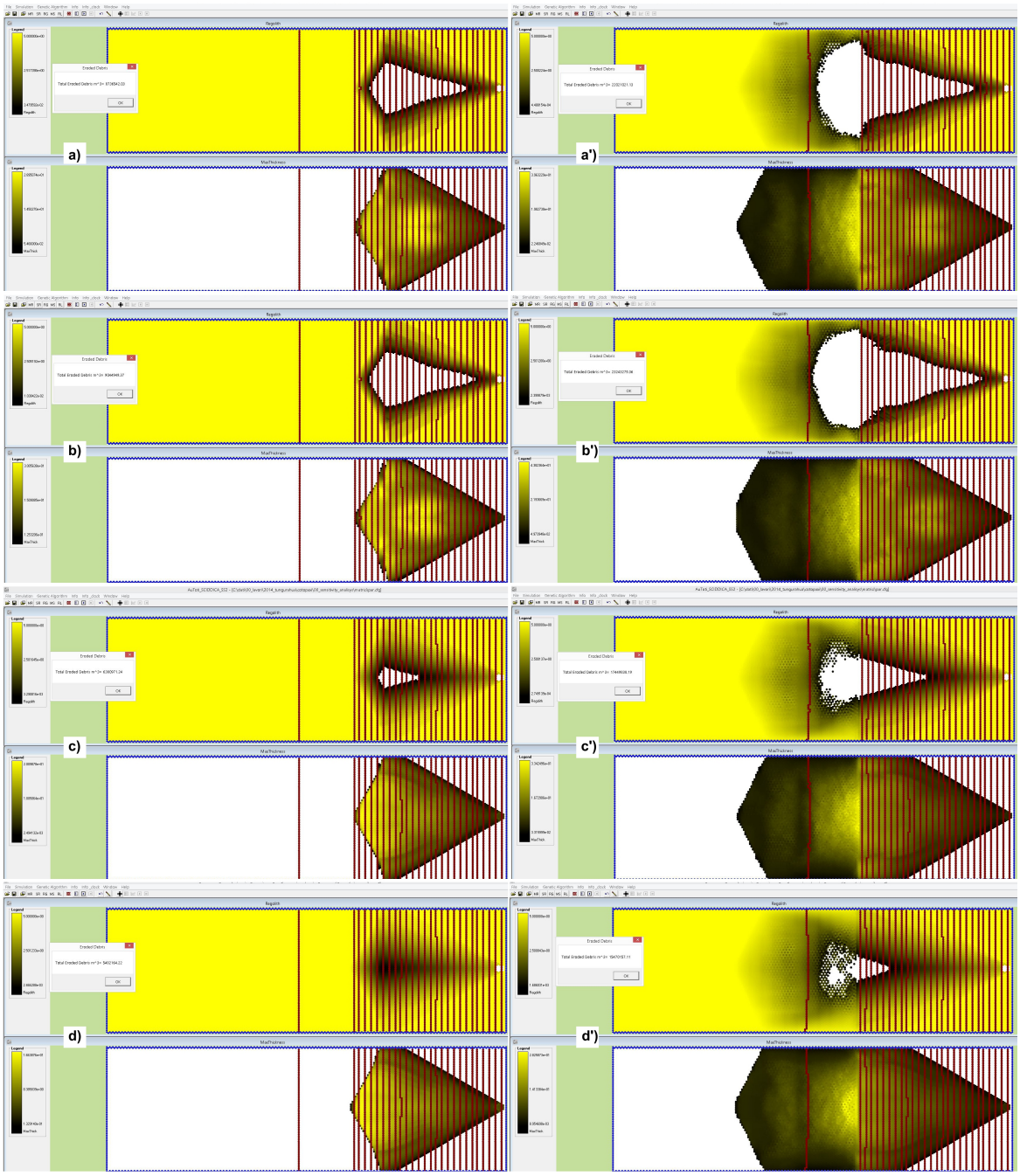

Fig. 6.20 Simulation with variation of the mobilization threshold parameters (p_{mt}) value.

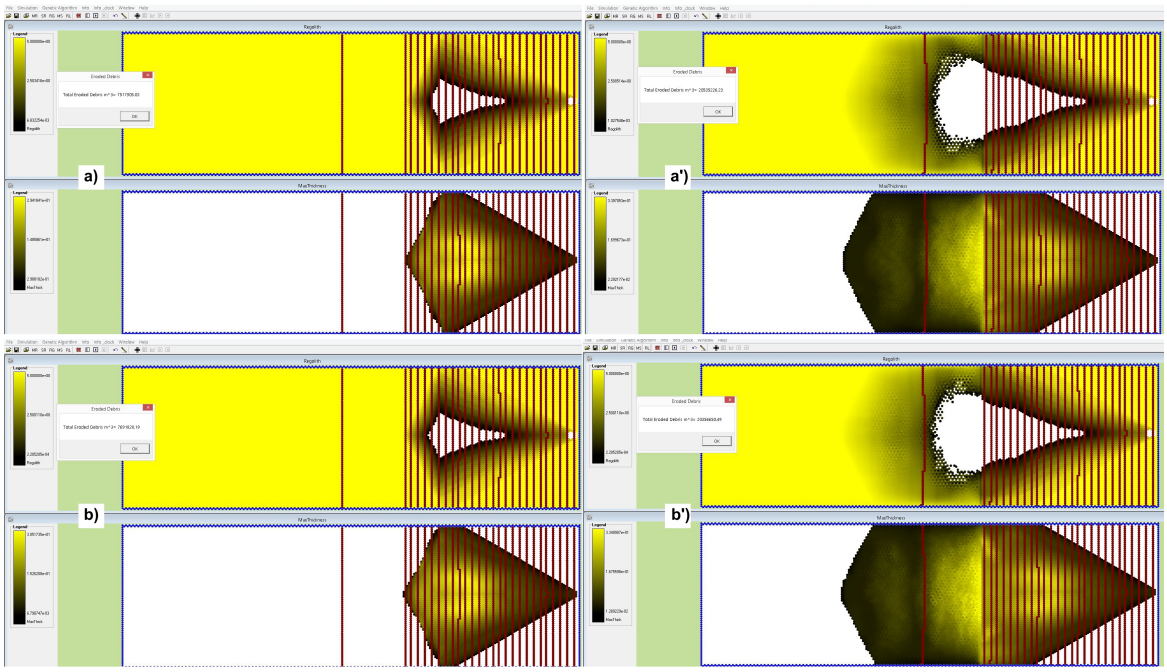

Fig. 6.21 Simulation with variation of the mobilization lahar friction coefficient (p_{fc}) value.

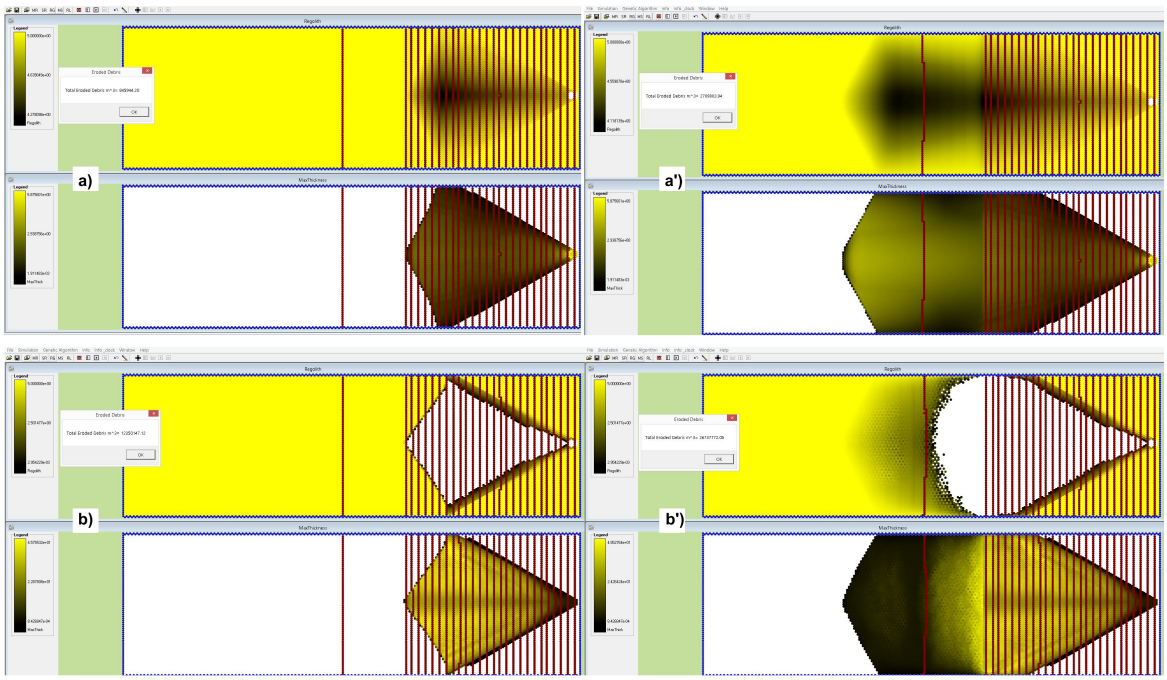

Fig. 6.22 Simulation with variation of the erosion dissipation of energy (p_{ed}) value.

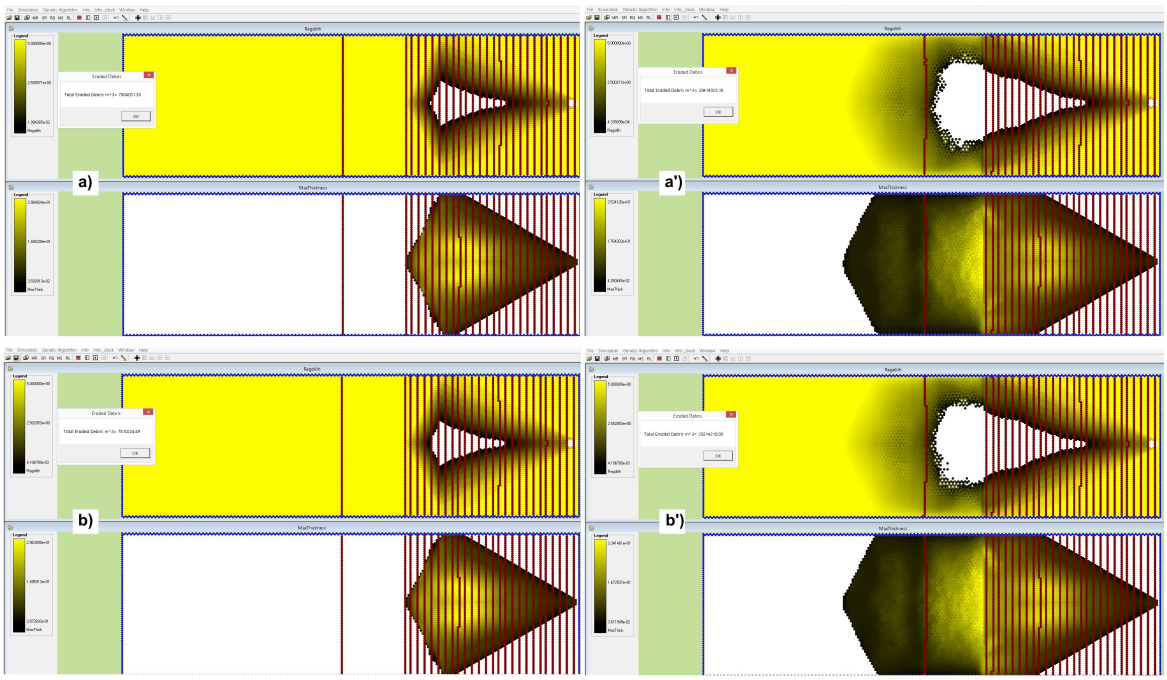

Fig. 6.23 Simulation with variation of the progressive erosion (p_{pe}) value.

Chapter 7

Conclusions and Recommendations

"...Die Kunst ist lang, und kurz ist unser Leben"

Johann Wolfgang von Goethe, 1808

Conclusions

As it may be evinced from many research, which are described in the previous chapters, the issues examined in this thesis, i.e., lahar M&S, belong to a multidisciplinary context (Computational Science) that for lahars it concerns, the fields of Computer Science, Geology, Mathematics and Physics. The contribution of these studies deals specifically with the phase of modeling based on the computational paradigm of Cellular Automata, together with validation of the model by successful simulations of real events of primary and secondary lahars.

The international scientific community recognizes well the potentiality of these models in both theoretical framework and applications for many different scientific and engineering areas (Chapter 2). Such potentialities are confirmed by the results of this research that appear in international publications.

The modeling phase is placed in the general context of the semi-empirical method, proposed by Di Gregorio and Serra (presented in Chapter 3) for modeling complex macroscopic phenomena with Cellular Automata.

This work is focused on the CA modeling of the complex phenomenon of primary and secondary lahars, whose dynamics are introduced in Chapter 4, and on the LLUNPIY model that was validated through simulations of 1877 Cotopaxi lahar and the 2005 and 2008 Tungurahua lahars.

There are different approaches for modeling this phenomenon (Chapter 4), these approaches reflect on one hand the availability of formal instruments to capture the phenomenon, on the other hand the partial scientific knowledge concerning the characteristics of the phenomenon and data about real events.

If such different approaches are compared in the light of the obtained results, it is possible to observe various visions of the phenomenon with significantly different methodologies.

A PDE approach (that wants to account for the physics of lahar as accurately as possible) must initially specify all the general characteristics of the phenomenon and lead them back to the related equations. Since lahars are complex systems, it is necessary to specify, for example, the characteristics of multiphase fluids, the third dimension must be explicit, etc. Such an approach could give rise to a complexity and multiplicity of interrelated equations, to be intractable also with the most sophisticated methods of numerical approximations for fast parallel computer simulations. Then, it is necessary a second smart phase of simplifying as much as possible the PDE in relations to the peculiarities of real cases. For example, the simulations with the model TITAN2D took the model back in two-dimensions. This smart simplification may be permitted also because the most path of 2005 lahar of Tungurahua volcano was depth channeled in the canyon of Rio Vascún. Therefore, the starting point is the specification of the phenomenon as faithful as possible in terms of equations and then to simplify according to the particular features of the case studies.

The CA approach is very different from this point of view. Firstly, it is necessary to recall that sometimes what is simple for CA, since it is easily described in terms of 'localism', it can be complicated in terms of PDE and vice versa. For example the sliding of a sphere of any diameter on a plane is trivial in terms of PDE, since there are analytical solutions, but they are not very manageable in terms of CA (only a fool would do that) for less than cheating by introducing the PDE solutions in the transition function of the CA. An opposite example is the falling snow, pushed by the wind against a barrier.

In this research, an incremental method of modeling was used, already experimented by other models for MCA. They are considered models apt to describe the phenomenon in the simpler way, but having as counterpart 'simple' case studies in the context of the CA, where simple is referred to the 'localism'. Positively overcome this phase, it is possible to starts in some way from the beginning introducing, in the modeling less simple cases.

Let's remember how LLUNPIY, as Cellular Automata model, is based on a partition of the area under examination in cells. The initial set of data, related to each cell, represents the beginning of the phenomenon and, after the repeated applications of the transitions function, the evolution of the system (Chapter 5).

In this research, some problems of a MCA approach are proposed. How large should be the cells? And then similarly, how long should be a temporal step? From an abstract viewpoint and taking into account the implicit parallelism and localism in CA, the best performance is obtained with the minimum size cell and therefore with a temporal step, that may be appropriate to such a size. But data precision or even the partial lacking of data implies a limit for such choices. The computational paradigm of Cellular Automata requires some questions related to the studied phenomenon, which other methods cannot consider (Chapter 4).

A feature characterizing models such as LLUNPIY (Chapter 5) is the knowledge of the system evolution for each cell sub-state at each step: an extraordinarily large amount of produced data, which does not have its counterpart in the field data. Then, it arises the problem to compare the evolution of the phenomenon in its emerging characteristics. Produced data must be analyzed according to 'ad hoc' criteria, which are dictated by the empirical knowledge or deduced by physical equations.

The starting assumptions are crucial for the model development; they consist in the definition of sub-states and parameters, which are considered essential for the evolution of the phenomenon. This can lead to revisit the physical processes from the local viewpoint for a description as complete as possible. For example, the determination of flows from one cell to its neighbors with the algorithm of minimization of differences is insufficient except in cases of purely gravitational flow with extremely high dissipation of energy. The LLUNPIY specification of the transition function for outflows (Chapter 5) was gradually enlarged to a wider spectrum of cases as occurred in SCIDDICA development.

Tommaso Toffoli highlights in his famous work "CA represent an alternative rather than an approximation to PDE in modeling Physics". The real laws of physics are conservation laws, which can be written in different formalisms with benefits and disadvantages that this involves. For example, magnetic spins have a better representation in discrete terms and then the CA are more advantageous.

In the case of MCA, the problem arises in a different way, it is not only a matter of accounting for the fundamental conservation laws, (which is never a problem for the mass conservation), but it is a matter of discovering and modeling the essential aspects of energy dissipation with the corresponding momentum variations. Robust empirical formulas, which account for statistically average conditions, can cope with the approximations of the available data.

Choices and attempts for the determination of parameters (in this highly non-linear context) may permit many times efficacious simulations on partial and approximated data.

Let's consider an example beyond these words: the empirical formula of the erosion and the corresponding loss of energy is valid for soils, which have similar characteristics only from a large-scale viewpoint. Although the model is deterministic, such rules have statistical value and their application cannot be extended to other cases except for similar geological characteristics; otherwise, the parameters values have to be changed or even new elementary processes and new sub-states have to be added.

The experience of models like SCIDDICA, SCIARA, PYR, VALANCA and SCAVATU is the background of LLUNPIY that was built on this basis.

At this point, it is important to pay attention to the following points regarding the reliability of the model that should be further investigated, although the satisfactory results of the simulations.

First phase of primary lahar: we started from a 'many sources' hypothesis to compare LAHARZ results with LLUNPIY ones; later the melting of the glacier of Cotopaxi Volcano was introduced in various ways. An immediate melting of 10 and 50 meters of thickness as the effect of pyroclastic flows was conjectured and applied in simulations; finally a gradual melting as the effect of pyroclastic bombs was considered, it represents a refinement of the model toward an event that is no longer possible to reconstruct in its true evolution. These three ways are representative of similar dynamics, which account for the event with gradually better approximations. It is necessary to take into account that in this thesis a series of tests and corrections are not reported. E.g. the frequency and duration of the pyroclastic bombs generates a mass of lahar, which produces almost equal effects with other values, different sets of values of parameters can be generate similar effects. Reported references for selecting parameters were accurately considered, but there are insufficient data.

With LAHARZ, the erosion process does not exist because of the simplicity of the model. With TITAN2D, for the opposite reason, because the complete PDE related to lahar behavior imply untenable computation times, the erosion process was necessarily omitted. LLUNPIY is able to manage the erosion process with satisfactory results (Chapter 6).

The management of erosion, which is a fundamental element of the phenomenon, is a LLUNPIY feature that is not present in the other simulation models. The candidate considers it as the main innovation of LLUNPIY model. The sensitive analysis, regarding the main parameters, highlights the importance of this LLUNPIY modeling development.

In this field, CA are able to develop a greater similarity in the simulation of the phenomenon, since, for their nature, they are a middle course between the great simplification of many empirical methods and the extreme precision of the PDE, which needs often to simplify equations because of the not sustainable computing times. A last note: CA are themselves a system with the same dynamical characteristics of the phenomena, which they model.

In the following, main critical points of LLUNPIY are enumerated:

1. Pyroclastic soil cover (regolith) data were considered almost homogeneous in terms of composition and thickness; such an assumption is critical, because the scarce data of soil tomography, that the candidate collected data by himself on the field and those were kindly interpreted by Rizzo and Straface show an heterogeneity, that is averaged in the studied cases. This part of the model has to be refined, when tomographic data will be available.

2. The exhaustion phase (lahar deposit and extruded water) of the model was not simulated because the reported lahar floods disappeared into the rivers. The elementary process in the model was deduced by SCIARA and it is well working if the opportune parameters are found.

3. The computations of lahar flows are based on the extension of Algorithm of Minimization of Differences (AMD) that is adopted in SCIDDICA-SS3. The simpler version of SCIDDICA-SS2 was used in simulations because results were approximately the same and computation times were very shorter. A GP-GPU version will be necessary in the future for getting on with the research.

Recommendations for future work

The model must be improved according to the previous enumerated critical points, but the semi-empirical approach needs more data and more precise information about the evolution of events. This implies that new events of lahars must be considered and the necessity of case studies in other areas as Peru, Mexico, Indonesia and so on. Only in this prospect, LLUNPIY will reach a higher level of reliability.

LLUNPIY was developed in order to be a forecasting tool and to provide with hazard maps that could be important for emergency situations. Another goal is to evaluate works for reduction of lahar hazard.

An unusually largest number of secondary lahars were triggered in the last fifteen years in a period of intense activity of Tungurahua volcano. The recent stratum of volcanic product, that fed lahars, did not reach dangerous thicknesses because of the high frequency of lahars, whose hazard was limited in these cases.

An idea, that arose during this research and that must be very well examined, is to find conditions for favoring the generation of secondary micro-lahars by LLUNPIY. In this way, the triggering of dangerous large lahars could be avoided by reducing the thickness of sensible stratum of pyroclastic matter, that could be eroded in a lahar event.

References

[1] Avolio, M. V., Crisci, G. M., D'Ambrosio, D., Di Gregorio, S., Iovine, G., Rongo, R., and Spataro, W. (2003). An extended notion of Cellular Automata for surface flows modelling. *WSEAS Transactions on Computers*, 2(4):1080–1085.

[2] Avolio, M. V., Crisci, G. M., Di Gregorio, S., Rongo, R., Spataro, W., and Trunfio, G. A. (2006). SCIARA γ 2: An improved Cellular Automata model for lava flows and applications to the 2002 Etnean crisis. *Computers & Geosciences*, 32(7):876 – 889.

[3] Avolio, M. V., Di Gregorio, S., Lupiano, V., and Mazzanti, P. (2013). SCIDDICA-SS3: a new version of Cellular Automata model for simulating fast moving landslides. *The Journal of Supercomputing*, 65(2):682–696.

[4] Avolio, M. V., Di Gregorio, S., Lupiano, V., Mazzanti, P., and Spataro, W. (2010a). Application Context of the SCIDDICA Model Family for Simulations of Flow-Like Landslides. In *Proceedings of The 2010 International Conference on Scientific Computing*, pages 40–46.

[5] Avolio, M. V., Di Gregorio, S., Spataro, W., and Trunfio, G. (2012). A Theorem about the Algorithm of Minimization of Differences for Multicomponent Cellular Automata. In Sirakoulis, G. and Bandini, S., editors, *Cellular Automata*, volume 7495 of *Lecture Notes in Computer Science*, pages 289–298. Springer Berlin Heidelberg.

[6] Avolio, M. V., Errera, A., Lupiano, V., Mazzanti, P., and Di Gregorio, S. (2010b). Development and calibration of a preliminary cellular automata model for snow avalanches. In Bandini, S. e. a., editor, *Cellular Automata*, volume 6350 of *Lecture Notes in Computer Science*, pages 83–94. Springer.

[7] Avolio, M. V., Lupiano, V., Mazzanti, P., and Di Gregorio, S. (2008). Modelling Combined Subaerial-Subaqueous Flow-Like Landslides by Cellular Automata. In Umeo, H., Morishita, S., Nishinari, K., Komatsuzaki, T., and Bandini, S., editors, *Cellular Automata*, volume 5191 of *Lecture Notes in Computer Science*, pages 329–336. Springer Berlin Heidelberg.

[8] Bar-Yam, Y. (1996). Polymer simulation using Cellular Automata: 2-D Melts, Gel-Electrophoresis and Polymer collapse. *Some New Directions in Science on Computers, eds. G. Bhanot, S. Chen, and P. Seiden (World Scientific, Singapore, 1996)*.

[9] Barca, D., Crisci, G., Di Gregorio, S., and Nicoletta, F. (1987). Lava flow simulation by cellular automata: Pantelleria's examples. In *Proceedings A.M.S. International Congress Modelling and Simulation, Cairo, Egypt*, pages 9–15.

[10] Barca, D., Di Gregorio, S., Nicoletta, F., and Sorriso-Valvo, M. (1986). A cellular space model for flow type landslides. In *Computers and their Application for Development, Proceedings of the International Symposium of the IASTED. Acta Press, Taormina, Italy*, pages 30–32.

[11] Barclay, J., Alexander, J., and Sušnik, J. (2007). Rainfall-induced lahars in the Belham Valley, Montserrat, West Indies. *Journal of the Geological Society*, 164(4):815–827.

[12] Beigy, H. and Meybodi, M. R. (2004). A mathematical framework for cellular learning automata. *Advances in Complex Systems*, 7(03n04):295–319.

[13] Bemmelen, R. v. (1949). The geology of Indonesia, vol. 1A–General geology of Indonesia and adjacent archipelagoes: The Hague, Netherlands, Govt. *Printing Office*, 732.

[14] Bennett, C. H. and Grinstein, G. (1985). Role of irreversibility in stabilizing complex and nonergodic behavior in locally interacting discrete systems. *Physical review letters*, 55(7):657.

[15] Berlekamp, E. R., Conway, J. H., and Guy, R. K. (2003). Winning ways for your mathematical plays, volume 4. *Applied Mathematics and Computation*, 10:12.

[16] Cáceres, B. et al. (2004). Determinación del volumen del casquete de hielo del volcán Cotopaxi. *IG-EPN, Instituto de Geofísica de la Escuela Politécnica Nacional. Quito*.

[17] Chen, H., Chen, S., and Matthaeus, W. H. (1992). Recovery of the Navier-Stokes equations using a lattice-gas Boltzmann method. *Physical Review A*, 45(8):5339, 5342.

[18] Chopard, B. (2012). Cellular automata modeling of physical systems. *Computational Complexity: Theory, Techniques, and Applications*, pages 407–433.

[19] Chopard, B., Dupuis, A., Masselot, A., and Luthi, P. (2002). Cellular Automata and lattice Boltzmann techniques: An approach to model and simulate complex systems. *Advances in complex systems*, 5(2):103–246.

[20] Chopard, B. and Masselot, A. (1999). Cellular Automata and lattice Boltzmann methods: a new approach to computational fluid dynamics and particle transport. *Future Generation Computer Systems*, 16(2):249–257.

[21] Clerici, A. and Perego, S. (2000). Simulation of the Parma River blockage by the Corniglio landslide (Northern Italy). *Geomorphology*, 33(1):1–23.

[22] Codd, E. F. (2014). *Cellular Automata*. Academic Press.

[23] Conway, J. (1970). The game of life. *Scientific American*, 223(4):4.

[24] Córdoba, G., Villarosa, G., Sheridan, M., Viramonte, J., Beigt, D., and Salmuni, G. (2015). Secondary lahar hazard assessment for Villa la Angostura, Argentina, using Two-Phase-Titan modelling code during 2011 Cordón Caulle eruption. *Natural Hazards and Earth System Science*, 15(4):757–766.

[25] Costa, J. E. (1997a). Hydraulic modeling for lahar hazards at Cascades volcanoes. *Environmental & Engineering Geoscience*, 3(1):21–30.

[26] Costa, J. E. (1997b). Hydraulic modeling for lahar hazards at cascades volcanoes. *Environmental & Engineering Geoscience*, 3(1):21–30.

[27] Crandell, D. R. (1971). Postglacial lahars from Mount Rainier volcano, Washington. Technical report, US Govt. Print. Off.

[28] Crisci, G., Di Gregorio, S., Pindaro, O., and Ranieri, G. (1986). Lava flow simulation by a discrete cellular model: first implementation. *International journal of modelling & simulation*, 6(4):137–140.

[29] Crisci, G., Di Gregorio, S., and Ranieri, G. (1982). A cellular space model of basaltic lava flow. In *Proceedings International AMSE Conference Modelling & Simulation (Paris, France, Jul. 1-3)*, pages 65–67.

[30] Crisci, G., Iovine, G., Di Gregorio, S., and Lupiano, V. (2008). Lava-flow hazard on the SE flank of Mt. Etna (Southern Italy). *Journal of Volcanology and Geothermal Research*, 177(4):778–796.

[31] Crisci, G. M., Avolio, M. V., Behncke, B., D'Ambrosio, D., Di Gregorio, S., Lupiano, V., Neri, M., Rongo, R., and Spataro, W. (2010). Predicting the impact of lava flows at Mount Etna, Italy. *Journal of Geophysical Research: Solid Earth*, 115(B4). B04203.

[32] Crisci, G. M., Di Gregorio, S., Rongo, R., and Spataro, W. (2005). PYR: a Cellular Automata model for pyroclastic flows and application to the 1991 Mt. Pinatubo eruption. *Future Generation Computer Systems*, 21(7):1019–1032.

[33] Crutchfield, J., Mitchell, M., and Das, R. (2002). *The evolutionary design of collective computation in Cellular Automata*.

[34] Crutchfield, J. P. (1994). The calculi of emergence: computation, dynamics and induction. *Physica D: Nonlinear Phenomena*, 75(1):11–54.

[35] Crutchfield, J. P. and Hanson, J. E. (1993). Attractor vicinity decay for a cellular automaton. *Chaos: An Interdisciplinary Journal of Nonlinear Science*, 3(2):215–224.

[36] D'Ambrosio, D., Di Gregorio, S., Gabriele, S., and Gaudio, R. (2001). A Cellular Automata model for soil erosion by water. *Physics and Chemistry of the Earth, Part B: Hydrology, Oceans and Atmosphere*, 26(1):33 – 39.

[37] D'Ambrosio, D., Di Gregorio, S., Gabriele, S., and Gaudio, R. (2002). Un metodo di trasformazione di reticoli a maglia quadrata in reticoli a maglia esagonale e viceversa. Technical Report 585, CNR-IRPI - Sezione di Cosenza.

[38] D'Ambrosio, D., Filippone, G., Marocco, D., Rongo, R., and Spataro, W. (2013). Efficient application of GPGPU for lava flow hazard mapping. *The Journal of Supercomputing*, 65(2):630–644.

[39] Denlinger, R. P. and Iverson, R. M. (2001). Flow of variably fluidized granular masses across three-dimensional terrain: 2. numerical predictions and experimental tests. *Journal of Geophysical Research: Solid Earth (1978–2012)*, 106(B1):553–566.

[40] Désérable, D., Dupont, P., Hellou, M., and Kamali-Bernard, S. (2007). Cellular automata models for complex matter. In *Parallel Computing Technologies*, pages 385–400. Springer.

[41] Deutsch, E. S. (1972). Thinning algorithms on rectangular, hexagonal, and triangular arrays. *Communications of the ACM*, 15(9):827–837.

[42] Di Gregorio, S. and Serra, R. (1999). An empirical method for modelling and simulating some complex macroscopic phenomena by cellular automata. *Future Generation Computer Systems* , 16(2–3):259 – 271.

[43] Di Gregorio, S., Serra, R., and Villani, M. (1997). A Cellular Automata Model of Soil Bioremediation. In *Complex Systems*, volume 11, pages 31–54.

[44] Doolen, G. D. (1990). *Lattice gas methods for partial differential equations: a volume of lattice gas reprints and articles, including selected papers from the workshop on large nonlinear systems, held August, 1987 in Los Alamos, New Mexico*, volume 4. Addison-Wesley Longman.

[45] Dragoni, M. (1993). Modelling the rheology and cooling of lava flows. *Active Lavas: Monitoring and Modelling, edited by: Kilburn, C. RJ and Luongo, G.,(UCL Press. London)*, pages 235–261.

[46] Ermentrout, G. B. and Edelstein-Keshet, L. (1993). Cellular automata approaches to biological modeling. *Journal of theoretical Biology*, 160(1):97–133.

[47] Escher, B. (1922). On the hot lahar of the valley of ten thousand smokes (alaska). *Proceedings Koninklijke Akademie van Wetenschappen, Amsterdam*, 24:282–293.

[48] Fagents, S. A. and Baloga, S. M. (2006). Toward a model for the bulking and debulking of lahars. *Journal of Geophysical Research: Solid Earth (1978–2012)*, 111(B10).

[49] Fischer, P. C. (1965). Generation of primes by a one-dimensional real-time iterative array. *Journal of the ACM (JACM)*, 12(3):388–394.

[50] Fisher, R. V. and Schmincke, H.-U. (2012). *Pyroclastic rocks*. Springer Science & Business Media.

[51] Fread, D. L. (1988). *The NWS DAMBRK model: Theoretical background/user documentation*. Hydrologic Research Laboratory, National Weather Service, NOAA.

[52] Fredkin, E. and Toffoli, T. (2002). *Conservative logic*. Springer.

[53] French, R. and Messinger, A. (1994). Genes, phenes and the baldwin effect: Learning and evolution in a simulated population. In *Artificial Life IV*, pages 277–282.

[54] Frisch, U., d'Humieres, D., Hasslacher, B., Lallemand, P., Pomeau, Y., Rivet, J.-P., et al. (1987). Lattice gas hydrodynamics in two and three dimensions. *Complex systems*, 1(4):649–707.

[55] Frisch, U., Hasslacher, B., and Pomeau, Y. (1986). Lattice-gas automata for the navier-stokes equation. *Physical review letters*, 56(14):1505.

[56] Gallavotti, G. (1996). Meccanica dei fluidi. *Quaderni CNR-GNAFA*, (52).

[57] Ganguly, N., Sikdar, B. K., Deutsch, A., Canright, G., and Chaudhuri, P. P. (2003). A survey on cellular automata.

[58] Gardner, M. (1970). Mathematical games: The fantastic combinations of john conway's new solitaire game "life". *Scientific American*, 223(4):120–123.

[59] Gardner, M. (2013). *Enigmi e giochi matematici*. BUR.

[60] Ghezzi, C. and Mandrioli, D. (1989). *Informatica teorica*. Città Studi.

[61] Goudie, A. (2004). *Encyclopedia of geomorphology*, volume 2. Psychology Press.

[62] Gray, L. (2003). A mathematician looks at Wolfram's new kind of science. *Notices-American Mathematical Society*, 50(2):200–211.

[63] Ha, S., Ku, N., Lee, K.-Y., et al. (2012). Lattice Boltzmann Simulation for the Prediction of Oil Slick Movement and Spread in Ocean Environment. In *The Twenty-second International Offshore and Polar Engineering Conference*. International Society of Offshore and Polar Engineers.

[64] Hanson, J. E. and Crutchfield, J. (1993). *Computational mechanics of cellular automata*. PhD thesis, University of California, Berkeley.

[65] Hanson, J. E. and Crutchfield, J. P. (1997). Computational mechanics of cellular automata: An example. *Physica D: Nonlinear Phenomena*, 103(1):169–189.

[66] Hardy, J. and Pomeau, Y. (1972). Thermodynamics and hydrodynamics for a modeled fluid. *Journal of Mathematical Physics*, 13(7):1042–1051.

[67] Hayes, B. (1984). The cellular automaton offers a model of the world and a world unto itself. *Scientific American*, 250(3):12–21.

[68] Hessel, R. (2006). Consequences of hyperconcentrated flow for process-based soil erosion modelling on the chinese loess plateau. *Earth Surface Processes and Landforms*, 31(9):1100–1114.

[69] Higuera, F. and Jimenez, J. (1989). Boltzmann approach to lattice gas simulations. *EPL (Europhysics Letters)*, 9(7):663.

[70] IGEPN (2005). Annual Review of the Activity of Tungurahua Volcano. Technical report, Instituto Geofísico, Quito, Ecuador. www.igepn.edu.ec.

[71] IGEPN (2008). Weekly Report from the Tungurahua Volcano Observatory (18-24 August, 2008). Technical Report 33, Instituto Geofísico, Quito, Ecuador. www.igepn.edu.ec.

[72] Ilachinski, A. (2001). *Cellular automata: a discrete universe*. World Scientific.

[73] Iverson, R. M. (1997). The physics of debris flows. *Reviews of geophysics*, 35(3):245–296.

[74] Iverson, R. M. and Denlinger, R. P. (2001). Flow of variably fluidized granular masses across three-dimensional terrain: 1. coulomb mixture theory. *J. Geophys. Res*, 106(B1):537–552.

[75] Janda, R. J., Scott, K. M., Nolan, K. M., and Martinson, H. (1981). Lahar movement, effects, and deposits. In *The 1980 Eruptions of Mount St. Helens, Washington*, volume 1250, pages 461–478. Washington, DC, USA: USGS.

[76] Kier, L. B., Seybold, P. G., and Cheng, C.-K. (2005). *Modeling chemical systems using cellular automata*, volume 1. Springer Science & Business Media.

[77] Kingsbery Jr, J. C. (2006). *Excluded Blocks in Cellular Automata*. PhD thesis, Citeseer.

[78] Kocabas, V. and Dragicevic, S. (2006). Assessing cellular automata model behaviour using a sensitivity analysis approach. *Computers, Environment and Urban Systems*, 30(6):921–953.

[79] Laigle, D. and Marchi, L. (2000). Example of mud/debris-flow hazard assessment, using numerical models. In *2nd International Conference on Debris-flow Hazard Mitigation: Mechanics, Prediction and Assessment*, pages 260–269. Balkema: Rotterdam.

[80] Langton, C. G. (1986). Studying artificial life with cellular automata. *Physica D: Nonlinear Phenomena*, 22(1):120–149.

[81] Langton, C. G. (1990). Computation at the edge of chaos: phase transitions and emergent computation. *Physica D: Nonlinear Phenomena*, 42(1):12–37.

[82] Lavigne, F. and Thouret, J.-C. (2003). Sediment transportation and deposition by rain-triggered lahars at Merapi Volcano, Central Java, Indonesia. *Geomorphology*, 49(1):45–69.

[83] Le Pennec, J. L., Jaya, D., Samaniego, P., Ramón, P., Moreno, S., Yánez, H., Egred, J., and van der Plicht, J. (2008). The eruptive periods at Tungurahua volcano, Ecuador, revealed by historical narratives, stratigraphy and radiocarbon dating. *Journal of Volcanology and Geothermal Research*, 176(1):70 – 81.

[84] Luo, L.-S. (2000). Theory of the lattice Boltzmann method: Lattice Boltzmann models for nonideal gases. *Physical Review E*, 62(4):4982.

[85] Lupiano, V., Machado, G., Crisci, G. M., and Gregorio, S. D. (2015). Modelling fast-moving flow-like landslides by cellular automata: Simulations of debris flows and lahars. In *WSEAS 2015 - Proceedings of the 8th International Conference on Environmental and Geological Science and Engineering (EG '15), Salerno, Italy, in: Advances in Environmental and Geological Science and Engineering.*, pages 53–61.

[86] Macedonio, G. and Longo, A. (1999). Lava flow in a channel with a bifurcation. *Physics and Chemistry of the Earth, Part A: Solid Earth and Geodesy*, 24(11):953–956.

[87] Machado, G., Lupiano, V., Avolio, M., Gullace, F., and Di Gregorio, S. (2015a). A cellular model for secondary lahars and simulation of cases in the Vascún Valley, Ecuador. *Journal of Computational Science. Sci. http://dx.doi.org/10.1016/j.jocs.2015.08.001*.

[88] Machado, G., Lupiano, V., Avolio, M. V., and Di Gregorio, S. (2014a). A Preliminary Cellular Model for Secondary Lahars and Simulation of 2005 Case of Vascún Valley, Ecuador. In Was, J., Sirakoulis, G., and Bandini, S., editors, *Cellular Automata*, volume 8751 of *Lecture Notes in Computer Science*, pages 208–217. Springer International Publishing.

[89] Machado, G., Lupiano, V., Avolio, M. V., and Di Gregorio, S. (2014b). LLUNPIY: Un modelo de Autómatas Celulares para la simulación de Lahares Secundarios. In *MEMORIAS / II WORKSHOP DE CIENCIA, INNOVACIÓN , TECNOLOGÍA Y SABERES*, Universidad Nacional de Chimborazo, Riobamba, Ecuador. ISBN: 978-9942-935-08-3.

[90] Machado, G., Lupiano, V., Crisci, G. M., and Gregorio, S. D. (2015b). LLUNPIY Preliminary Extension for Simulating Primary Lahars - Application to the 1877 Cataclysmic Event of Cotopaxi Volcano. In *SIMULTECH 2015 - Proceedings of the 5th International Conference on Simulation and Modeling Methodologies, Technologies and Applications, Colmar, Alsace, France, 21 - 23 July, 2015.*, pages 367–376.

[91] Major, J., Pierson, T., Dinehart, R., and Costa, J. (2000). Sediment yield following severe volcanic disturbance. — A two-decade perspective from Mount St. Helens. *Geology*, 28(9):819–822.

[92] Major, J. J. and Newhall, C. G. (1989). Snow and ice perturbation during historical volcanic eruptions and the formation of lahars and floods. *Bulletin of volcanology*, 52(1):1–27.

[93] Malamud, B. D. and Turcotte, D. L. (2000). Cellular-automata models applied to natural hazards. *Computing in Science & Engineering*, 2(3):42–51.

[94] Manville, V. (2004). Palaeohydraulic analysis of the 1953 Tangiwai lahar; New Zealand's worst volcanic disaster. *Acta Vulcanologica*, 16(1/2):1000–1015.

[95] Manville, V., Hodgson, K., and Nairn, I. (2007). A review of break-out floods from volcanogenic lakes in New Zealand. *New Zealand Journal of Geology and Geophysics*, 50(2):131–150.

[96] Manville, V., Hodgson, K. A., Houghton, B. F., Keys, J. R. H., and White, J. D. L. (2000). Tephra, snow and water: complex sedimentary responses at an active snow-capped stratovolcano, Ruapehu, New Zealand. *Bulletin of Volcanology*, 62(4-5):278–293.

[97] Manville, V., Major, J. J., and Fagents, S. A. (2013). Modeling lahar behavior and hazards. In Fagents, S. A., Gregg, T. K. P., and Lopes, R. M. C., editors, *Modeling Volcanic Processes*, pages 300–330. Cambridge University Press.

[98] Margolus, N. (1984). Physics-like models of computation. *Physica D: Nonlinear Phenomena*, 10(1):81–95.

[99] McNamara, G. R. and Zanetti, G. (1988). Use of the Boltzmann equation to simulate lattice-gas automata. *Physical Review Letters*, 61(20):2332.

[100] Miyamoto, H. and Sasaki, S. (1997). Simulating lava flows by an improved cellular automata method. *Computers & Geosciences*, 23(3):283–292.

[101] Mothes, P. and Vallance, J. (2015). Lahars at Cotopaxi and Tungurahua Volcanoes, Ecuador. In J.F.Shroder and Papale, P., editors, *Volcanic Hazards, Risks, and Disasters*, pages 141–167. Elsevier.

[102] Muñoz-Salinas, E., Castillo-Rodríguez, M., Manea, V., Manea, M., and Palacios, D. (2009). Lahar flow simulations using LAHARZ program: Application for the Popocatépetl volcano, Mexico. *Journal of Volcanology and Geothermal Research*, 182(1-2):13–22.

[103] Murray, A. B. and Paola, C. (1994). A cellular model of braided rivers.

[104] Murray, A. B. and Paola, C. (1997). Properties of a cellular braided-stream model. *Earth Surface Processes and Landforms*, 22(11):1001–1025.

[105] Oertel, H., Erhard, P., Asfaw, K., Etling, D., Muller, U., Riedel, U., Sreenivasan, K., and Warnatz, J. (2010). *Prandtl-essentials of fluid mechanics*, volume 158. Springer Science & Business Media.

[106] Ostrovsky, B., Crooks, G., Smith, M., and Bar-Yam, Y. (2001). Cellular automata for polymer simulation with application to polymer melts and polymer collapse including implications for protein folding. *Parallel Computing*, 27(5):613–641.

[107] Owens, R. G. and Phillips, T. N. (2002). *Computational rheology*, volume 2. World Scientific.

[108] Peterson, D. W. (1986). Volcanoes: tectonic setting and impact on society. *Active Tectonics, Geophysics Study Committee, National Research Council. National Academy Press, Washington DC*, pages 231–246.

[109] Petitot, J. (1977). Centrato/acentrato. *Enciclopedia Einaudi*, 2:894–954.

[110] Pierson, T. (1986). Flow behavior of channelized debris flows, Mount St. Helens, Washington. *Hillslope processes*, pages 269–296.

[111] Pierson, T. C. (1995). Flow characteristics of large eruption-triggered debris flows at snow-clad volcanoes: constraints for debris-flow models. *Journal of Volcanology and Geothermal Research*, 66(1):283–294.

[112] Pierson, T. C. (2005). Hyperconcentrated flow—transitional process between water flow and debris flow. In *Debris-flow hazards and related phenomena*, pages 159–202. Springer.

[113] Pierson, T. C., Janda, R. J., Thouret, J. C., and Borrero, C. A. (1990). Perturbation and melting of snow and ice by the 13 November 1985 eruption of Nevado del Ruiz, Colombia, and consequent mobilization, flow and deposition of lahars. *J. Volcanol. Geotherm*, 41:17–66.

[114] Pierson, T. C., Janda, R. J., Umbal, J. V., and Daag, A. S. (1992). *Immediate and long-term hazards from lahars and excess sedimentation in rivers draining Mt. Pinatubo, Philippines*. US Department of the Interior, US Geological Survey.

[115] Pierson, T. C. and Scott, K. M. (1985). Debris flow to hyperconcentrated streamflow. *Water resources research*, 21(10):1511–1524.

[116] Pistolesi, M., Cioni, R., Rosi, M., and Aguilera, E. (2014). Lahar hazard assessment in the southern drainage system of Cotopaxi volcano, Ecuador: Results from multiscale lahar simulations. *Geomorphology*, 207(0):51 – 63.

[117] Pitman, E., Nichita, C., Patra, A., Bauer, A., Sheridan, M., and Bursik, M. (2003). Computing granular avalanches and landslides. *Physics of Fluids*, 15(2):3638–3646.

[118] Pitman, E. B. and Le, L. (2005). A two-fluid model for avalanche and debris flows. *Philosophical Transactions of the Royal Society of London A: Mathematical, Physical and Engineering Sciences*, 363(1832):1573–1601.

[119] Procter, J., Cronin, S., Fuller, I., Sheridan, M., Neall, V., and Keys, H. (2010). Lahar hazard assessment using Titan2D for an alluvial fan with rapidly changing geomorphology: Whangaehu River, Mt. Ruapehu. *Geomorphology*, 116(1):162–174.

[120] Qian, Y., d'Humières, D., and Lallemand, P. (1992). Lattice bgk models for navier-stokes equation. *EPL (Europhysics Letters)*, 17(6):479.

[121] Quarteroni, A. and Valli, A. (2008). *Numerical approximation of partial differential equations*, volume 23. Springer Science & Business Media.

[122] Rizzo, E. and Straface, S. (2015). Personal communication. CNR IMAA, Potenza and Department of Environmental and Chemical Engineering, University of Calabria, Italy.

[123] Rodolfo, K. S., Umbal, J. V., Alonso, R. A., Remotigue, C. T., Paladio-Melosantos, M. L., Salvador, J. H., Evangelista, D., and Miller, Y. (1996). Two years of lahars on the western flank of Mount Pinatubo: Initiation, flow processes, deposits, and attendant geomorphic and hydraulic changes. *Fire and mud: eruptions and lahars of Mount Pinatubo, Philippines*, pages 989–1014.

[124] Rosenfeld, A. and Wu, A. Y. (1981). Reconfigurable cellular computers. *Information and Control*, 50(1):64–84.

[125] Rothman, D. H. and Zaleski, S. (1994). Lattice-gas models of phase separation: interfaces, phase transitions, and multiphase flow. *Reviews of Modern Physics*, 66(4):1417.

[126] Salles, T., Lopez, S., Cacas, M., and Mulder, T. (2007). Cellular automata model of density currents. *Geomorphology*, 88(1):1–20.

[127] Saltelli, A., Tarantola, S., and Campolongo, F. (2000). Sensitivity analysis as an ingredient of modeling. *Statistical Science*, pages 377–395.

[128] Sassa, K. (1989). Special lecture: geotechnical model for the motion of landslides: Proc 5th international symposium on landslides, lausanne, 10–15 july 1988v1, p37–55. publ rotterdam: Aa balkema, 1988. In *International Journal of Rock Mechanics and Mining Sciences & Geomechanics Abstracts*, volume 26, page 88. Pergamon.

[129] Savage, S. B. and Hutter, K. (1989). The motion of a finite mass of granular material down a rough incline. *Journal of fluid mechanics*, 199:177–215.

[130] Schilling, S. P. (1998). *LAHARZ: GIS programs for automated mapping of lahar-inundation hazard zones*. U.S. Geological Survey.

[131] Schmidt, K. (1934). *Die Schuttströme am Merapi auf Java nach dem Ausbruch von 1930*. Kolff.

[132] Schowalter, W. R. (1978). *Mechanics of non-Newtonian fluids*. Pergamon press Oxford.

[133] Segre, E. and Deangeli, C. (1995). Cellular automaton for realistic modelling of landslides. *Nonlinear Processes in Geophysics*, 2:1–15.

[134] Sheridan, M., Stinton, A., Patra, A., Pitman, E., Bauer, A., and Nichita, C. (2005). Evaluating titan2d mass-flow model using the 1963 little tahoma peak avalanches. *Mount Rainier, Washington: Journal of Volcanology & Geothermal Research*, 139:89–102.

[135] Shroder, J. F. and Papale, P. (2014). *Volcanic Hazards, Risks and Disasters*. Academic Press.

[136] Sieburg, H. B., McCutchan, J. A., Clay, O. K., Cabalerro, L., and Ostlund, J. J. (1990). Simulation of hiv infection in artificial immune systems. *Physica D: Nonlinear Phenomena*, 45(1):208–227.

[137] Slimi, R. and El Yacoubi, S. (2009). Spreadable cellular automata: modelling and simulations. *International Journal of Systems Science*, 40(5):507–520.

[138] Sloane, N. J. (2007). The on-line encyclopedia of integer sequences. In *Towards Mechanized Mathematical Assistants*, pages 130–130. Springer.

[139] Smith, G. A. (1986). Coarse-grained nonmarine volcaniclastic sediment: terminology and depositional process. *Geological Society of America Bulletin*, 97(1):1–10.

[140] Smith, G. A. (1991a). Lahars: Volcano hydrologic-events and deposition in the debris flow—hyperconcentrated flow continuum. *Special Publications of SEPM*.

[141] Smith, G. A. and Fritz, W. J. (1989a). Volcanic influences on terrestrial sedimentation. *Geology*, 17(4):375–376.

[142] Smith, G. A. and Fritz, W. J. (1989b). Volcanic influences on terrestrial sedimentation. *Geology*, 17:375–375.

[143] Smith, R. (1991b). The application of cellular automata to the erosion of landforms. *Earth Surface Processes and Landforms*, 16(3):273–281.

[144] Sodiro, L. (1877). Relación sobre la erupción del Cotopaxi acaecida el dia 26 de junio de 1877. *Imprenta Nacional, Quito, Ecuador (40 pp.)*.

[145] Sparks, R., Wilson, L., and Hulme, G. (1978). Theoretical modeling of the generation, movement, and emplacement of pyroclastic flows by column collapse. *Journal of Geophysical Research: Solid Earth (1978–2012)*, 83(B4):1727–1739.

[146] Spezzano, G. and Talia, D. (1999). *Calcolo parallelo, automi cellulari e modelli per sistemi complessi*, volume 9. Franco Angeli s.r.l., Milano, Italy.

[147] Succi, S. (1991). *Automi cellulari: una nuova frontiera del calcolo scientifico*. Franco Angeli.

[148] Succi, S. (2001). *The lattice Boltzmann equation: for fluid dynamics and beyond*. Oxford University press.

[149] Succi, S. (2002). Lattice Boltzmann schemes for quantum applications. *Computer physics communications*, 146(3):317–323.

[150] Thatcher, J. W. (1964). Universality in the von Neumann cellular model. Technical report, DTIC Document.

[151] Thouret, J.-C. and Lavigne, F. (2000). Lahars: occurrence, deposits and behaviour of volcano-hydrologic flows. *Volcaniclastic rocks from magma to sediments. Gordon and Breach Science Publishers*, pages 151–174.

[152] Toffoli, T. (1977). Computation and construction universality of reversible cellular automata. *Journal of Computer and System Sciences*, 15(2):213–231.

[153] Toffoli, T. (1984). Cellular automata as an alternative to (rather than an approximation of) differential equations in modeling physics. *Physica D: Nonlinear Phenomena*, 10(1):117–127.

[154] Vallance, J. W. (2000). *Lahars. Encyclopedia of Volcanoes*, pages 601–616. Academic press.

[155] Vallance, J. W. (2005). Volcanic debris flows. In *Debris-flow Hazards and Related Phenomena*, pages 247–274. Springer.

[156] Vichniac, G. Y. (1984). Simulating physics with cellular automata. *Physica D: Nonlinear Phenomena*, 10(1):96–116.

[157] Victor, J. D. (1990). What can automaton theory tell us about the brain. *Cellular Automata: Theory and Experiment*, pages 205–207.

[158] Von Neumann, J. (1951). The general and logical theory of automata. *Cerebral mechanisms in behavior*, pages 1–41.

[159] Von Neumann, J., Burks, A. W., et al. (1966). Theory of self-reproducing automata. *IEEE Transactions on Neural Networks*, 5(1):3–14.

[160] Wainwright, R. T. (1974). Life is universal! In *Proceedings of the 7th conference on Winter simulation-Volume 2*, pages 449–459. Winter Simulation Conference.

[161] Weimar, J. R. (1997). *Simulation with cellular automata*. Logos-Verlag Berlin.

[162] Whitman, R. V. and Bailey, W. A. (1967). Use of computers for slope stability analysis. *Journal of Soil Mechanics & Foundations Div*.

[163] Williams, R., Stinton, A., and Sheridan, M. (2008). Evaluation of the Titan2D two-phase flow model using an actual event: Case study of the 2005 Vazcún Valley Lahar. *Journal of Volcanology and Geothermal Research*, 177(4):760 – 766. Volcanic Flows and Falls A Special Issue to Honor Michael F. Sheridan.

[164] Wolf, T. S. (1877). Memoria sobre El Cotopaxi y su última erupción, acaecida el 26 de junio de 1877. *Imprenta del Comercio, Guayaquil, Ecuador.*

[165] Wolfram, S. (1983). Statistical mechanics of cellular automata. *Reviews of modern physics*, 55(3):601.

[166] Wolfram, S. (1986). Cellular automaton fluids 1: Basic theory. *Journal of Statistical Physics*, 45(3-4):471–526.

[167] Wolfram, S. (1994). *Cellular automata and complexity: collected papers*, volume 1. Addison-Wesley Reading.

[168] Wolfram, S. (2002). *A new kind of science*, volume 5. Wolfram media Champaign.

[169] Wright, T. L. and Pierson, T. C. (1992). Living with volcanoes. Technical report, USGPO,.

[170] Wuensche, A. (1999). Classifying cellular automata automatically: finding gliders, filtering, and relating space-time patterns, attractor basins, and the z parameter. *Complexity*, 4(3):47–66.

[171] Wuensche, A. and Lesser, M. (1992). *The global dynamics of cellular automata: An atlas of basin of attraction fields of one-dimensional cellular automata*. Number 1. Andrew Wuensche.

Appendix A

Notation

Nomenclature	Description
CA	Cellular Automata (Cellular Automaton)
M&S	Modeling and Simulation
MCA	Multicomponent (or Macroscopic) Cellular Automata
PDE	Differential Partial Equations
fa	finite automaton (finite state automaton)
ea	elementary automata
S_A	cell **A**ltitude
S_{D}	tephra stratum **D**epth
$S_{\mathrm{D1}}, S_{\mathrm{D2}}$	upper erodible stratum (D1) and lower stratum (D2)
S_{SR}	mobilizable stratum: **S**tratum **R**eceptivity,
S_{SWC}	**S**tratum **W**ater **C**ontent,
S_{MIR}	**M**ax **I**nfiltration **R**ate
S_{WL}	**W**ater **L**evel
S_{WKH}	**W**ater **K**inetic **H**ead
S_{WO}	**W**ater **O**utflows
S_{WKHO}	**W**ater **K**inetic **H**ead of **O**utflows
S_{LT}	**L**ahar **T**hickness
S_{KH}	Lahar **K**inetic **H**ead
S_{LWC}	**L**ahar **W**ater **C**ontent
S_{X},	the co-ordinate **X** of the lahar barycenter
S_{Y}	the co-ordinate **Y** of the lahar barycenter
S_{MX},	the component **x** of the lahar **M**omentum
S_{MY}	the component **y** of the lahar **M**omentum
S_{E}	**E**xternal flow normalized to a thickness
$S_{\mathrm{EX}}, S_{\mathrm{EY}}$	**E**xternal flow co-ordinates **X** and **Y**
S_{KHE}	**K**inetic **H**ead of **E**xternal flow

Nomenclature	Description
S_I	**I**nternal flow normalized to a thickness
S_{IX}	**I**nternal flow co-ordinate **X**
S_{IY}	**I**nternal flow co-ordinate **Y**
S_{KHI}	**K**inetic **H**ead of **I**nternal flow
p_a	cell **a**pothem (m)
p_t	**t**emporal correspondence of a CA step (s)
p_{fc}, p_{wfc}	lahar and water **f**riction **c**oefficient parameters (-)
p_{td}	**t**urbulence **d**issipation (-)
p_{ed}	**e**rosion **d**issipation of energy (-)
p_{pe}	lahar parameter of **p**rogressive **e**rosion (-)
p_{mt}	**m**obilization **t**hreshold (m)
p_{slt}	**s**lope **t**hreshold $(^\circ)$
p_{wct}	**w**ater **c**ontent **t**hreshold $(\%)$
p_{khl}	**k**inetic **h**ead **l**oss (m)
p_{dft}	lahar complete **d**eposit **f**ormation **t**hreshold $(\%)$
p_{adh1}	minimum **adh**erence (m)
p_{adh2}	maximum **adh**erence (m)